STABILIZATION OF A RING DYE LASER

By

CHARLES CHARBEL HARB

A thesis submitted for the degree of Master of Science

of The Australian National University.

STABILIZATION OF A RING DYE LASER

By

CHARLES CHARBEL HARB

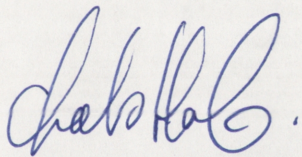A thesis submitted for the degree of Master of Science

of The Australian National University.

May 14, 1992

Statement of Authorship

The contents of this thesis, except where indicated by references, are entirely my own work.

Charles Harb

May 14, 1992

ACKNOWLEDGEMENTS

ABSTRACT

We have developed an external stabilization unit, based on an acousto-optic modulator operating in a feedback loop, that can dramatically improve the stability of a commercial ring dye laser. The frequency stability of the this laser has been reduced from a few MegaHertz to below twenty kiloHertz, and its intensity stability has been reduced from approximately two and one half percent to below one half a percent.

This thesis outlines the development of this stabilization system. Emphasis is given to the technology and techniques required to frequency and intensity stabilize the ring dye laser. A review is given of the control theory for such a stabilization system, and the elements of the control loop. We summarise the appropriate concepts of standard control theory applying to laser control, and link these concepts to illustrate how the control loop elements interact with each other.

We introduce the *effective locking potential* curve of a locking scheme. This is a numerical integration of the error signal in a locking scheme. The curve provides a new way of visualizing the capture range and strength of a locking system. We have compared several different locking schemes, and highlighted their strengths with the aid of the effective locking potential.

An understanding of the properties of the laser source is essential if we wish to control its output. The ring dye laser is a complicated laser source that has extensive literature describing its operation. We have condensed the available literature, extracting the aspects necessary for a comprehensive understanding of its operation.

The electronic developments have also been addressed. The electronics of a control loop is extremely important. We required high gain, low noise, high bandwidth, low drift electronics. The technology to produce these electronic circuits is presented, and the techniques involved have been refined.

A summary of the different stabilization methods is presented, where we consider the advantages, disadvantages, and feasibility of the different options in relation to our needs. We propose a novel feedforward technique for frequency stabilization. It is based around an AOM, and uses an optical fibre imposed optical delay as compensation for the intrinsic delays of the AOM.

Finally, we present the results of a set of experiments using the stabilization unit. The results of these experiments clearly show an improvement, due to the stabilization unit, in the quality of the data.

TABLE OF CONTENTS

ACRONYMS AND NOTATIONS

This thesis is written in, and adheres to, the SI units system.

The following acronyms and notations are presented in the order in which they appear in the given chapter.

AOM	:	acousto-optic modulator
EOM	:	electro-optic modulator
FWHM	:	full-width-half-maximum
VCO	:	voltage controlled oscillator
VCA	:	voltage controlled attenuator
PZT	:	piezoelectric transducer
PID	:	proprotional-integrating-differentiating amplifier
RF	:	radio frequency
LO	:	local oscillator
IF	:	intermediate frequency
DBM	:	double balanced mixer
PCB	:	printed circuit board

CHAPTER 1

INTRODUCTION

1.1   MOTIVATION

Noise is an important consideration in physics. The presence of noise limits the accuracy of measurement processes. In laser physics, noise is generated by random electromagnetic fields oscillating at the same frequency as the desired signal. Chief among these are mechanical vibrations, thermal drifts, and laser medium variations. As a result of these intrinsic noise processes the laser's linewidth is degraded, both in frequency and intensity. The motivation behind laser stabilization then comes from the desire to produce a laser oscillator with an output free of such excess noise.

The applications for a low noise laser system are numerous and in many research areas including both quantum optics and high resolution spectroscopy. These projects require the laser oscillator to have its frequency, intensity, and output spacial characteristics all stabilized.

This project develops a stabilization unit for a ring dye laser, for use in laser spectroscopy and quantum optical research. We will concentrate on an external stabilization technique. External stabilization uses a correcting element, such as an electrooptic modulator (EOM) or acoustooptic modulator (AOM), placed outside the laser cavity.

External techniques have been studied for many years, primarily by J.L. Hall, at the Joint Institute for Laboratory Astrophysics, Boulder, Colorado, (JILA) [Hall 84]. Hall has already reduced the dye laser linewidth to the hertz level by using an EOM–AOM combination. However, this system requires a complex electronic delay inside the servo system to link the two modulators. A simpler approach is to use only one AOM to correct for any laser frequency changes, which we have done in this work.

1.2   REVIEW OF PREVIOUS WORK

Control of the laser output has a long historical background, spanning back to the laser's conception [Schawlow & Townes 58]. This early work, dealing with the "extension of maser techniques to the infrared and visible regions", gave the basic limit for laser stabilization, which is now known as the *Schawlow-Townes* limit. The frequency limit was calculated for a passively stabilized laser. This limit on the laser's spectral purity is set by quantum noise fluctuations caused by spontaneous emission from the atoms inside the laser cavity.

It was quickly realised that the Schawlow-Townes limit could be reduced by actively "locking" the laser field to some frequency reference that was not affected by spontaneous emission, such as a Fabry-Perot cavity.

Many of the initial investigations into laser stabilization were performed on low power gas lasers such as Helium-Neon lasers (He-Ne) [White 65, Wallard 73]. Techniques were developed for locking the laser to the centre of the Lamb dip, to low finesse Fabry-Perot cavities, Zeeman split atomic lines, and narrow linewidth electronic transitions [Barger 69, Hanes 69]. The linewidth of the laser system was reduced from tens of GHz to the sub-GHz level. The lasers used in the initial investigation stage were single fixed frequency devices, which were useful for some areas of research, but not all. High resolution spectroscopy [Stacey 89], for example, requires a stable tunable laser source for probing atomic systems.

A new era came with the development of the tunable cw dye laser, in the early 70's. Bager *et al.* [1973] stabilized a dye laser to a transmission fringe of a high finesse Fabry-Perot cavity using the very popular "fringe side" method (which has since been employed in many commercially built dye lasers). This system used a 0-100kHz servo system and achieved a frequency stability of 50MHz over a period of 1 second. Further improvements in dye flow, mounting of optics, and reference cavity temperature stabilization have given us commercially built single mode cw dye lasers [Johnston 82] with residual linewidths of a few MHz. The tunability and linewidths of these lasers satisfy the majority of needs for modern research, but not the needs of the newest areas of research.

Reducing the linewidth of a dye laser, and other laser systems, to below one MHz has required a great deal of effort. Concurrent development of optics and electronics have drastically improved our ability to stabilize both the laser frequency and intensity

output. In conjunction with traditional frequency transducers such as resonator mirrors on piezoelectric (PZT) stacks and galvo driven optical plates, we now have acoustooptic modulators (AOM) and electrooptic modulators (EOM). These devices have a much higher bandwidth, and consequently reduced response time. Also, developments in integrated circuitry have produced low noise, low drift, high gain, high bandwidth operational amplifiers, suitable to drive these frequency transducers.

In 1984 Hall & Hänsch [Hall 84] reported that they were able to reduce the linewidth of a commercial ring dye laser from about 3MHz to approximately 20kHz using an external frequency stabilizer. This stabilizer was based on the combination of an EOM and AOM as a frequency transducer (this will be discussed in a later chapter). Soon after this report, a dye laser was stabilized to 200Hz [Hough 84] using an intracavity EOM to correct for the high frequency laser fluctuations. Since this initial work, several dye lasers have been stabilized to around the kilohertz regime [Kallenbach 89, Steiner 89, Fisk 91]. All these systems used an intracavity EOM to act as the fast frequency transducer.

The next major step came in 1988 with the publication by Salomon *et al*. [Salomon 88] entitled "Laser stabilization at the millihertz level". They were able to lock two independent He-Ne lasers onto adjacent cavity orders of a high-finesse Fabry-Perot cavity so that their relative phase coherence was preserved for 8 seconds, which corresponded to a linewidth for each laser of approximately 50mHz. Since this work Day *et al*. [1991] reported that they were successful in stabilizing two independent diode pumped Nd:YAG ring oscillators to a commercial Fabry-Perot interferometer yielding a beatnote linewidth of 330mHz.

These stabilities are well beyond our requirements. However, we want to use similar methods to achieve our design specification (that will be discussed in section 1.3). The technology developed during the course of this project has placed us in the position to push closer to the sub-hertz regime should the need arise.

1.3   SUMMARY OF THIS WORK

The aim of this investigation is to develop an active stabilization system for use at the Department of Physics and Theoretical Physics, Australian National University. Our main areas of interest are in the fields of quantum optics and laser spectroscopy, and the requirements of these fields have been considered in this work. We wish the stabilization system developed to fill the following three criteria:

(I)   It can be used to frequency stabilize the laser oscillator down to ≈ 20kHz.

(II)   It can be used to intensity stabilize the laser oscillator down to ≈ 0.5%.

(III)   It should be capable of isolating the laser oscillator from the experiment.

The lasers used in this project were the Spectra-Physics 380D, and the Coherent CR-699-21, travelling wave ring dye lasers. We used the Coherent for the frequency stabilization experiments, and the Spectra-Physics for the intensity stabilization experiment. Their usage was solely based on the availability of the lasers at the required time.

The frequency noise associated with the CR-699-21 is shown in figure 1-1. The noise is measured by detecting the lasers transmission through an optical spectrum analyser (Newport SuperCavity), and recording this on a Hewlett-Packard [Model 54200A/D] digitizing oscilloscope

The CR-699-21 is actively stabilized to a temperature controlled Fabry-Perot confocal reference cavity. The stabilization system is able to reduce the frequency noise on the laser output from at least 20MHz ("free running") to approximately 1MHz FWHM ("locked") for short time periods (5ms), as measured from the width of the solid trace in fig. 1-1, and ≈ 8MHz for longer time periods, 5s in this case (see appendix a for an explanation of how fig. 1-1 was recorded).

The instantaneous laser linewidth (solid curve in fig.1-1) has frequency noise which is attributed to thickness fluctuations in the dye jet-stream [Hall 86]. Typically, the phase of the laser radiation can change by as much as 1 radian in a microsecond with respect to an ideal sine wave oscillator. The varying phase of the laser field manifests itself as a frequency broadening of the laser field. That is, the output field contains the fundamental laser oscillation frequency as well as extra Fourier components arising from the fluctuating dye-stream. Hence, the output appears to be frequency broadened. A secondary affect is seen in the intensity output of the
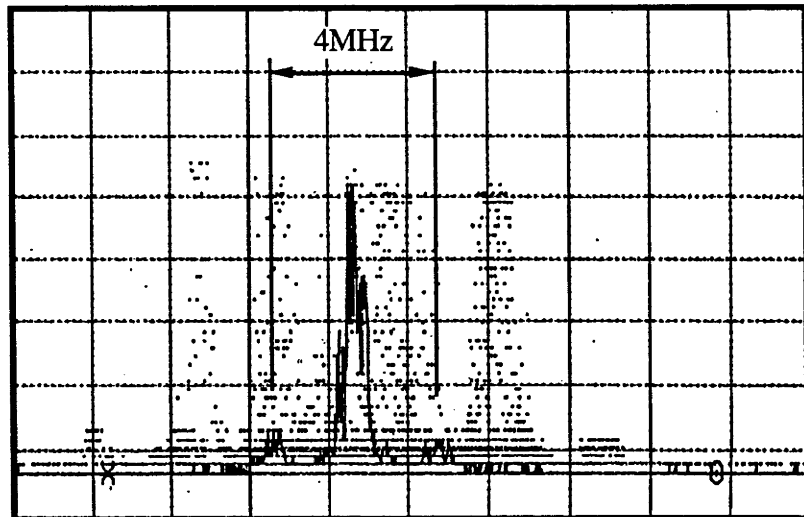
Figure 1-1. Illustration of the laser frequency output. This is the transmission of the laser light through an optical spectrum analyser: the solid curve shows the instantaneous linewidth of the laser field, and the dots indicate the deviation of the field around the central frequency. The sidebands were superimposed on the laser field by phase modulating the laser light at two MegaHertz, to calibrate the frequency scale. The trace is recorded on a Hewlet-Packard digital storage oscilloscope. The HP was working in acquisition mode; that is it was displaying the present acquisition on the screen as well as the previous acquisitions. Each trace was recorded over the 23ms sweep time of the SuperCavity, and the total set of traces was recorded over a 5s period.

laser. As the laser medium thickness fluctuates so to does the output intensity because the laser gain is dependent on the medium thickness.

The long-term laser linewidth (illustrated by the dots in fig.1-1) is due to mechanical vibrations of the reference cavity and by directional fluctuations of the laser beam with respect to the reference cavity. These force the laser frequency to jump by many MHz.

We are able to determine the requirements of the servo system from figure 1-1. The servo system must be able to correct for both the fast small frequency changes, (occurring at MHz rates) caused by the dye jet instabilities, and it must also be able to correct for the slow large frequency jumps caused by the reference cavity instabilities.

The external stabilizer built at this university was based on the system developed by Hall & Hänsch (1984) at JILA, which used an AOM/EOM frequency transducer. The AOM is used to correct for the slow large frequency changes and the EOM is used to correct for the fast small frequency changes. The two modulator system is

required because neither of the modulators can satisfy the requirements for the servo completely. Unfortunately, it is technically very difficult to build such a system. To reduce the complexity of the servo we chose to use only the AOM as a frequency correcting element. Advances in electronic technology has made it possible for us to build this system.

Our error signal was derived from a high finesse Fabry-Perot cavity using the Pound-Drever method [Drever 83]. The electronics to control the stabilizer were designed and built by myself as part of this project. An analysis of the stabilizing systems error signal indicated that the stability of the laser is about 20kHz over periods in excess of 1 minute.

Two experiments were performed using this external stabilizer. The first was a hole burning experiment in K Eu (WO_4) in collaboration with Dr. P.T.H. Fisk and Mr. M. Sellars at the Laser Physics Centre, ANU. The second experiment was a saturated absorption experiment in a vapour of Samarium in collaboration with Dr. R.J. McLean and Dr. P. Hannaford (CSIRO Division of Materials Science and Technology, Vic.). Both these experiments showed an improvement in the signals obtained when the stabilization system was used. The results of these two experiments are presented in this thesis.

The intensity output of the Spectra-Physics laser is shown in figure 1-2. This Figure shows the total photodetector output of the laser and the AC component on an expanded scale. The signal was taken from a low noise UDT PIN 6D photodetector, and displayed on a Tektronix 2211 digital storage oscilloscope. The majority of the noise in the output of the dye laser originates at the switch mode power supply of the pump laser. This power supply induces spikes in the output of the pump laser (at 50 and 100Hz) that carried through into the dye laser causing large variations in the output intensity of the dye laser. Faster intensity fluctuations are produced by mechanical vibrations of the laser cavity which reduces the lasing efficiency, and also the dye jet fluctuations mentioned earlier.

The principle of operation of the intensity stabilizer built at this department is based on controlling the RF power supplied to the acoustooptic modulator (AOM) in a feedback configuration. The intensity stability was reduced from $\approx 2.5\%$ to below 0.4%.

The elegance of the stabilization systems developed here is that they can be combined

Time 5ms/DIV
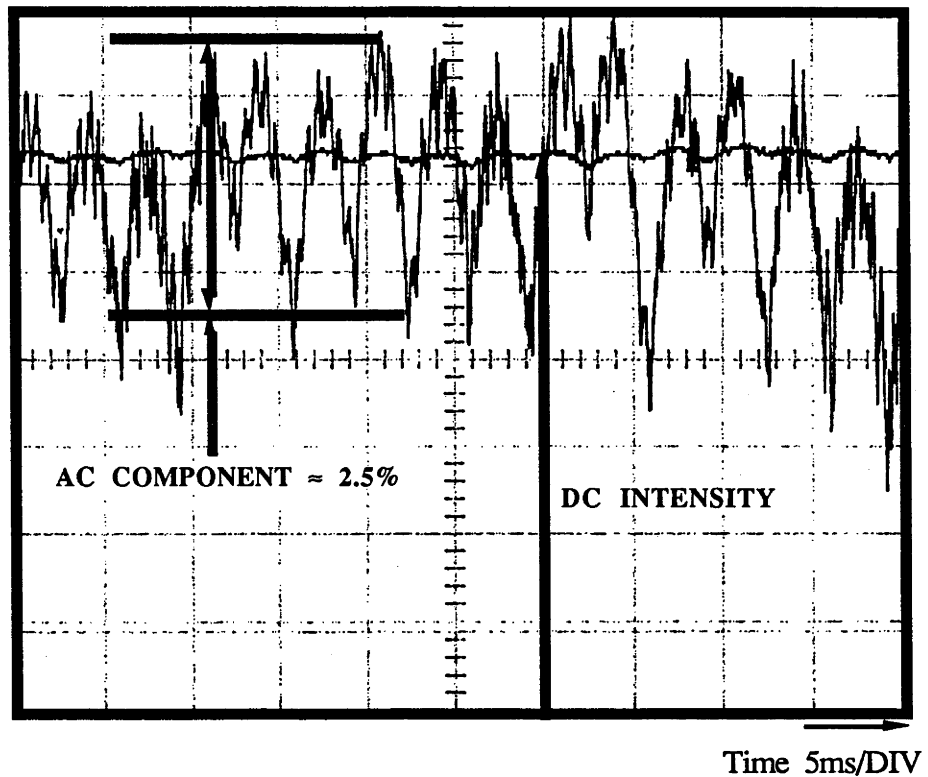
Figure 1-2. This shows the intensity fluctuations of the Spectra-Physics 380D
ring dye laser. The AC scale is 20mV/DIV, the DC scale is 0.5V/DIV.

into one system which is capable of satisfying all three criteria mentioned earlier.
The acoustooptic modulator is an isolation unit, any laser light reflected back towards
the laser experience a frequency shift that detunes the light away from the laser
wavelength. Frequency stabilization can be achieved by controlling the RF frequency
supplied to the acoustooptic modulator. Finally, the intensity stability can be
achieved by altering the RF power supplied to the same acoustooptic modulator.

In this project we have also devoted research time to designing a fast response (>
200kHz) high voltage (1000V) DC power supply, with minimal phase lag between
the input and output signals, to drive mirrors on PZT stacks and EOM's. The
commercially available HV supplies are designed to control only PZT's with
resonances at low frequencies ($\approx$ 2-10kHz), but recently, the group in Stanford
University [Levenson 91] have developed a PZT with first resonance around 200kHz,
which is ideal for this type of stabilization work. Our development work has
shown that it is possible to build a high voltage supply with the required characteristics.
The circuit diagram and phase response of the first prototype are presented in this
thesis.

1.4   STRUCTURE OF THIS THESIS

This thesis is laid out as follows:-

Chapter 2 outlines the control theory required for laser stabilization, and the components for such a system. Chapter 3 describes the ring dye laser used in this work. Chapter 4 is devoted to a review of alternative techniques used in laser frequency and intensity stabilization. Chapter 5 outlines the electronics developed in this project. Chapter 6 is a presentation of the experiments and results obtained using the frequency and intensity stabilizers. Finally chapter 7 will give the conclusions and recommendations for future work.

CHAPTER 2

LASER CONTROL

INTRODUCTION

Active stabilization allows us to eliminate the noise associated with the classical processes such as mechanical vibrations. This chapter defines the concepts of active stabilization.

Figure 2.1-1 is a schematic representation of the control problem [Hall 86, Dorf 89] associated with stabilizing the laser output frequency. The problem is to actively adjust the laser frequency so that it is held to some stable reference. The control

Conversion of the amplified error
signal V into a frequency shift f.

Stabilized laser
output
oscillating at
frequency v .

Laser
Oscillating
with a central
frequency v
and a frequency
linewidth of Δv .

Frequency Transducer

Frequency
$v + \Delta v$
is sent to be
measured.

Amplification and
phase compensation of
error voltage to V.

PID Amplifier

Frequency
Reference

Conversion of the frequency
error f into a voltage v that is
negative if f is negative and
positive if f is positive.

Frequency
Discriminator

$f = v_0 - v + \Delta v$

Measurement of the difference
between the reference
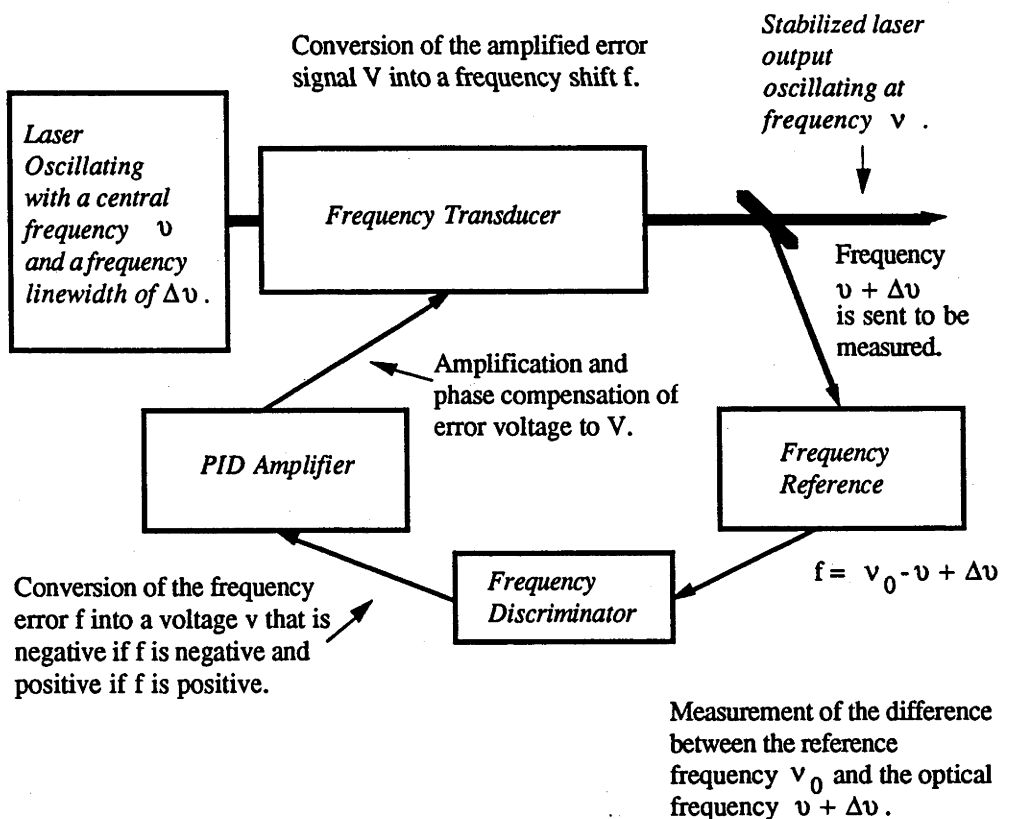frequency v_0 and the optical
frequency $v + \Delta v$.

Fig.2.1.1. Schematic of the control system used in frequency locking of lasers.

system illustrated in figure 2.1-1 is called a feedback system because the control loop measures the error on the output of the laser then creates a correction signal and sends this signal to a frequency transducer placed before the sampling point. Ideally the correction signal should be sent back to the frequency transducer exactly π radians out of phase with the error signal so that it can counteract the error from the output. In practice, however, there exist within the control loop some elements that have frequency dependent phase lags and resonances. It is therefore very difficult to feed a signal back to the frequency transducer that is exactly π radians out of phase with the error signal for all possible frequencies. Hence, we need to be able to identify the phase lags in a control loop and tailor the loop so that the signal fed back is as close to π radians out of phase with the output as is possible, and for as many frequencies as possible.

The performance of a control loop depends on the characteristics of the loop, the noise in the laser, the noise in the detection electronics, and the response times of the frequency transducers. These characteristics set limits on the maximum gain of the loop, and hence on the strength of the control loop. In order to produce an active stabilization system we must therefore design the system so that we have the largest possible gain in the loop without sending the loop into oscillations.

This chapter is divided into the following sections:

(2.1)   *Control theory* : the theory developed to describe the elements of an automated control system.

(2.2)   *Frequency reference* : the laser can either be locked to an atomic transition or a high finesse temperature stabilized optical resonator.

(2.3)   *Frequency discriminator* : there are many methods for generating an error signal to be used in a control system. These include : *Saturated Absorption* in some atomic medium; *Transmission* through an optical resonator; or *Reflection* off an optical resonator. Reasons are given as to why we use the Pound/Drever [Drever 83] method to generate the error signal.

(2.4)   *PID amplifier* : this is a frequency and phase dependent electronic amplifier circuit which is used as an intermediate stage between the frequency discriminator and the frequency transducer.

(2.5)   *Frequency transducers* : these can be piezoelectric (PZT) driven

mirrors inside the laser cavity; electrooptic modulators (EOM) internal or external to the laser cavity; or an acoustooptic modulator (AOM) external to the laser cavity.

2.1   CONTROL THEORY

The servomechanism controlling the laser frequency is most effectively dealt with in frequency space. The laser is considered to be an oscillator with output Fourier frequency υ that is being perturbed by some noise process $S(f)_{Las}$ where f stands for the fluctuation frequency, so that the observed laser frequency is $(\upsilon+f)$. $S(f)_{Las}$ is a measure of the fractional noise per unit bandwidth and hence has units $Hz/\sqrt{Hz}$.

A very practical approach to the analysis and design of a servomechanism to compensate for $S(f)_{Las}$ is called the frequency response method which is defined as the steady-state response of a system to a sinusoidal input signal. In order to use this method we will need to outline the properties of the elements in the feedback loop.

The laser frequency is monitored in comparison to a frequency reference which defines the optical frequency, ν_0, that must be maintained. Instantaneous variations in the optical frequency from the reference are assessed by an appropriate discriminator (a Fabry-Perot cavity for example), that converts the frequency fluctuations, f, to voltage fluctuations, v. This signal from the discriminator, $D(f\Rightarrow v)$, is called the systems error signal and has units V/Hz.

A signal proportional to $D(f\Rightarrow v)$ could, in principle, be amplified by a wide bandwidth operational amplifier and sent back π radians out of phase with the output but, as mentioned earlier, phase lags in the control loop need to be addressed. A proportional-integrating-differentiateing (PID) electronic amplifier is used instead of a simple proportional amplifier to produce a control signal. The control signal from the PID is a frequency dependent amplification of the error signal, which can compensate for phase shifts in the controlled loop that would cause undesired oscillations. This frequency dependent gain, $G(v\Rightarrow V)$, has units V/V . The amplified voltage is negatively fed back to a frequency transducer which alters the optical frequency with a conversion gain $K(V\Rightarrow f)$ (units Hz/V).

The functions that I have defined above, namely K, G and D, are called the transfer functions of their respective elements. K, G and D represent the dynamics of the system under consideration. A transfer function is the ratio of the output to input signal where the input is a sinusoid: that is, $T(f) = \dfrac{OUTPUT(f)}{INPUT(f)}$. This function can be obtained analytically by taking the Laplace transform of the differential equations describing the properties of the elements. This method is called the Laplace transform method. However, it is generally easier to experimentally determine the transfer function using the frequency response method mentioned earlier. T(f) is, generally, complex in nature and describes the frequency response of an individual stage in the control loop or of a combination of stages. The magnitude of T(f) describes the attenuation that a sinusoid would experience when passing through a stage, and the argument of T(f) describes the phase change between the input and output sinusoid.

The spectral density of laser frequency noise, $S(f)_{Las}$, can be suppressed over the bandwidth of the control loop by using active frequency control [Dorf 89 Ch. 3]. The noise is reduced to:

$$S_{closed\ loop} = \frac{S_{Las}}{|1 + KGD|} \tag{2.1}$$

In a realistic environment, however, there is noise in the other sections of the control loop which adds to the noise from the laser. Let us define $S_{Amplifier}$ (units $V/\sqrt{Hz}$), and $S_{Discriminator}$ (units $V/\sqrt{Hz}$) as being the spectral density of voltage noise associated with the amplifier and discriminator respectively; $S_{Discriminator}$ includes the noise of the frequency reference. The equation for the closed loop spectral density of frequency noise taking into account the other contributions is:

$$S_{closed\ loop} = \frac{\sqrt{S_{Las}^2 + |K\ S_{Amplifier}|^2 + |K\ G\ S_{Discriminator}|^2}}{|1 + KGD|} \tag{2.2}$$

In the limit of very high servo gain, G, we find:

$$S_{closed\ loop} = \frac{S_{Discriminator}}{D} \tag{2.3}$$

Which states that the minimum spectral density of frequency noise depends only on the discriminator, given sufficiently high servo gain. As a consequence of this

result much effort has gone into finding the best frequency discriminator, as will be discussed in section 2.3.

2.2   FREQUENCY REFERENCE

Laser frequency stabilization has been studied since the early 60's and at that time the major stumbling block was in obtaining a frequency reference which was very stable and also highly sensitive to small frequency changes. Initially the best results were obtained using atomic transitions as frequency discriminators because they gave an absolute frequency reference that was very narrow, FWHM was typically tens of MHz or less. Presently, however, Fabry–Perot cavities [Hough 84] gave much larger frequency discrimination. The change from atomic transitions as frequency discriminators to optical cavities is largely due to advances in optical coating techniques which allow cavities with finesse of the order of 40000 to be readily available. These cavities have bandwidths on the order of 200KHz. Also, a further advantage of Fabry-Perot cavities is that their resonant frequency can be changed, which is not the case for atomic transitions.

We have chosen to lock to a Fabry-Perot cavity. This section will discuss the properties of the Fabry-Perot cavity, and the two cavities used in this experiment.

2.2.1   PROPERTIES OF A FABRY-PEROT CAVITY

The Fabry-Perot cavity is a multiple-beam interferometer capable of extremely high resolution. This device is called a division-of-amplitude interferometer because the interfering beams are produced by splitting the incident beam at a partially reflecting surface. In the Fabry-Perot a series of such beams are produced by multiple reflection between two mirrors. The effective number of interfering beams depends on the reflectivity of the mirrors.

The geometry for a Fabry-Perot etalon with a beam incident at angle θ, normal to the axis of the input mirror, is shown schematically in fig. 2.2.1-1. The optical path difference between successive rays is given by the relation:

$$\Lambda = 2 \ n \ d \ \cos[\theta] \tag{2.4}$$

where n is the refractive index between the mirrors, d is the distance between the mirrors, an θ is the incident angle of the light rays. The optical phase shift induced by the path length difference is given by the relation:

$$\delta = 2 \ n \ d \ \cos[\theta] \ \frac{2\pi}{\lambda} \ = \ \frac{2nd}{c} \ \cos[\theta] \ \omega \tag{2.5}$$

where c is the speed of light, λ is the wavelength of the radiation, and ω is the angular frequency of the radiation.

An electromagnetic field oscillating with angular frequency ω and amplitude E_o can

Fig. 2.2.1-1. The reflection and transmission of a light field when incident on a Fabry-Perot cavity. The reflected amplitude is r, and the transmitted amplitude is s. The mirrors are separated by a distance d.
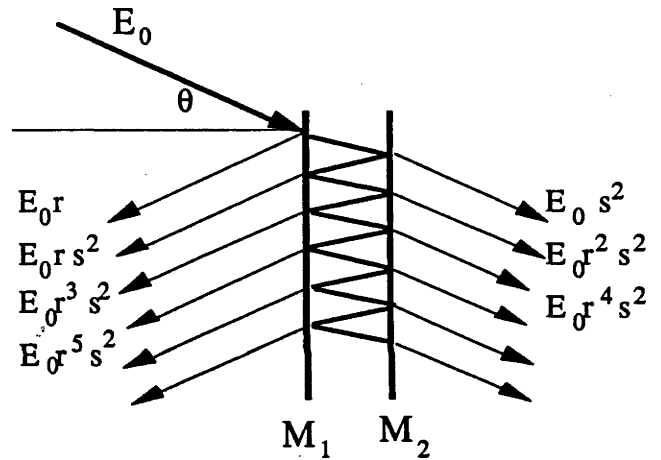
be represented in the complex form:

$$E \ (t) \ = \ E_0 \ e^{j \ \omega \ t} + c.c \tag{2.6}$$

Let us define the amplitudes of the reflected and transmitted field at an interface, such as surface of a mirror, as r and s respectively. They are related to each other by the relationship:

$$r^2 + s^2 = 1 = R + S \tag{2.7}$$

and R and S are the reflectivity and transmittance of the interface. We are assuming that the cavity has low losses due to absorption and scattering. Then the field due to a single reflection at the interface is:

$$E \ (t) \ = \ E_0 \ r \ e^{j \ \omega \ t} + c.c \tag{2.8}$$

and the first transmitted field through the Fabry-Perot cavity is:

$$E(t) = E_0 \, s^2 \, e^{j(\omega t + \delta)} + c.c \qquad (2.9)$$

Each subsequent double pass through the cavity introduces a factor r^2 to the amplitude and a phase shift δ to the field.

The total field reflected by the Fabry-Perot cavity is the sum of all the reflected beams:

$$E_{reflection}(t) = E_0 \, r \, e^{j\omega t}\left[1 + s^2 e^{-j\delta} + s^2 r^2 e^{-j2\delta} \ldots + s^2 r^{(2N-4)} e^{-j\delta}\right]$$

$$(2.10)$$

which simplifies to:

$$E_{reflection}(t) = E_0 \, r \, e^{j\omega t}\left[\frac{1 - e^{-j\delta}}{1 - r^2 e^{-j\delta}}\right] + c.c \qquad (2.11)$$

From a similar argument we find the complex field amplitude of the transmitted field is:

$$E_{transmission}(t) = E_0 \, e^{j\omega t} e^{-j\delta/2}\left[\frac{1 - r^2}{1 - r^2 e^{-j\delta}}\right] + c.c \qquad (2.12)$$

The amplitude transfer functions for reflection and transmission [Siegman 86 Ch. 11] are thus:

$$T_{reflection} = r\left[\frac{1 - e^{-j\delta}}{1 - r^2 e^{-j\delta}}\right] \qquad (2.13)$$

$$T_{transmission} = r \, e^{-j\frac{\delta}{2}}\left[\frac{1 - r^2}{1 - r^2 e^{-j\delta}}\right] \qquad (2.14)$$

and contain the wavelength dependent amplitude attenuation and phase shift experienced by incident electromagnetic field.

The reflected and transmitted intensity is calculated from the relation: $I = E.\hat{E}$, where $\hat{E}$ is the complex conjugate of the field.
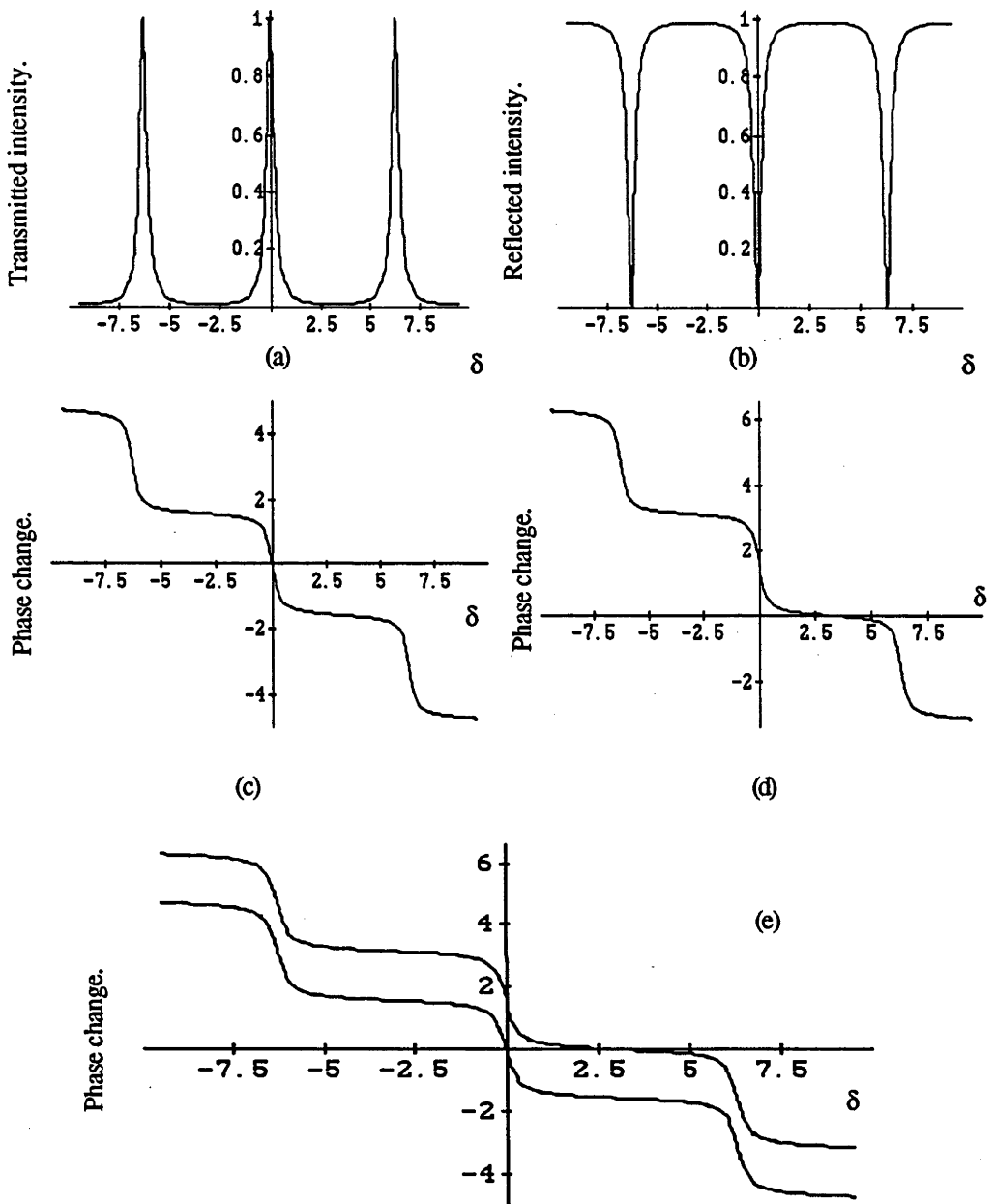
Fig. 2.2.1-2. Diagram showing the intensity & phase differences as a function of optical phase difference (or cavity length) for the transmitted (a & c) and reflected (b & d) cases. There is a 90 degree phase difference between the transmitted and reflected beams, as is shown in (e).

$$I_r = E_{ref}(t).\hat{E}_{ref}(t)$$

$$= E_0^2 \, r^2 \left[\frac{1-e^{-j\delta}}{1-r^2e^{-j\delta}}\right]\left[\frac{1-e^{+j\delta}}{1-r^2e^{+j\delta}}\right]$$

$$I_r = E_0^2 \left[\frac{\left[2r/(1-r^2) \right]^2 \sin^2(\delta/2)}{1 + \left[2r/(1-r^2) \right]^2 \sin^2(\delta/2)} \right]$$

(2.15)

and similarly for transmission,

$$I_t = E_0^2 \left[\frac{1}{1 + \left[2r/(1-r^2) \right]^2 \sin^2(\delta/2)} \right]$$

(2.16)

The finesse of the cavity is $F = \left[2r/(1-r^2) \right]^2$ (2.17)

and the term $\left[1 + \left[2r/(1-r^2) \right]^2 \sin^2(\delta/2) \right]^{-1} \equiv \mathfrak{A}(\delta)$ (2.18)

is known as the Airy function. It represents the transmitted field and is shown in figure 2.2.1-2a. Conservation of energy tells us that the reflected intensity (fig. 2.2.1-2b) is the incident intensity minus that transmitted. Also shown in figure 2.2.1-2 is the phase shift, δ, experienced by the incident field verses frequency through an interferometer.

2.2.2 THE FABRY-PEROT CAVITIES

The laser was locked to two different types of commercial cavities. The first was a Tropel cavity (Model 216) : a confocal, low finesse ($\approx$100-200), 300MHz free spectral range (FSR) cavity with a linewidth of approximately 3MHz. This unit has no temperature control supplied. We were able to lock the laser accurately to this cavity (error signal measurements indicated that it was locked to below 40kHz), but we observed large frequency drifts (over 20MHz per minute) which were due to thermal expansion of this reference cavity.

The second cavity used was a Newport SuperCavity (Series SR-130): a non-confocal, high finesse ($\approx$ 40000), 6GHz FSR cavity with has a linewidth of approximately 150kHz. This cavity proved to be very satisfactory for our purposes. Laser frequency drifting induced by thermal expansion of the reference cavity was still unavoidable but occurred at much slower rates (typically 1MHz per minute). This

cavity allowed us to reduce the locking error to below 20kHz measured over several minutes (see appendix A).

Better results were obtained using this cavity for several reasons. First, the low bandwidth of the cavity gave a frequency discriminating slope of 2kHz/V as opposed to 30kHz/V for the Tropel. Secondly, the SuperCavity control electronics included a temperature controller[1] for the cavity which decreased the frequency drift. Thirdly, the SuperCavity is securely mounted in a five-axis positioning mount which minimises the effects of vibrations (as well as increasing the ease of alignment).

Our SuperCavity is the high finesse version SR-120. It has a centre wavelength of 550nm and the finesse drops down to 30% (12000) at the wavelengths 515 and 585nm.

The specifications for the SuperCavity are as follows:

Finesse	> 10000 over bandpass of cavity, and typically 40000 at centre wavelength;
Free Spectral Range	6GHz (for the SR-100 series);
Bandpass	515nm to 585nm;
Mirror radius of curvature	30cm;
Cavity length	25.4mm;
Fringe width	< 300kHz @ centre wavelength
	< 600kHz @ edge of bandpass;
Fringe stability	Stabilization to 3E-5 @ 633nm under normal laboratory conditions;
Operating environment	$25^0 \pm 5^0$;
Transverse mode splitting	784 ± 40 MHz;
Longitudinal mode splitting	5.984 ± 0.3 GHz.

---

[1] The temperature control had an unfortunate fault in its temperature sensing which arose from cross talk with the high voltages used to scan the cavity. Increased electrical insulation between the two sections would probably solve the problem, but it is easier to avoid adjusting the sweep controls.

The disadvantage of using a cavity is that the long term stability of the cavity is not as good as that of an atomic transition due to mechanical expansion as a result of environmental changes. The ideal frequency reference will utilise both systems to achieve good short and long term stability. This could be done by locking the Fabry–Perot to an atomic transition (to ensure long term stability) and then locking the laser to the Fabry–Perot cavity.

2.3   FREQUENCY DISCRIMINATOR

This section will discuss the signals obtained from the reference cavity, and these will be called the *frequency discriminating* or *error signals*.

Before considering how an error signal is generated, let us examine the logic behind laser frequency stabilization. This can be described easily using the diagrams in figure 2.3-1. An error signal is shown in fig. 2.3-1a. We wish to lock the laser frequency to a part of the fringe that can discriminate frequency changes, that is, a part having a non-zero slope. This point is indicated in figure 2.3-1a. If the lock point is displaced from zero volts (or ground) by some amount V then this voltage is electronically subtracted from the error signal so that it is symmetric about ground.
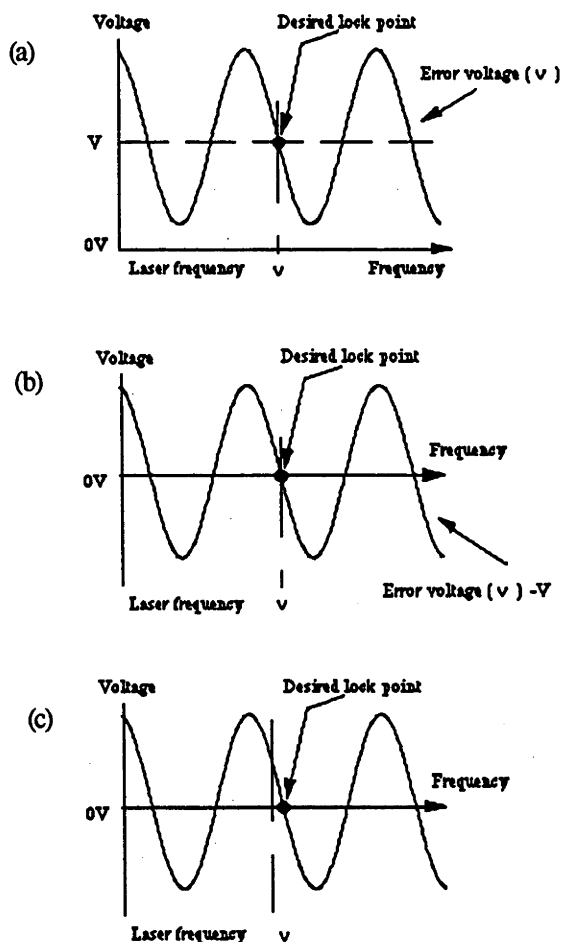

Fig. 2.3-1. Pictorial representation of the logic behind laser frequency locking. (a) show the desired lock point on the error signal. (b) biasing the error signal the desired lock point is at 0V. (c) any laser frequency changes can be detected and forced back to the lock point.

The bipolarity of the error signal can be used as follows:

If the laser frequency is too low then a positive error voltage will be present which can be used, in conjunction with a frequency transducer, to increase the laser frequency.

Similarly, if the laser frequency is too high then a negative voltage is obtained, which can be used to force the laser frequency to decrease.

2.3.1   ERROR SIGNAL GENERATION FROM CAVITIES

2.3.1.1   FRINGE SIDE ERROR SIGNAL

One of the simplest ways to produce an error signal is to detect the transmission of the laser field through a Fabry-Perot cavity. This is called the *fringe side method* [Barger 73]. This method and the error signal in this system are shown in fig. 2.3.1-2. The error signal is the Airy Function [eqn. 2.18] for the transmitted intensity through a Fabry–Perot cavity.

A portion of the laser output beam is split off by a beam splitter and sent to the reference cavity. This beam is used as the test beam, leaving the majority of the laser output for use in an experiment. A second beam splitter divides the test beam once again. The first test beam is passed through a Fabry-Perot cavity that is tuned so that the laser frequency falls near its half maximum transmission points. Any laser frequency change results in an amplitude change in the transmitted beam, which can be used as an error signal. However, an error signal generated in this way is laser amplitude sensitive, and must be normalized to eliminate the laser amplitude dependence. The second test beam is used as a laser output intensity monitor, which can be subtracted from the error signal to remove this dependence. We would ideally wish to divide the two signals but don't because of electronic difficulties such as delays in the chips that are used as divider chips.

At this point it is useful to introduce the concept of the *effective locking potential* (fig. 2.3.1-2c) of an error signal (fig. 2.3.1-2b). The magnitude of the error signal, measured from the lock point, represents the size of the driving force of the controller. As the laser frequency moves further away from the desired lock point
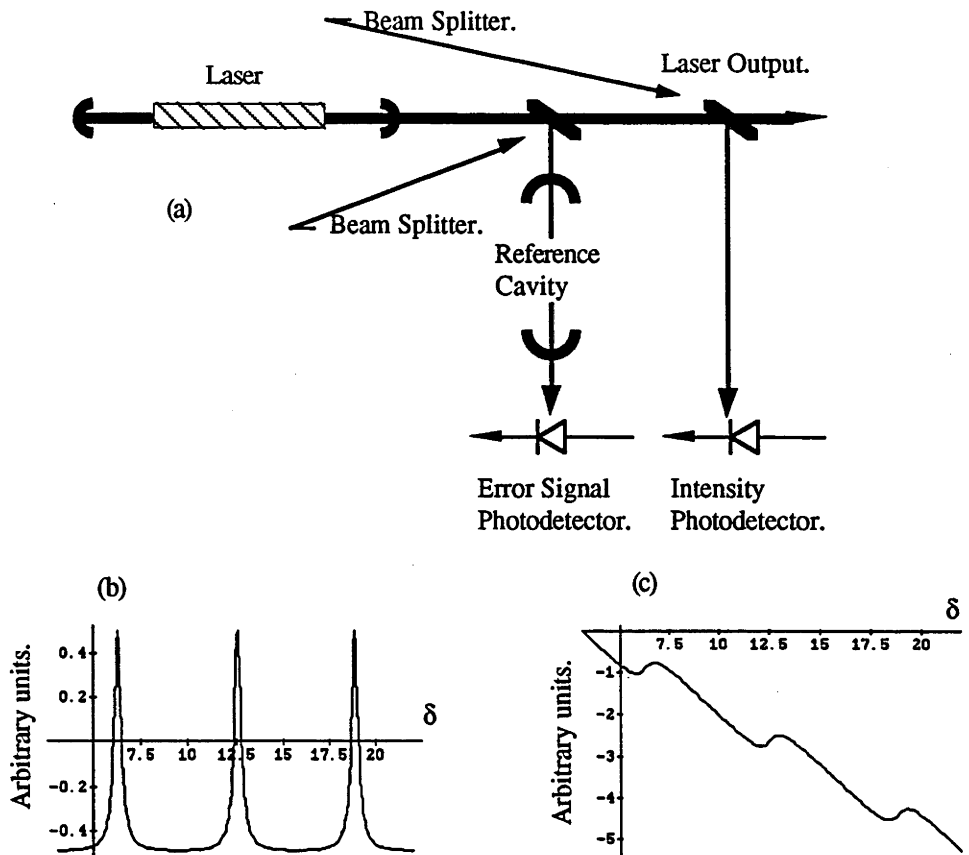
Fig. 2.3.1-2. (a) Schematic of the fringe side method. (b) The error signal generated in this scheme. (c) the effective potential of this error signal.

the signal driving it back increases. However, a sufficiently large frequency excursion will take the frequency beyond the capture range of the controller. Hence, the error signal has both a maximum restoring force and capture range. The effective locking potential is a diagrammatic representation of the driving force and shows directly the capture range of an error signal. This potential 'well' is analogous to the potential well in a mechanical system, such as a ball rolling into a well of a certain depth and width. In order to find an analogy to the mechanical case, the locking potential is calculated by integrating the error signal. The depth of the well illustrates the strength of the driving force for that error signal and the width of the well illustrates the capture range for the error signal.

Using this locking potential we can quickly compare the characteristics of the different types of discriminator. Moreover, we are able to choose the technique that best suits us.

2.3.1.2 THE DITHER ERROR SIGNAL

In a second approach [White 65] the laser cavity length is modulated (dithered) to produce a phase modulated field, which is passed through a Fabry-Perot cavity. The transmitted field is detected by a photodetector. The corresponding signal [Hils 87] is a mapping of the cavities dispersion profile, and is shown in fig. 2.3.1-3. In this particular example the modulation frequency is approximately 2kHz.

(a)

Laser

PZT Stack

Beam Splitter.

Oscillator   Double balanced mixer.

Reference Cavity

Error Signal

Photodetector.

(b)

Arbitrary units.

δ

(c)

Arbitrary units.

δ
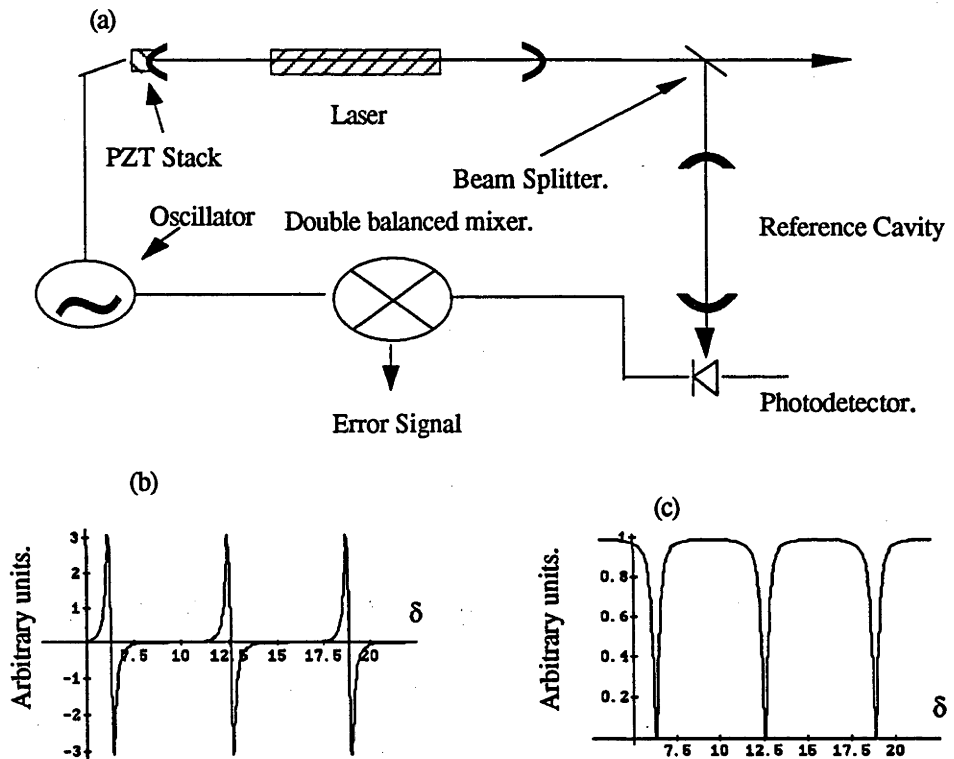
Fig. 2.3.1-3. (a) Schematic of the dither error signal generation method. (b) The error signal obtained from this scheme. (c) The effective potential of this scheme.

The electric field amplitude of a laser oscillating with angular frequency ω_0 that is being phase modulated at a frequency ω_m is given by :

$$E(t) = E_0 \, e^{j\left(\omega_0 \, t + \alpha \, cos(\omega_m \, t)\right)}$$

(2.19)

where α is the modulation index. The sidebands induced by frequency modulation are given by the expansion,

$$e^{j\alpha \cos(\omega_m t)} = \sum_{k=-\infty}^{\infty} a_k e^{jk\omega_m t} \text{ , where } a_k = j^k J_k(\alpha)$$

(2.20)

where J_n is the nth-order Bessel function, and a Fourier decomposition of the electric field shows clearly the frequency components in the field, expressed as a sum of Bessel functions:

$$E(t) = E_0 . e^{j\omega_0 t} \left[J_0(\alpha) + J_1(\alpha)\left(e^{j\omega_m t} - e^{-j\omega_m t}\right) \right] + c.c \qquad (2.21)$$

This approximation assumes that the higher harmonics of ω_m are negligibly small in magnitude. It can be seen from this expression that the phase modulated field has three frequency components. One at the carrier frequency and the other two at the carrier plus and minus the modulation frequency. Furthermore, the beat signal between the carrier and one of the sidebands is 180 degrees out of phase with the beat signal between the carrier and the other sideband. This field is then scanned across the cavity (which has a transfer function for transmission that is given by equation [2.14]) and the amplitude of component oscillating at the modulation frequency is measured. That is,

$$E_{Trans}(t) = E_0 . e^{j\omega_0 t} \begin{bmatrix} J_0(\alpha) r\, e^{-j\frac{\delta_0}{2}} \left[\dfrac{1-r^2}{1-r^2 e^{-j\delta_0}} \right] + \\[2em] J_1(\alpha) e^{j\omega_m t} r\, e^{-j\frac{(\delta_0+\delta_m)}{2}} \left[\dfrac{1-r^2}{1-r^2 e^{-j(\delta_0+\delta_m)}} \right] - \\[2em] J_1(\alpha) e^{-j\omega_m t} r\, e^{j\frac{(\delta_0-\delta_m)}{2}} \left[\dfrac{1-r^2}{1-r^2 e^{j(\delta_0-\delta_m)}} \right] \end{bmatrix}$$

(2.22)

where δ_0 and δ_m are the values δ takes for the angular frequencies ω_0 and ω_m respectively. The intensity incident on the photodetector is then obtained by multiplying E_{ref} by its complex conjugate. The error signal is extracted from the photocurrent by phase sensitive detection of the signal at the modulation frequency. That is, the phase sensitive detection process isolates the coefficients of the terms

containing $e^{j\,\omega_m\,t}$. The expression for the magnitude and phase of the detected signal is thus:

$$I_{dither}(t) \ = \ E_0^2 \exp[j\omega_m t] * J_0(\alpha) * J_1(\alpha) * r^2 * \exp[-j\omega_m/2] *$$

$$\left[\left[\left[\frac{1-r^2}{1-r^2 e^{-j\delta_o}}\right] * \left[\frac{1-r^2}{1-r^2 e^{-j(\delta_o-\delta_m)}}\right]\right] - \right.$$

$$\left.\left[\left[\frac{1-r^2}{1-r^2 e^{-j(\delta_o+\delta_m)}}\right] * \left[\frac{1-r^2}{1-r^2 e^{-j\delta_o}}\right]\right]\right]$$

(2.23)

This signal permits the laser to be locked to the centre of the cavity resonance. This method has the disadvantage that the signal drops to zero within a few cavity fringe widths making it difficult to compensate for large frequency jumps.

2.3.1.3 THE DC POUND DISCRIMINATOR

Two of the most powerful schemes for obtaining a frequency error signal involve measuring the optical phase shift near a resonance of the cavity. The first is known as the "Pound/Drever" [Pound 46, Drever 83] discriminator which is named after Pound who was the first to apply such a technique to NMR research and Drever who applied it at optical frequencies. This technique measures the optical phase shift near a cavity resonance that a phase modulated laser field experiences. The second technique is known as the "dc Pound stabilizer" or the "Pound/Hänsch" discriminator once again after Pound and Hänsch [Hänsch 80] who applied the principle to the optical domain. This uses homodyne detection with a quadrature-phase local oscillator field.

The experimental arrangement for the latter method is shown in figure 2.3.1-4. Linearly polarized light from a single mode laser is incident on a confocal reference cavity. A polarizer is placed inside the cavity and aligned at an angle θ with respect to the polarization axis of the laser. The component of the laser field parallel to the axis of the polarizer sees a low loss cavity and experiences a frequency dependent
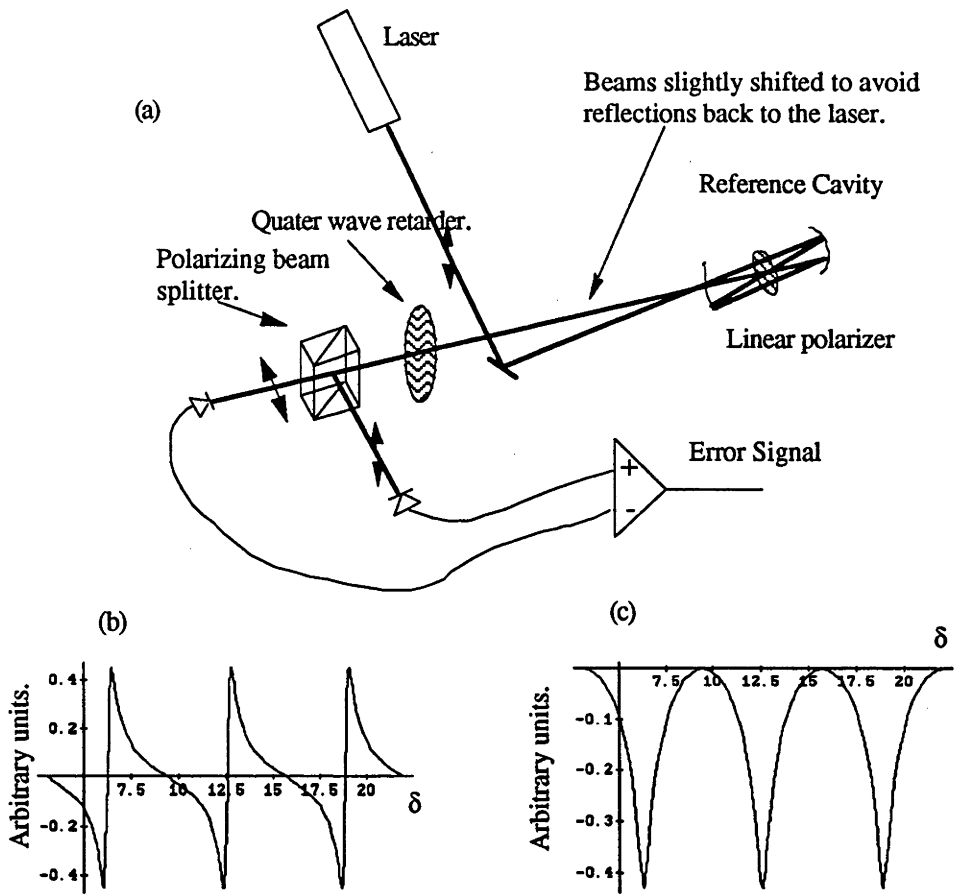
Fig. 2.3.1-4. (a) Schematic representation of the Pound/Hänsch method for generating a frequency error signal. (b) The error signal generated in this method. (c) The effective potential of this method.

phase shift in reflection. The component perpendicular to the axis of the polarizer sees a high loss cavity and is totally reflected. On recombination, the relative phase difference between the two components will yield a laser field that is elliptically polarized. Detection of the ellipticity of the beam is accomplished by the use of a quarter wave retarder followed by a polarizing beam splitter separating the two components. These are individually monitored by two photodetectors and compared in a differential amplifier. The intensity difference for the two components, I_{PH}, is the system error signal, and is given by the expression:

$$I_{PH} = I_{max}.2.\cos(\theta).\sin(\theta).\frac{T.R.\sin(\delta)}{(1-R)^2 + 4.R.\sin^2(\delta/2)} \qquad (2.24)$$

where θ is the angle that the intra-cavity polarizer makes with the laser polarization, and T is the cavity transmittance.

It should be noted that this technique dose not necessarily require a figure of eight cavity or ring cavity.

2.3.1.4 THE POUND-DREVER ERROR SIGNAL

Finally, the Pound-Drever method is shown schematically in figure 2.3.1-5. As mentioned earlier, this technique examines the response a Fabry-Perot cavity to phase modulated light. In this work we used this technique to produce the error signal. The phase modulation is superimposed onto the laser beam by passing the beam through an electrooptic phase modulator which has its refractive index oscillating at some radio frequency.

Equation (2.21) gives us the electric field for phase modulated light. When this field strikes a Fabry-Perot cavity, which has a transfer function for reflection that is given by equation [2.13], the electric field is modified to:.
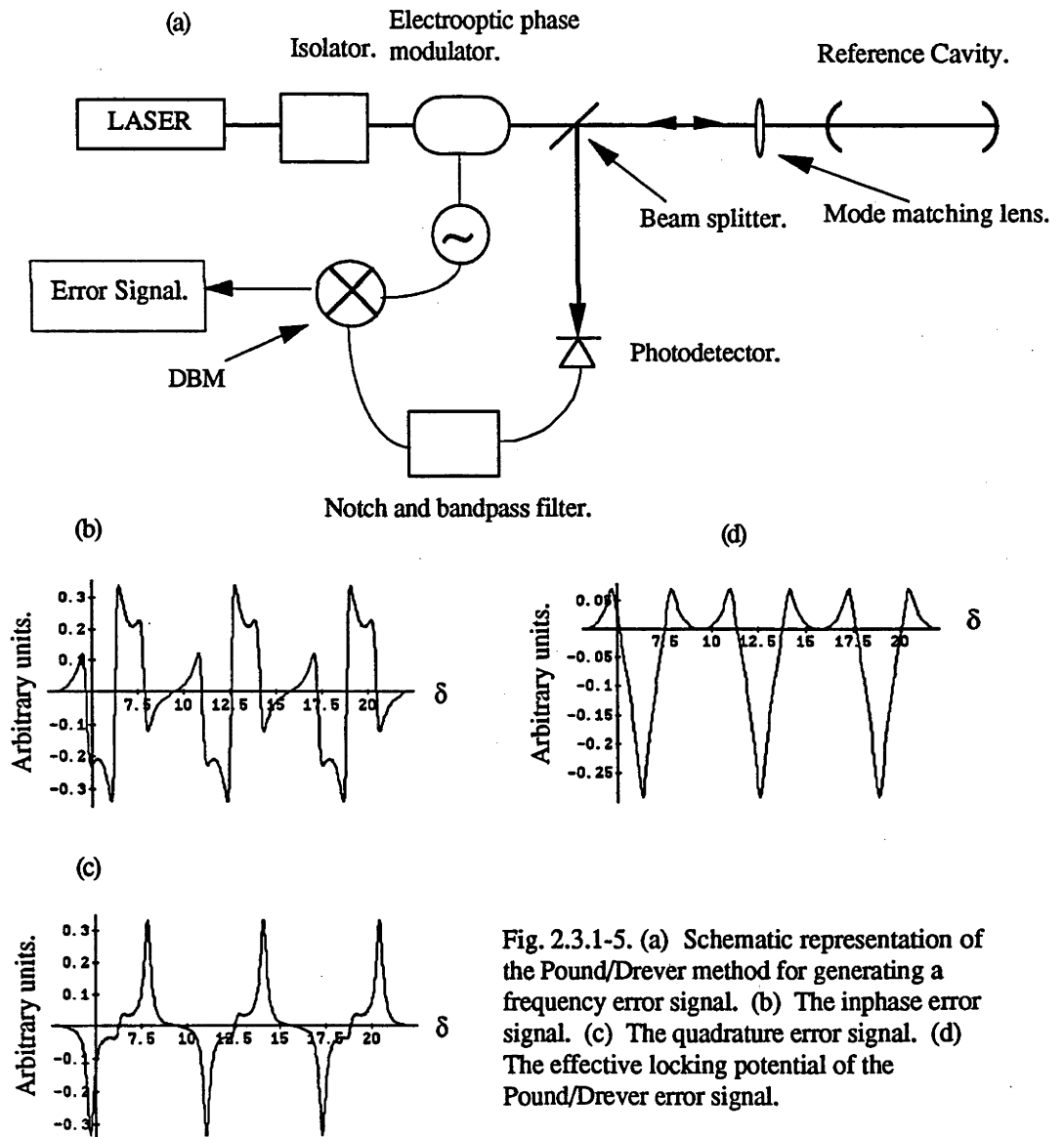

Fig. 2.3.1-5. (a) Schematic representation of the Pound/Drever method for generating a frequency error signal. (b) The inphase error signal. (c) The quadrature error signal. (d) The effective locking potential of the Pound/Drever error signal.

$$E_{ref}(t) = E_0.e^{j\,\omega_\circ\,t} \begin{bmatrix} J_0(\alpha)\;r\left[\dfrac{1-e^{-j\delta_\circ}}{1-r^2e^{-j\delta_\circ}}\right] + \\[2ex] J_1(\alpha)e^{j\,\omega_m\,t}\;r\left[\dfrac{1-e^{-j(\delta_\circ+\delta_m)}}{1-r^2e^{-j(\delta_\circ+\delta_m)}}\right] - \\[2ex] J_1(\alpha)e^{-j\,\omega_m t}\,r\left[\dfrac{1-e^{-j(\delta_\circ-\delta_m)}}{1-r^2e^{-j(\delta_\circ-\delta_m)}}\right] \end{bmatrix} + c.c$$

$$(2.25)$$

where δ_0 and δ_m are the values δ takes for the angular frequencies ω_0 and ω_m respectively. The intensity incident on the photodetector is then obtained by multiplying E_{ref} by its complex conjugate. The error signal is extracted from the photocurrent by phase sensitive detection of the signal at the modulation frequency. That is, the phase sensitive detection process isolates the coefficients of the terms containing $e^{j\,\omega_m\,t}$. The expression for the magnitude and phase of the detected signal is thus:

$$I_{ref}(t) = E_0.^2\;R\;J_0(\alpha)\;J_1(\alpha)\begin{bmatrix} \left[\dfrac{1-e^{-j\delta_\circ}}{1-r^2e^{-j\delta_\circ}}\right]\left[\dfrac{1-e^{+j(\delta_\circ-\delta_m)}}{1-r^2e^{+j(\delta_\circ-\delta_m)}}\right] + \\[2ex] \left[\dfrac{1-e^{-j(\delta_\circ+\delta_m)}}{1-r^2e^{-j(\delta_\circ+\delta_m)}}\right]\left[\dfrac{1-e^{+j\delta_\circ}}{1-r^2e^{+j\delta_\circ}}\right] \end{bmatrix} + c.c$$

$$(2.26)$$

The real and imaginary parts of the first term of equation (2.26) give the inphase and quadrature components of the error signal. These have been plotted in fig. 2.3.1-5. We observe that the profile of the quadrature components have a complicated structure.

The inphase error signal, figure 2.3.1-5b, is a bipolar signal that crosses the zero volts axis five times about each cavity resonance. The other error signal mentioned above only cross the zero axis a maximum of three times about each cavity resonance.

This error signal also has more peaks than the other error signals. They occur at the cavity resonance frequency (the two central peaks) and at the cavity resonance frequency plus or minus the modulation frequency (the outer most peaks). Hence the capture range is dependent on the modulation frequency.

The quadrature error signal, figure 2.3.1-5c, has two main peaks, occurring at the cavity resonance frequency plus or minus the modulation frequency (the outer most peaks), and two central peaks. These central peaks were observed experimentally before they were calculated from the theory [Schenzle 82] presented above. Prior to the calculations workers assumed that the central feature should be set to zero to produce best inphase error signal, but Schenzle *et. al.* showed this not to be the case.

It can be see from figure 2.3.1-5d, the effective locking potential of the Pound/Drever error signal, that we can simultaneously have an error signal that has a very well defined lock point and also has a large capture range. The definition of the lock point is determined by the FWHM of the cavity which is 150kHz in the case of the SuperCavity, and the capture range can be set arbitrarily (1MHz to 100MHz if necessaries).

2.3.2   COMPARISON OF ERROR SIGNALS

Let us start by emphasizing that the systems shown here are only a minor subset of all the different systems used for laser stabilization. The four systems outlined above are the most commonly used for the control of dye lasers. The different methods are attributed to the long history, and high activity of the laser stabilization field.
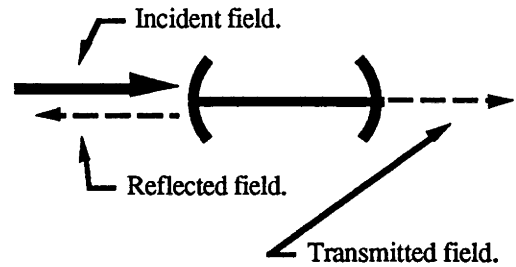
Where and when each should be used depends greatly on the particular laser. It is not uncommon to use more than one system to achieve the desired stabilization, utilizing the different capture ranges and steepness of the locking potential. For example, it would not be possible to lock the dye laser to a high finesse cavity such as the SuperCavity (which has a linewidth of approximately 150kHz FWHM) using the fringe side method because the capture range would be too small. But we could, however, lock the laser to a low finesse cavity (one with a linewidth of say 3MHz such as the Tropel) using the fringe side method to utilize its large capture

range and then use the Pound/Drever system to lock the laser to a high finesse cavity.

We chose Pound/Drever locking for several reasons. First, we were able to obtain an error signal that was unaffected by the DC noise of both the laser and the electronic circuitry, because we were working with RF detection techniques. Secondly, the capture range could be set arbitrarily to an convenient value. We chose 10MHz because the laser frequency jitter is approximately half this value and thus will be contained within the capture range of the error signal. Thirdly, the steepness of the locking potential was very high due to the high finesse of the SuperCavity, and hence the laser could be locked tightly to the lock point.

Finally, this technique responds very quickly to frequency jumps. An error signal generated from the light reflected off a cavity does not get affected by the cavity. That is, the storage time of the cavity does not limit the response time of the error signal. For example, the SuperCavity has a storage time of $6.7\mu s$ (which is the inverse of its linewidth). Fluctuation occurring at rates faster than $6.7\mu s$ can not be seen by the method based on the transmission through the cavity
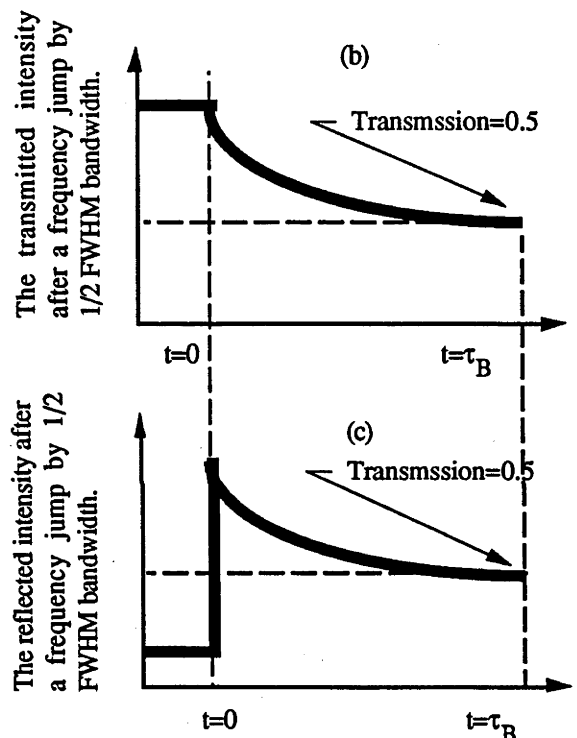

Build-up time of the cavity is τ_B

Fig. 2.3.2-1. Response of the (b) transmitted and (c) reflected fields to a change of the laser frequency. Up to time t=0 the laser field is resonant with the cavity (a) so the transmitted intensity is high and the reflected intensity is low At t=0 the laser frequency suddenly changes so the transmitted field remains at approximately the same intensity due to the field inside the cavity and slowly decays to some equilibrium value. The reflected field, on the other hand, immediately sees a highly reflecting surface and consequently has a large and sudden change in intensity.

because the cavity integrates them out, Fig 2.3.2-1b. On the other hand, the reflected method does not get effected by the storage time of the cavity, as is

illustrated in figure 2.3.2-1c, and thus can respond to the fluctuations occurring at rates faster than $6.7\mu s$.

In order to physically interpret the response of the an error signal in the time domain equaling or exceeding the build-up time of the reference cavity, we need to re-evaluate the error signals taking in to consideration that the intensity output does not have time to reach steady state. The error signals shown through out section 2.3.1 are not correct in this domain because they are assuming steady state has been reached. A full analysis has of the error signals in this time domain has yet to be done. We can say, however, that the signals are not those shown in section 2.3.1 and that the Pound/Drever is able to generate a signal where as the others can not.

2.3.3 THE ERROR SIGNALS GENERATED IN THE SPECTRA-PHYSICS 380D & COHERENT CR-699-21 DYE LASERS
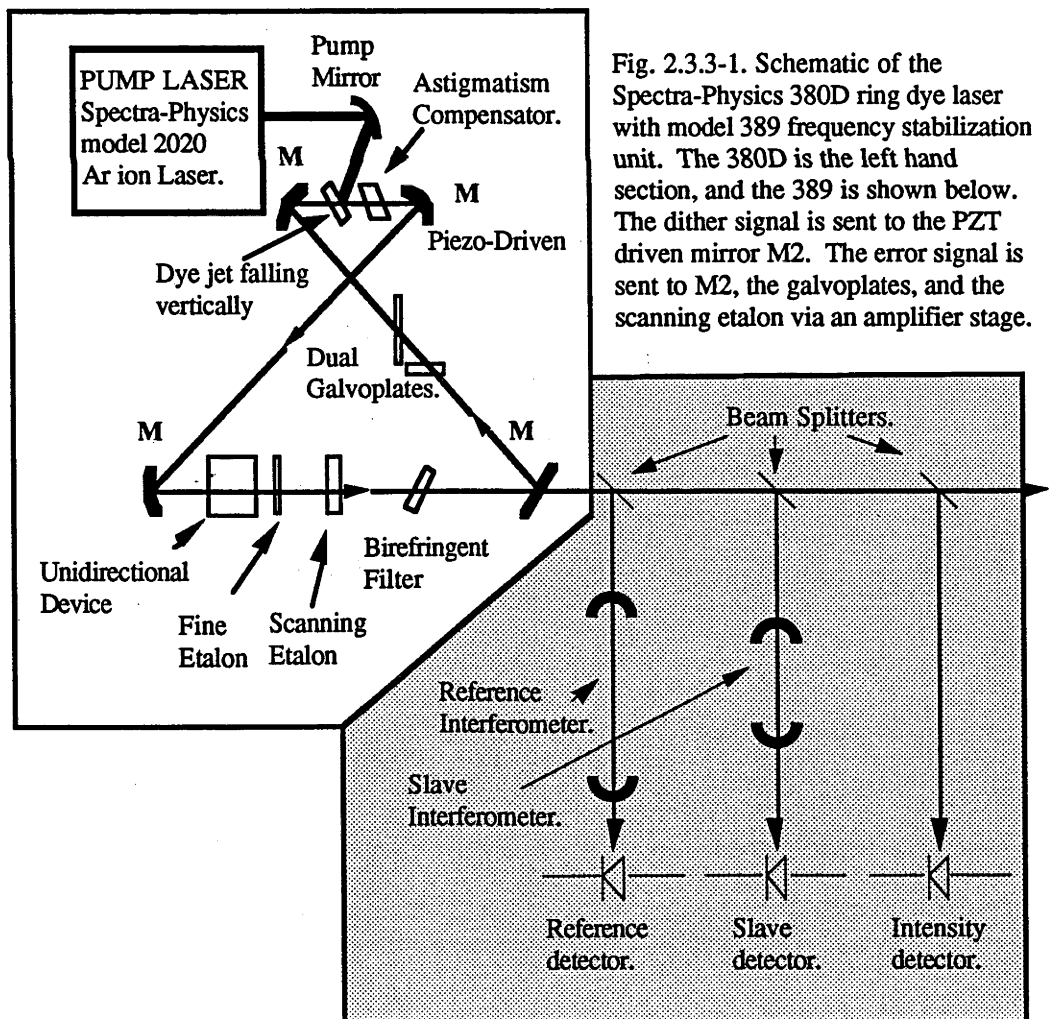

Fig. 2.3.3-1. Schematic of the Spectra-Physics 380D ring dye laser with model 389 frequency stabilization unit. The 380D is the left hand section, and the 389 is shown below. The dither signal is sent to the PZT driven mirror M2. The error signal is sent to M2, the galvoplates, and the scanning etalon via an amplifier stage.

To illustrate the practical application of error signal generation in the commercial systems used in this department I shall consider a specific example of its implementation in our commercially built Spectra-Physics ring dye laser model 380D, with stabilization unit model 389. The laser is shown in figure 2.3.3-1 along with the stabilization unit.

The stabilization unit has three main components:

(1)   *Reference   interferometer* : FSR ≈ 500MHz and finesse ≈ 3. This is the main optical component for frequency stabilization. The laser frequency is locked to the peak of one of its cavity transmission modes. Inside this interferometer is a galvoplate that is used for scanning purposes. It is made out of glass and is used to change the optical length of the interferometer. As the optical length alters so to does the resonant cavity frequency and the laser frequency is forced to follow the cavity by the control electronics.

(2)   *Slave interferometer* :   FSR ≈ 10GHz and finesse ≈ 3.   This interferometer is used as a backup element for the reference interferometer during a mode-hop. Its fringes are set so that the light frequency is positioned within the capture range of one of its cavity modes. Laser frequency jumps have a high probability of jumping outside the capture range of the reference interferometer, however, there is a low probability that they will cause a jump which takes the laser frequency outside the capture range of the slave interferometer. If a disturbance induces a large jump then control of the laser is switched to the slave interferometer, and returned to the reference interferometer when the disturbance has passed.

(3)   *Intensity diode* : A reverse-bias pin photodiode identical to the diodes used for the reference and slave interferometers. This is used to monitor the laser power and to normalize the signals from the two interferometers.

The 380D employs the fringe side locking technique.

The CR-699 has only one reference cavity. The stabilization unit has two main components:

(1)   *Reference   interferometer* : FSR ≈ 1GHz and finesse ≈ 3. It is a confocal cavity, with mirror a separation of 7.5cm. Two different methods are used to generate the error signal from this reference interferometer.

Both of these are shown in figure 2.3.3-2.

(2)   *Intensity diode* : A reverse-bias pin photodiode identical to the diodes
used for the reference interferometer. This is used once again to monitor
the laser power and to normalize the signal from the reference interferometer.
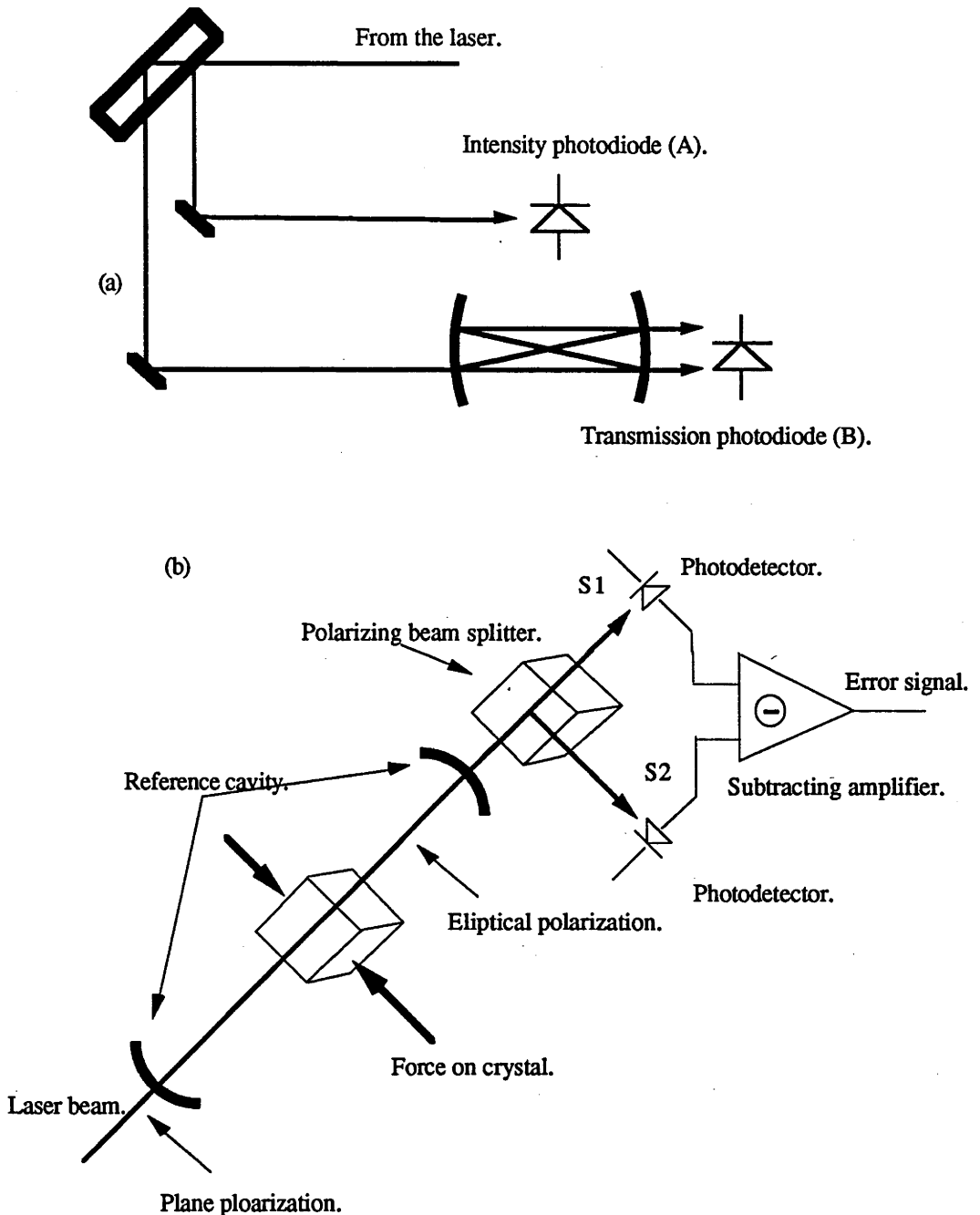
Fig. 2.3.3-2. Schematic of the error signal generation scheme used in the Coherent CR-699-21.
(a) The error signal used in the CR-699 at the department. It is generated by detecting the
transmission through the reference cavity.
(b) An alterative error signal configuration. The laser beam is passed through a reference cavity
containing a birefringent element. The elliptical polarization produced is separated into its
orthogonal components, and these are used to produce the error signal.

The method illustrated in fig. 2.3.3-2a is used in our CR-699 to generate the error signal. Information of the output frequency is obtained by taking a portion of the output, using a beam splitter, and passing it through the reference interferometer in a figure of eight configuration, giving the Airy function transmission curves (equation 2.18). The transmission of the interferometer (signal B) is frequency and amplitude dependent. In order to eliminate the amplitude dependence from the signal B, the laser amplitude is also sampled (signal A). The signals A and B are electronically subtracted from each other to produce a normalized Airy function signal that is intensity independent. The laser frequency is then locked to the fringe side of this signal.
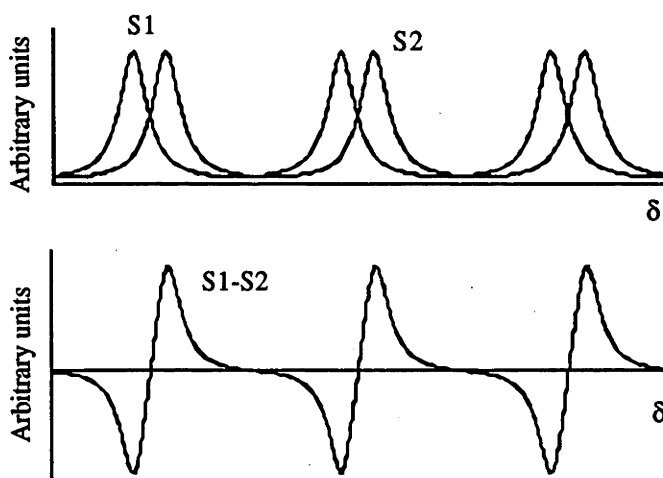
Fig. 2.3.3-3. Top curve shows the transmission of the tw polarizations. The bottom curve is the error signal obtained from subtracting the two transmissions.

In the second method (figure 2.3.3-2b) the error signal is also derived by looking at the transmission through the reference cavity [Johnston 79]. However, the CR-699 has within it's optical cavity a birefringent element which is orientated such that its direction of birefringence is at 45^0 to the polarization of the laser output beam. The birefringence induces a difference in the optical path length for the two orthogonally polarized beam components. The resulting transmission fringes for each component has a frequency shift, as shown in figure 2.3.3-3a. The two polarizations are separated by passing the transmission beam through a polarizer or beam separator. They are then sent to separate photodetectors, and electronics that subtract one transmission fringe from the other producing the error signal shown in figure 2.3.3-3b. This signal is also normalized to the output intensity of the laser.

2.4 PROPORTIONAL-INTEGRATING-DIFFERENTIATING (PID) AMPLIFIER

The purpose of this controller is to bring a physical quantity to a predetermined value and to hold it at this value. The control signal should be exactly out of phase with any perturbation that may alter the value of the physical quantity in order for the servo to be able to counteract its influence. This is called negative feedback (see figure 2.1-1) : the output signal is fed back so that it is subtracted from the input. Thus the phase of the correction signal sent back to the frequency transducer from the control electronics has to be π radians out of phase with respect to the measured error signal.

The control signal can be, in principle, a proportional amplification of the systems error signal. In a normal control system, however, there exists some element (for example a mirror mounted on a PZT) that has a frequency dependent phase lag in its response. This may eventually alter the negative feedback process into a positive feedback process : the output signal is fedback so that it adds to the input signal. Positive feedback causes oscillation rather than stabilization.

A PID controller is generally used instead of a proportional controller in most feedback systems. PID is an acronym for a three mode controller consisting of a proportional stage, integrating stage, and differentiating stage. The output of the PID is a sum of a proportional term, an integrating term, and a differentiating term. Each of these terms has adjustable
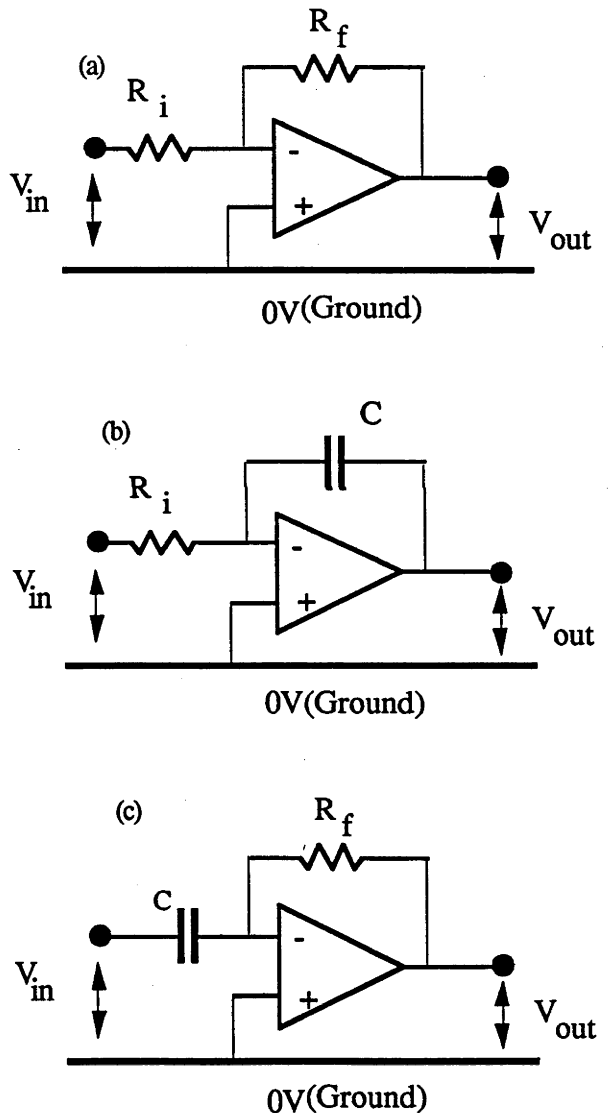

Fig. 2.4-1. Schematic of the component in a PID. (a) the proportional amplifier (b) the integrating amplifier. (c) the differentiating amplifier.

gain. Each term is produced by an operational amplifier, and the basic configuration for each term is shown in fig. 2.4-1. The total PID is shown in fig.2.4-2.
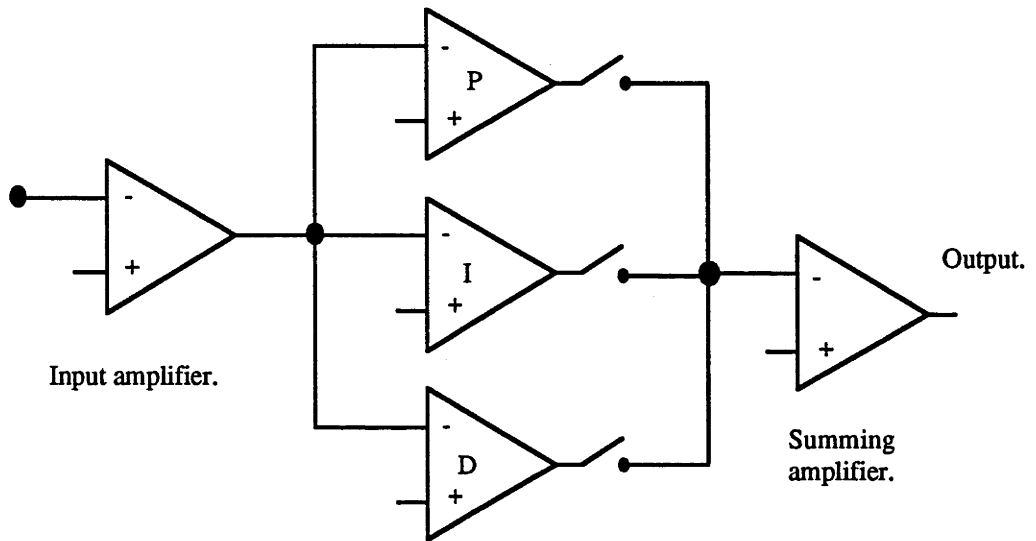

Fig. 2.4-2. The PID. The signal is sent to each stage of the PID via an isolating amplifie then the amplified signals are added together using a summing aplifier.

A PID can be tailored to increase the frequency response of the total control loop by careful phase control. To illustrate how a PID works I will introduce the Bode Plot [Dorf 89 Ch. 7].

The Bode plot consists of two graphs plotted separately. The first is the logarithm of the magnitude of the transfer function versus frequency, and the second is the phase of the transfer function versus frequency. This plot indicates the frequency response of a system: the steady-state response of a system to a sinusoidal input.

The complex transfer functions for the proportional, integrating and differentiating circuits shown above are:

$$v_{out}/v_{in} = \frac{R_f}{R_i} = A \quad \text{where A is the gain of the amplifier.} \tag{2.27}$$

$$v_{out}/v_{in} = \frac{1}{j \, \omega \, R_i \, C + 1} \tag{2.28}$$

$$v_{out}/v_{in} = \frac{j \, \omega \, R_f \, C}{j \, \omega \, R_f \, C + 1} \tag{2.29}$$

and the corresponding Bode plots for these three sections are shown in fig. 2.4-3.

20 $Log_{10} |T|$

Proportional

-10   -20   -30   -40

2 3 4 5 6 7 8

$Log_{10} [\omega]$

Magnitude constant with frequency.

Arg [T]

1.5 1 0.5 -0.5 -1 -1.5

Output is inphase with the input.

2 3 4 5 6 7 8

$Log_{10} [\omega]$

(a)

20 $Log_{10} |T|$

Integral

-10   -20   -30   -40

2 3 4 5 6 7 8

$Log_{10} [\omega]$

Magnitude decreases at high frequencies.

Arg [T]

1.5 1 0.5 -0.5 -1 -1.5

Output lags behind the input by $-\pi/2$ radians.

2 3 4 5 6 7 8

$Log_{10} [\omega]$

(b)

20 $Log_{10} |T|$

$Log_{10} [\omega]$

Differential

-10   -20   -30   -40

2 3 4 5 6 7 8

Magnitude increases at high frequencies.

Arg [T]

1.5 1 0.5 -0.5 -1 -1.5

2 3 4 5 6 7 8

$Log_{10} [\omega]$

Output leads the input by $\pi/2$ radians.

(c)

20 $Log_{10} |T|$

$Log_{10} [\omega]$

P + I + D.

-10   -20   -30   -40

2 3 4 5 6 7 8

Combined magnitude overlaid with its different components.

Arg [T]

1.5 1 0.5 -0.5 -1 -1.5

2 3 4 5 6 7 8

$Log_{10} [\omega]$

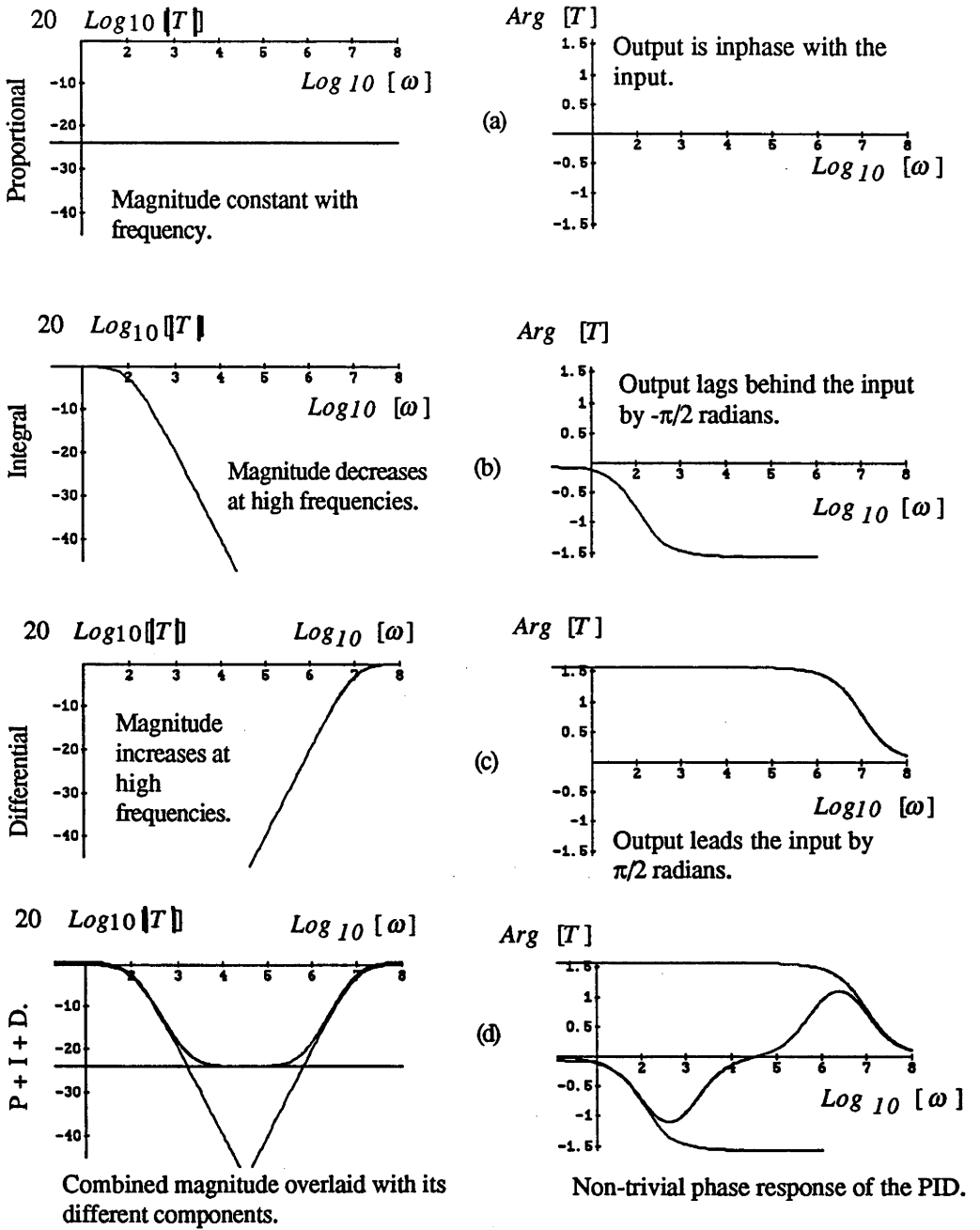Non-trivial phase response of the PID.

(d)

Fig. 2.4-3. Bode plots for the (a) proportional, (b) integrating, (c) differentiating anplifiers and the combination to give PID characteristics shown in (d). T is the transfer function for each stage.

The proportional amplifier sends a signal back to the controlled system that is 180 degrees out of phase with the error signal and is of constant gain for all perturbing frequencies. The P of a controller effectively amplifies the error signal and returns it to the controlled system with a fixed phase. This will only be sufficient in a servo if the controlled system is able to respond to a perturbation instantaneously and if its response is frequency independent.

An integrator circuit, sometimes called a low pass filter, has a frequency dependent gain. It has maximum gain at low frequencies, and an attenuated gain at higher frequencies. For a single stage integrator, as shown in fig. 2.4-1b, the gain roll-off is -6dB/Octave (or equivalently -20dB/Decade). Accompanying this frequency dependent gain is a frequency dependent input-output phase variation. At low frequencies the output signal is in phase with the input signal. At higher frequencies the output phase lags behind the input, eventually reaching a $\pi/2$ radians phase lag.

A differentiator circuit, or high pass filter, has the opposite characteristics to the integrator. High gain is obtained at high frequencies, low gain at low frequencies. Furthermore, the output phase at low frequencies leads the input by $\pi/2$ radians, and eventually reaches a frequency where the two are inphase.

A PID sums these individual stages to give the overall transfer function:

$$v_{out}/v_{in} = \frac{R_f}{R_i} + \frac{1}{j \omega R_i C + 1} + \frac{j \omega R_f C}{j \omega R_f C + 1} \tag{2.30}$$

the corresponding Bode plots for the PID is also shown, fig. 2.4-3d. This figure shows that the gain and phase properties of a PID are vastly different than each of it's individual stages.

To illustrate the effect of having a PID in the feedback loop let's consider the case where a control system has an element with a transfer function given by:

$$T = \frac{1}{\left[1 + j \omega \left(\frac{2\kappa}{\omega_n} \right) + \left(\frac{j \omega}{\omega_n} \right)^2 \right]} \tag{2.31}$$

where ω_n is the element's resonant frequency, and κ is a damping constant. The Bode plots for this element is shown in fig. 2.4-4a. There are two features to note from the Bode plots. Firstly, at the resonance frequency the magnitude increases dramatically for a given input amplitude. Secondly, there is a π change in phase from one side of the resonance to the other. Hence, negative feedback on one side of the resonance will become positive feedback on the other side of the resonance. Positive feedback quickly forms large oscillations, and hence instability.

To avoid feeding back an oscillatory signal, we can pass the error signal through

the PID illustrated in fig. 2.4-4b. This PID-element combination (fig. 2.4-4c) gives the control loop high gain at low frequencies, a unity gain at the resonance frequency (hence no oscillations) and improved gain at high frequencies. Also, the phase characteristics are improved. There is no longer a π phase change occurring at the resonance frequency, The π phase change is pushed to much higher frequencies.
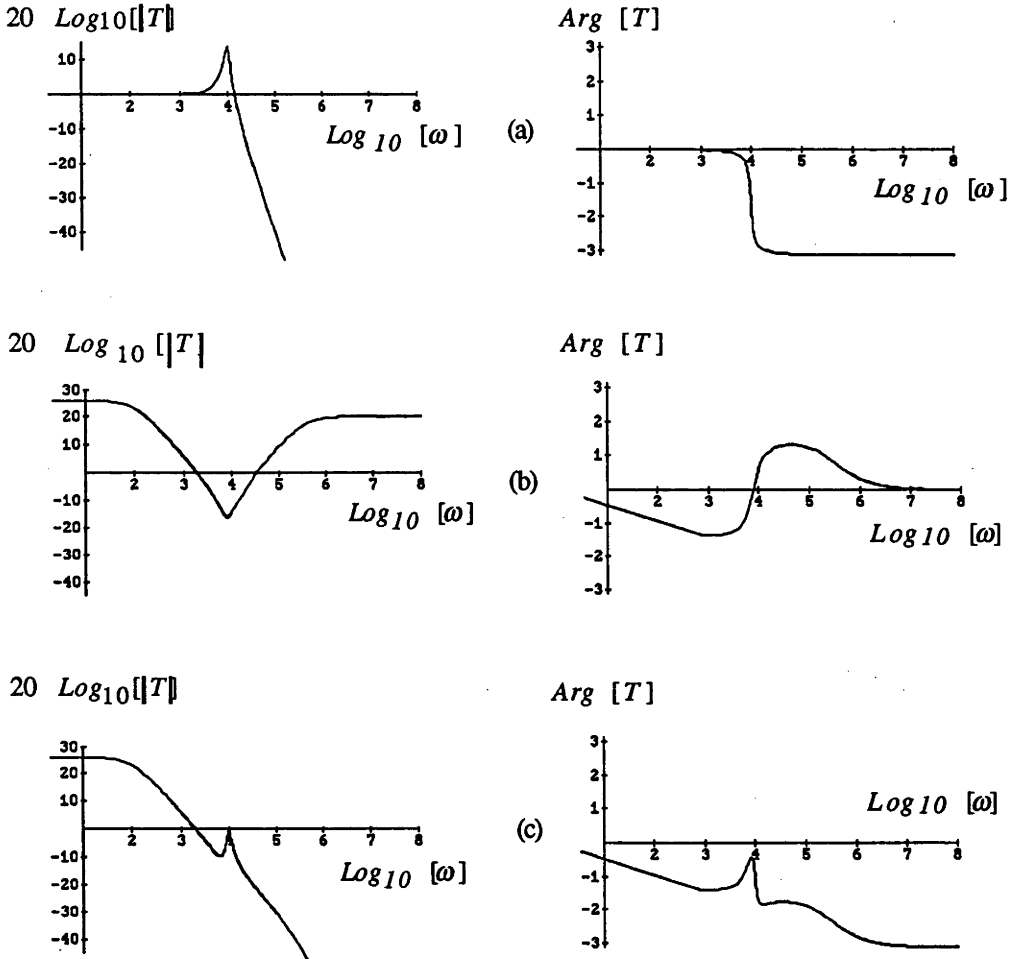

Fig. 2.4-4. Bode plots for (a) an element with a resonance. (b) a PID tailored to selectively amplify the error signal. (c) the combination of the (a) & (b). T is the transfer function for each element.

The transfer function for the total control loop is simply the product of the individual transfer functions. That is:

$$T_{\text{Control loop}} = \frac{\left[\dfrac{R_f}{R_i} + \dfrac{1}{j\,\omega\,R_i\,C + 1} + \dfrac{j\,\omega\,R_f\,C}{j\,\omega\,R_f\,C + 1}\right]}{\left[1 + j\,\omega\left(\dfrac{2\kappa}{\omega_n}\right) + \left(\dfrac{j\,\omega}{\omega_n}\right)^2\right]}$$

(2.32)

2.5 FREQUENCY TRANSDUCERS

There are three common frequency and intensity transducers. Piezoelectric elements (PZT), Acoustooptic modulators (AOM), and Electrooptic modulators (EOM). The frequency response and principle of operation of these devices is different. In general a stabilization scheme utilizes at least one of these transducers, and in our case, all three are used. Hence, it is appropriate to describe the properties and implementation of these devices.

2.5.1 PIEZOELECTRIC TRANSDUCERS

The piezoelectric element or PZT as it is commonly known is an electronically controllable positioning element which functions on the basis of the piezoelectric effect. When certain crystals are compressed or stretched in a certain direction, electric charges appear on the surfaces of the crystal that are perpendicular to the axis of strain. Conversely, when such crystals are placed between two metallic surfaces between which a difference of potential exists, then the crystal expands or contracts. An alternating potential results in an alternating expansion-contraction of the crystal. Commercially available crystals can only oscillate over a small frequency band, typically up to about 40kHz, before their first crystal resonance is reached.

A PZT can alter a laser's frequency if it is attached to one of its resonator mirrors. This is illustrated in fig. 3-4 which shows the components of the Coherent CR-699-21 ring dye laser. The tweeter of this laser is mounted on a PZT, and is used as a frequency transducer. A single PZT can move a distance equivalent to many wavelengths of light, $\approx 20\mu m$, and hence a resonator mirror mounted on a PZT has a large dynamic range. This element alone is able to reduce the laser linewidth from tens of MHz to $\approx$ one MHz.

The major problems with the PZT is its requirement for high voltages (> 1kV) and its limited frequency response. The later is by far the most important because ring dye lasers have noise beyond 1MHz Fourier frequency. In order to reduce the laser linewidth further than commercially available, transducers with faster response times are required. These are available in the form of AOMs and EOMs.

2.5.2 ACOUSTOOPTIC TRANSDUCERS

An acoustooptic modulator operates via the Acoustooptic effect. A sound wave incident on a crystal, such as TeO_2 which is used in this project, induces a sinusoidal perturbation of the density of the crystal. This density grating in turn causes the refractive index of the crystal to change.

If n is the refractive index and the sound wave has the form $x = v_s t$, (where x is the distance travelled in time t and v_s is the sound speed), then the induced refractive index change can be expressed as

$$\Delta n = \Delta n_0 \sin (\omega_s t - k_s x) ; \qquad\qquad \omega_s / k_s = v_s \qquad (2.33)$$

We can think of the refractive index modulation as a series of partially reflecting mirrors separated by the sound wavelength λ_s moving at a velocity v_s. If a beam is incident on the medium at angle θ_i then a diffraction at angle θ_r is obtained when the path difference AC-BD (see fig. 2.5.2-1) is a multiple of the optical wave length λ/n, that is,

$$z (\cos \theta_i - \cos \theta_r) = m\lambda/n \qquad\qquad (2.34)$$

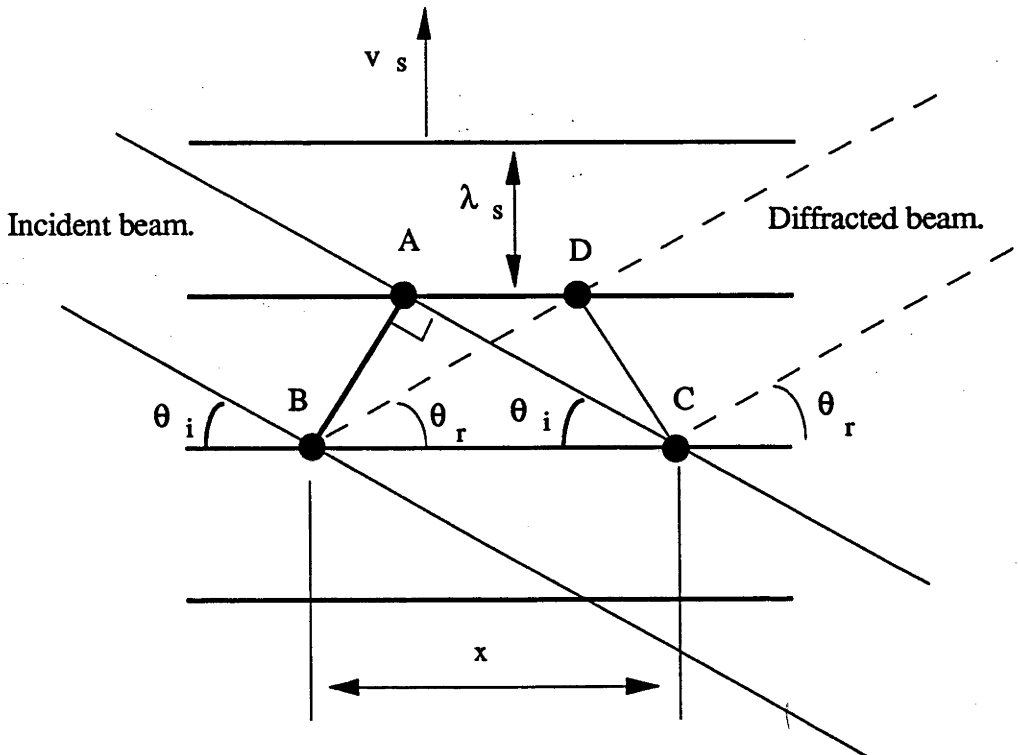or $\quad \cos \theta_r = \cos \theta_i - m\lambda/zn \qquad\qquad (2.35)$

Fig. 2.5.2-1. Diffraction of an optical beam off a density grating induced by a sound wave.

However for all the waves to constructively interfere we require the diffracted wave to have no dependence on z. Thus m = 0 is our only possibility, which implies that $\theta_i = \theta_r$.

Also, the diffraction from any two acoustic wave fronts must add up in phase along the direction of the reflected beam. So the path difference AO + OB, (see fig. 2.5.2-2), must equal the optical wave length, and this leads to the Bragg Diffraction condition:

$$2\lambda_s \sin \theta = \lambda/n ; \qquad \theta_i = \theta_r = \theta \tag{2.36}$$

To derive the resultant frequency shift due to the acoustic wave we consider the Doppler effect. Assuming that the optical beam is incident on a mirror moving at the sound speed, v_s, and the Bragg condition is satisfied. The Doppler frequency shift for a wave reflected from this moving object is:

$$\Delta\Omega = 2\omega\, v\, (c/n)^{-1} \quad \text{and} \quad v = v_s \sin\theta, \tag{2.37}$$

So $\Delta\Omega = 2\,\omega\, v_s \sin\theta\, (c/n)^{-1} \equiv 2\pi v_s/\lambda_s = \omega_s$, $\tag{2.38}$

from the Bragg condition. Thus $\Omega_{\text{diffracted}} = \Omega_d = (\Omega + \omega_s)$, and for the case of the
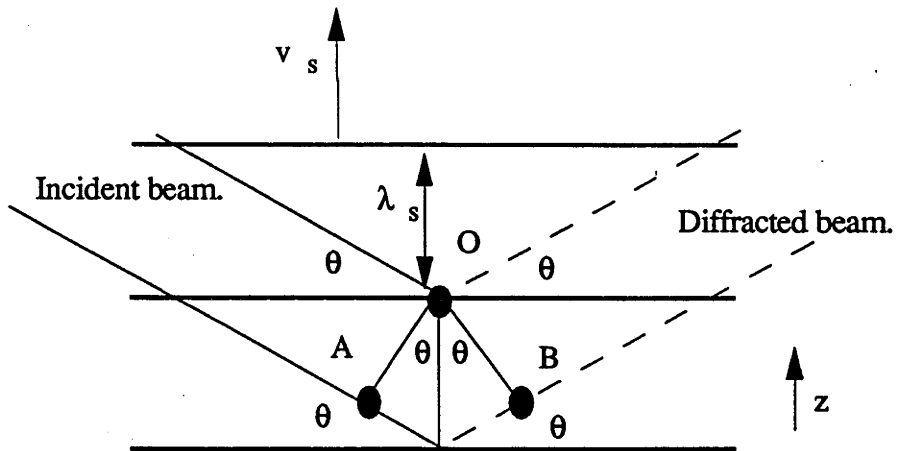

Fig. 2.5.2-2. Constructive interference of the optical waves producing a Doppler shifted beam.

sound wave receding from the optical beam the Doppler shift changes sign and the diffracted beam has the frequency $\Omega_d = (\Omega - \omega_s)$. In practice, however, the modulation of the refractive index is not sinusoidal, it is a Fourier series in ω_s, that is,

$$\Delta n = a_1 \sin\omega_s t + a_2 \sin 2\omega_s t + a_3 \sin 3\omega_s t + ... \tag{2.39}$$

This is due to the non perfect nature of the transducer producing the modulation.

This in turn gives us higher order diffracted beams at frequencies such that

$$\Omega_d = (\Omega \pm \omega_s), (\Omega \pm 2\,\omega_s), (\Omega \pm 3\omega_s), \ldots \qquad (2.40)$$

An AOM can only alter the laser frequency if it sitting outside the laser cavity. The frequency, ω_s, of the sound wave being sent to the modulator is varied so that the frequency of the one of the diffracted beams is locked to the reference cavity.

Furthermore, the intensity diffracted into the beams can be controlled by controlling the RF power sent to the modulator. The sound transducer of the AOM looks like a 50Ω load to a voltage source. For 1W of RF power ($\approx 10V_{P\text{-}P}$) approximately 80% of the incident beam can be diffracted into one of the first order beams. Varying the RF power alters the diffraction efficiency, thus an AOM can be used as an intensity noise eater by controlling the RF power sent to the AOM.

2.5.3   ELECTROOPTIC TRANSDUCERS

The third frequency transducer is the electrooptic modulator (EOM), and operates in accordance with the electrooptic effect. Certain crystals when subjected to an electric field change their refractive index. Optical radiation incident on such a crystal experiences an optical path length change which is governed by the strength and frequency of the electric field.

The crystals are generally birefringent. The "ordinary" and "extraordinary" directions of the crystal vary in phase at the same frequency but with different amplitudes which is determined by the applied field and the EO coefficient. An EOM can thus be used as either an amplitude or phase modulator depending on the orientation of the crystal with respect to the direction of polarization of laser field.

An EOM can change the laser frequency if it is placed inside or outside the laser cavity. Internally it requires a voltage signal that is proportional to the frequency change because it changes the optical path length of the resonator cavity. Externally it requires a voltage ramp which is the integral of the laser frequency change because the frequency change is a sum of the instantaneous phase changes it imposes on the beam [Hall 84].

CHAPTER 3

DYE LASERS

INTRODUCTION

There are many types of laser systems. The diagram below illustrates the range of different categories of lasers. The work carried here deals with atomic spectroscopy and quantum optics which requires laser radiation tunable over a wide range of wavelengths. The ring dye laser is the only wide range tuneable laser source that suits this particular experimental work. The lasing medium is an organic dye, dissolved in a liquid, and is optically pumped by an Argon ion gas laser.

The department owns two ring dye lasers: a Spectra-Physics 380D, and a Coherent CR-699-21. My frequency stabilization was carried out on the CR-699-21. This chapter will discuss the operation of this laser.
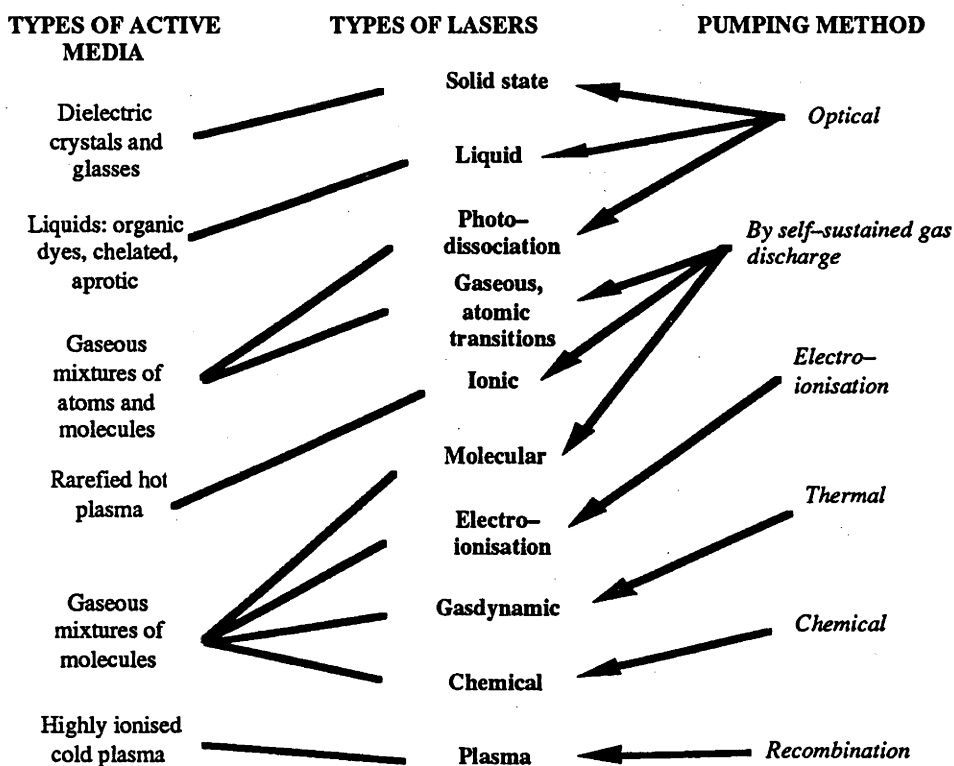

Fig.3.1. Summary of the various laser systems

For a discussion on other types of laser systems see [Tarasov 83].

3.1 DYE LASER OPERATION

The energy level diagram below (fig.3.1-1) shows the typical lasing scheme for a dye molecule. It consists of a ground state S_0, a series of singlet levels S_1, S_2, ..., and a series of triplet levels T_1, T_2,... .

In the singlet states the spin of the active electrons and that of the remainder of the molecule are antiparallel, while in the triplet states the spins are parallel. Intense absorption and fluorescence is thus obtained between singlet $\leftrightarrow$ singlet states while the singlet $\leftrightarrow$ triplet radiative transitions involve a spin flip
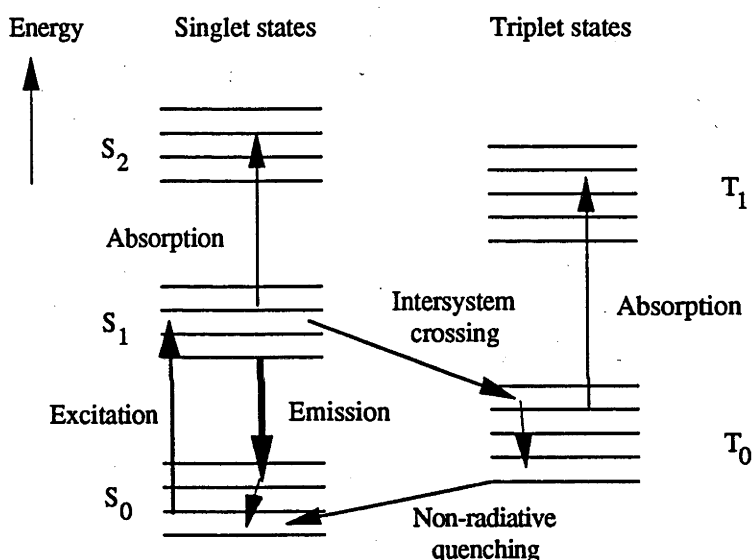

Fig. 3.1-1. The energy level diagram for a dye laser.

and are therefore less probable. In addition to the electron transitions are vibrational and rotational transitions which increase the absorption band to form a broad continuous energy band. The colour of the dye is determined by the broad absorption band $S_0 \leftrightarrow S_1$ which results from the excitation of an electron in a π–orbital.

A ground state electron is optically pumped into one of the vibrational–rotational levels in S_1. Collisions with other molecules dissipates any excess energy from the pump source and leaves the electron in the lowest vibrational level. Lasing then occurs from the lowest vibrational level to any vibrational–rotational level in the ground state. Finally the electrons relax to the $v = 0$ level of the ground state.

In the absence of frequency sensitive feedback the dye laser will oscillate on a band approximately 100GHz in bandwidth. With feedback this can be reduced to ≈ 1MHz for commercial dye lasers and to mHz in specific laboratories [Hall 88, Day 91].

There are several processes that compete with the lasing process to increase the losses of the laser. These processes arise from the depletion of the S_1 level electron population by spontaneous emission, two photon absorption, and intersystem crossing to the triplet states.

3.2   CR–699–21 DYE LASER

The CR-699 ring dye laser (shown in fig.3.2-1) is the laser used in this project. It is a travelling wave laser consisting of a four mirror resonator. This laser is a single mode laser that can be tuned over a wide range of frequencies (depending on the dye used). It is frequency stabilised to approximately 5MHz by locking the laser output to a temperature controlled reference cavity.
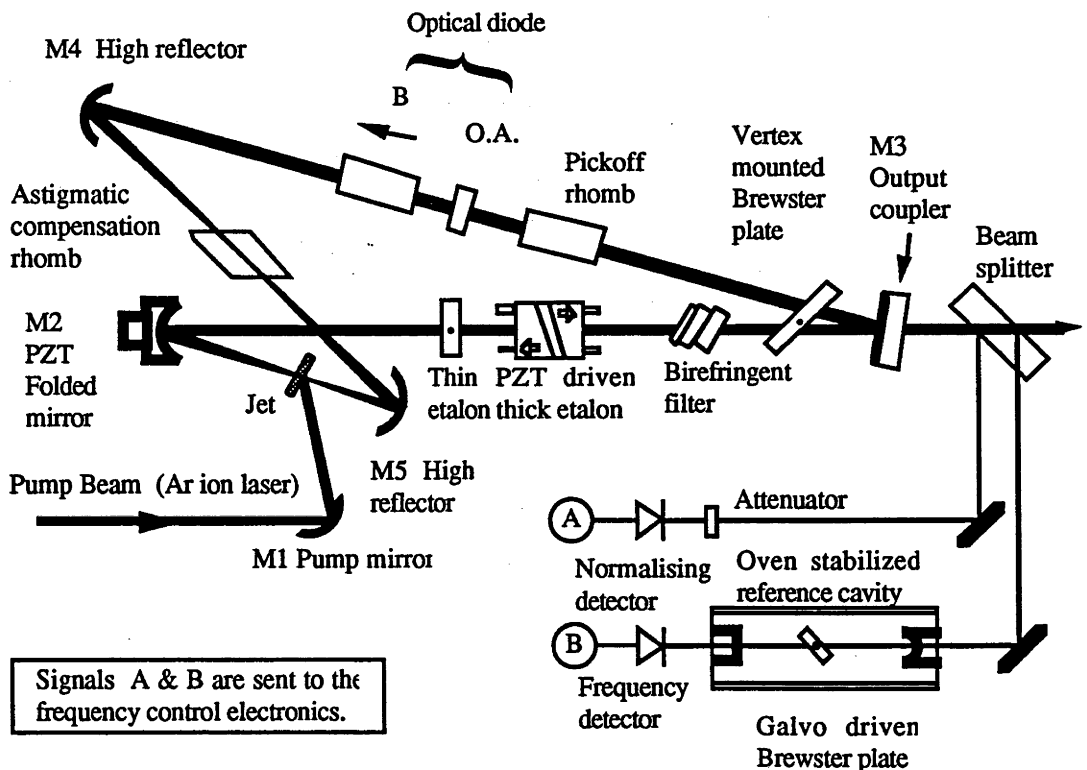

Fig. 3.2-1. Schematic representation of the Coherent CR-699-21 ring dye laser.

All components in the dye laser head are mounted on a 2-inch diameter solid invar rod, for mechanical and thermal stability. The laser has several internal components which are discussed briefly below.

3.2.1   RESONATOR MIRRORS

There are five mirrors in the ring dye laser. They are labelled M1, ..., M5.

M1 is a high reflecting mirror (coated to reflect the two Argon ion lines). It has a radius of curvature of 50mm, and is positioned 50mm from the dye jet.

M2 is a high reflecting mirror with a radius of curvature of 100mm. It is referred to as the *tweeter mirror*, and is mounted on a PZT stack to provide the fast (10KHz bandwidth) cavity length adjustments required to reduce the dye laser frequency jitter (frequency error) to ≈ 1MHz. It is set 50mm from the dye jet. This mirror can produce 1μm of optical path length change with a 50kHz first resonance.

M3 is the output coupler and is partially transmitting (≈ 97%). It has a long radius of curvature, > 1m and is set 570mm away from the tweeter mirror.

M4 is a high reflector and has a radius of curvature of 150mm. It is called the *fold mirror*.

M5 is another high reflector a with radius of curvature of 100mm. It is set 80mm from the dye jet and 220mm from the fold mirror.

3.3 SINGLE MODE SELECTION AND THE INTRACAVITY ELEMENTS

A dye can lase over a wide range of wavelengths. The cavity elements described below, are designed to restrict the output to a chosen sharp frequency by introducing cavity losses at all wavelengths other than that required. The laser contains three wavelength selecting elements. These are the birefringent filter and the thin and thick etalons. Each element will allow a certain band of wavelengths to be transmitted, as shown in figure 3.3-1. The selected wavelength corresponds to the wavelength that can be simultaneously transmitted through the three filters. Scanning of the laser field can be easily achieved by changing the relative positions of each filter's transmission.
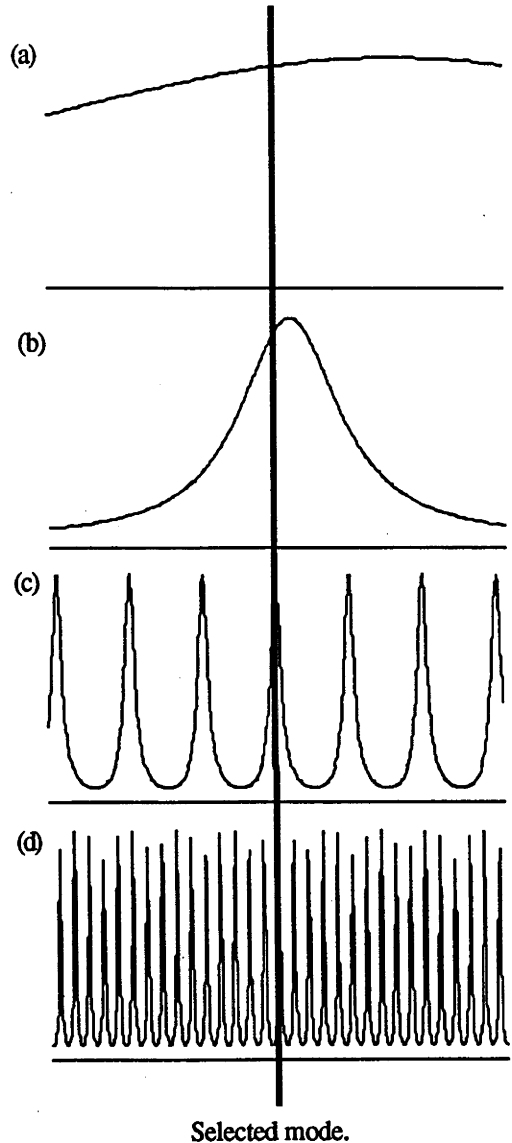

(a)

(b)

(c)

(d)

Selected mode.

Fig. 3.3-1. The single mode selection of a ring dye laser. (a) the laser gain profile. (b) The birefringent filter's transmission. (c) The thin etalon's transmission. (d) the thick etalon's transsmission.

OPTICAL DIODE: A ring dye laser has the ability to lase in two directions, from M2 to M3 or M4 to M3. To ensure unidirectional operation of the laser an optical diode is placed inside the cavity. The diode is designed to induce a polarization rotation on one of the light paths which, subsequently, causes reflection losses at the Brewster surfaces inside the cavity. Light travelling in the opposite direction is unaffected by the diode. The net result is such that lasing in one direction is suppressed.

The optical diode employs the Faraday effect. A small piece of optical glass with high Verdet constant that is immersed in a DC magnetic field. The Faraday effect in this glass rotates both the forward and backward propagating electromagnetic waves by the same amount and in the same direction. The forward wave is selected by applying initial rotation to it, by means of a reciprocal polarization-rotating element which rotates its polarization back into the plane of incidence of the Brewster plates and the laser cavity. Thus, the forward wave is unaffected by the diode. For the backwards travelling wave, however, the two rotations add causing increased reflections off the Brewster surfaces in the cavity, and result in a net loss. A small additional loss of less than 1% is sufficient to allow the forward wave to be the dominant oscillation.

BIREFRINGENT FILTER: This is a three plate filter manufactured from crystalline quartz. The three plates are in the thickness ratio 1:4:16. It has a passive bandwidth of about 380GHz, however, when used inside the laser it reduces the laser linewidth to approximately 2GHz. The orientation of the filter is such that the forward light strikes it at Brewster angle.

THIN ETALON: The thin etalon has a free spectral range of 200GHz, which is sufficient to enforce single mode operation. It is mounted on a galvanometer for electric angle tuning.

THICK ETALON: The thick etalon has a free spectral range of 10GHz and permits the longitudinal mode to be scanned. It is constructed from two Littrow prisms mounted on PZT's.

The birefringent filter, thin etalon and thick etalon are used to obtain single frequency operation that is tuneable. These three elements reduce the laser linewidth to about 20MHz.

ASTIGMATIC COMPENSATION RHOMB: A Brewster angled rhomboid of silica is used to compensate for the astigmatism inherent in the operation of the three spherical mirrors in an off axis manner.

VERTEX MOUNTED TUNING (Brewster) PLATE: This allows continuous scanning of the cavity length. This arrangement provides compensation for the displacement caused in tipping the plate that would otherwise misalign the ring and cause power modulation with scanning. The plate also functions to provide large scale and low frequency jitter corrections. It can produce 30μm of optical path length change with its first mechanical resonance at 1kHz.

DYE JET: The liquid dye is inserted into the cavity as a free-standing jet stream. Its optical quality surfaces are oriented at Brewster's angle for low loss

3.4   THE INTRACAVITY ASSEMBLY (ICA)

The ICA houses the thick and thin etalons. Incorrect optical alignment of this element can greatly reduce the scanning range of the laser. Both etalons are electronically controlled, and are used to scan the laser frequency. The thin etalon is a quartz plate and the thick etalon is a Fabry-Perot cavity.

The thick etalon [Berg 78] consists of a pair of closely spaced identical prisms mounted along the optical axis of the laser. The configuration of the prisms is shown in figure 3.4-1. Scanning of the laser frequency is achieved by moving the prisms with respect to each other. Surface 1 is at an angle α with respect to the normal of the incident beam. α is the minimum angle necessary to
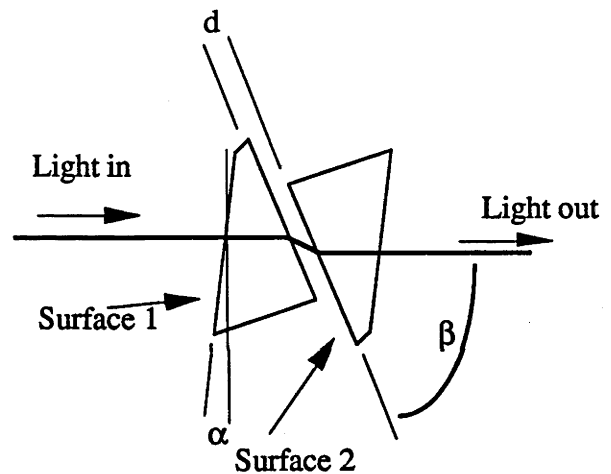

Fig. 3.4-1. The prisms inside of the thick etalon.

prevent coupling of the laser energy back into the cavity from surface 1. Surface 2 is inclined at an angle β to the direction of the laser beam. β is within a few degrees of Brewster's angle for the nominal radiation wavelength of the laser. Having surface 2 at an angle β eliminates the need to anti-reflection coat this surface. However, it is necessary to anti-reflection coat surface 1. The two prisms have a distance d between them, which is of the order of 1mm. This small gap minimizes the offset between the incoming and outgoing beams.

3.5   FREQUENCY OUTPUT OF THE RING LASER

Siegman [Ch. 1] states that the round trip phase shift condition for the phase shift inside the cavity must be some integer multiple of 2π. That is:

$$\frac{\omega P}{c} = q.2\pi \tag{3.1}$$

or

$$\omega = q.2\pi\left(\frac{c}{P}\right) \tag{3.2}$$

where ω is the angular frequency of the radiation, c is the speed of light, P is the round-trip path length of the ring laser (fig. 3.5-1), and q is an integer.

The CR-699-21 has a total perimeter of $\approx$ 1.5m. If the laser is running at 580nm then q is of the order of $2.5*10^6$.

We can rearrange [3.2] to show that the relative frequency stability is equal to the relative length stability:

$$\frac{\Delta v}{v} = \frac{\Delta P}{P} \tag{3.3}$$

Fig. 3.5-1. Schematic of a simple ring laser.

where v ($=\omega/2\pi$) is the laser frequency. Commercial ring dye lasers have a linewidth in the megahertz regime, which is thus 1 part in 10^{-8} relative frequency stability (assuming a wavelength of 580nm). The relative cavity length change required to maintain this level of stability is also 1 part in 10^{-8}.
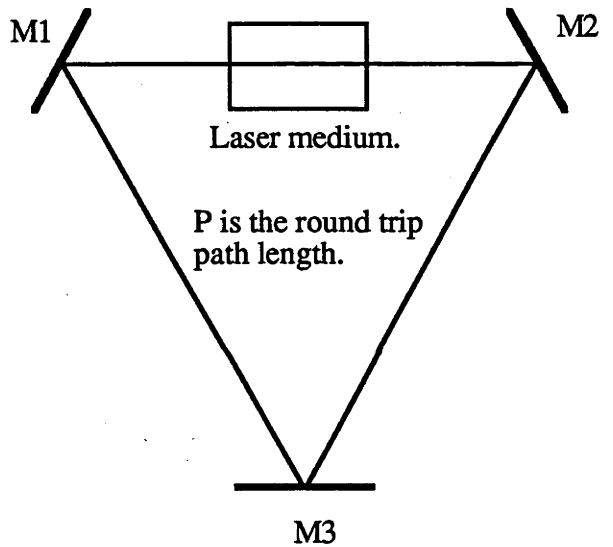
3.6   GAIN CURVES FOR THE CR-699-21 FREQUENCY TRANSDUCERS

The CR-699-21 uses the Brewster plate and the tweeter mirror (M2) as its frequency transducers. The gain curves [Grzesik 85] for these two elements are shown in figure 3.6-1.

The Brewster plate controls the low frequency changes. It can not be driven quickly because its first mechanical resonance is at $\approx$ 1kHz. The servo controlling this transducer is thus designed so that its roll over point is at $\approx$ 0.8Hz, and has unity gain at 120Hz. The higher frequency changes are sent to the tweeter mirror. The servo control electronics the tweeter is designed so that it has very little control at low frequencies, <1Hz, hence the two control loops work independently. The tweeter has gain all the way out to 10kHz, and its first mechanical resonance at $\approx$ 60kHz.

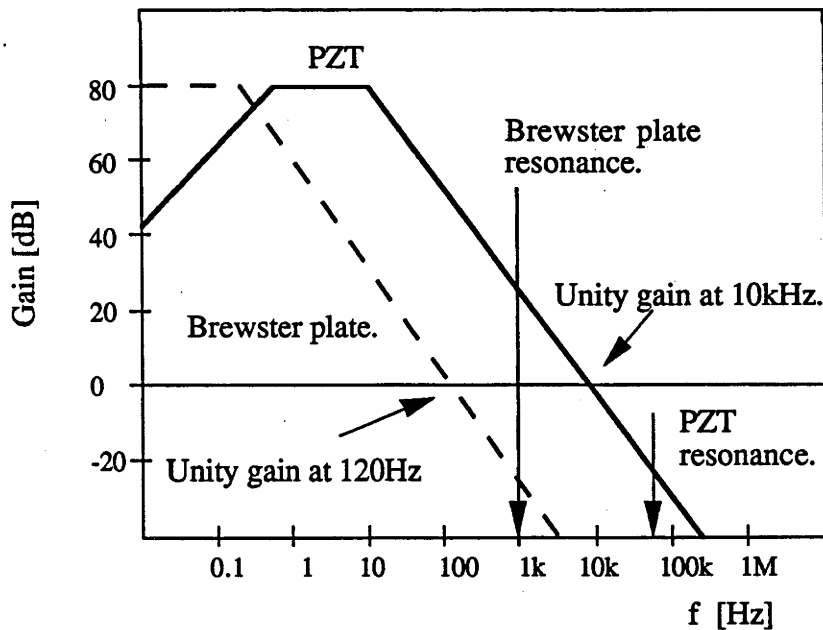Fig. 3.6-1. Bode plot (magnitde) for the frequency transducers in the CR-699-21.

CHAPTER 4

ALTERNATIVE LOCKING SYSTEMS

INTRODUCTION

This chapter outlines the different ways to frequency and intensity stabilize a ring dye laser. We considered three methods to frequency stabilize, and two different intensity stabilization systems. The advantages and disadvantages are discussed.

4.1   FREQUENCY STABILIZATION

The laser frequency can be altered by changing the resonator length or changing the laser frequency outside the cavity. A stabilization system using the first method is called internal stabilization because the frequency transducer is inside the cavity. A stabilization system using the second method is called external stabilization because the frequency transducer is outside the cavity.

4.1.1   INTERNAL STABILIZATION

The internal stabilization elements of a commercial dye laser have been discussed in chapter 3. These intracavity devices can reduce the linewidth of a typical dye laser from tens of MHz to approximately 1MHz. Further reduction of the linewidth requires devices that can alter the laser cavity length at a much faster rate than Brewster plates and PZT mounted mirrors. The EOM was, until recently, unusable because it stopped the lasing process when it was placed inside the laser cavity.
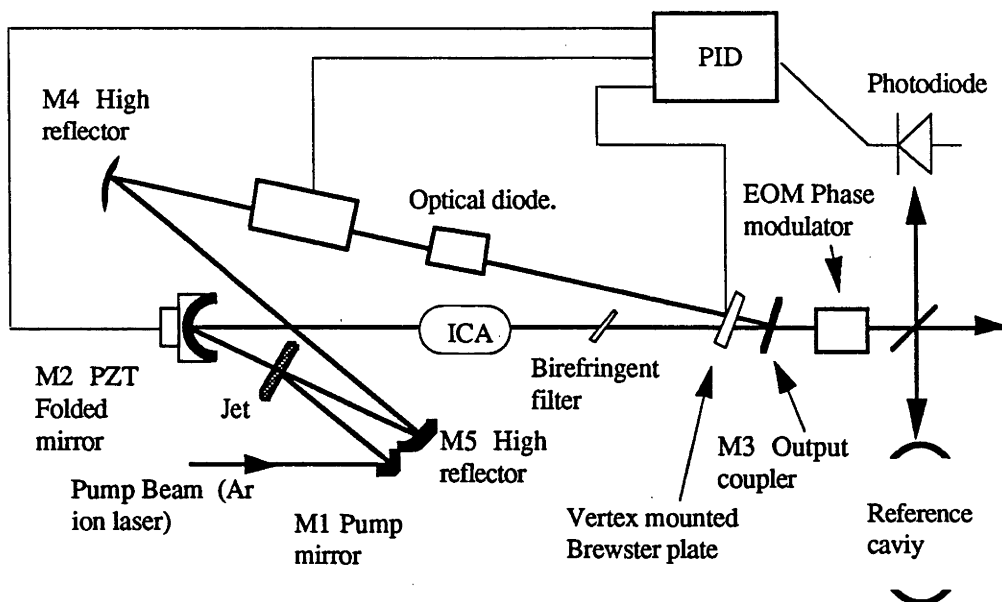
Fig. 4.1.1-1. Schematic of an internal stabilization scheme. This diagram does not include the phase sensitive detection to generate the error signal.

Now, however, there exists an EOM from Gsänger[1] that has been used successfully in several internal stabilization systems. It has been reported [Fisk 91] that the output power of a ring dye laser dropped only by ≈20% after insertion of the modulator into the ring dye laser cavity.

The simplest way to understand the internal stabilization scheme is to look at the system's response to a sudden change in frequency. The response diagrams are shown in figure 4.1.1-2.

It was pointed out in section 3.5 that the frequency output of a laser is dependent on the resonator length. To compensate for a sudden frequency change, such as that illustrated in fig. 4.1.1-2a, the control electronics must supply an equally sudden voltage change to the frequency transducers, fig. 4.1.1-2b. The resulting frequency change due to the change in cavity length is shown in fig. 4.1.1-2c. Figure 3.6-1 shows that a commercial system cannot respond to a frequency change that occurs in a time less than 0.1ms (the PZT unity gain point is at 10kHz). Insertion of the EOM allows the control loop to extend its bandwidth so that it can respond to changes that occur on time scales less than 0.1ms. The EOM can in principle respond at a GHz rate, which indicates that ns changes can be addressed. However, the existing electronics limit the systems response to the point where μs changes are out of the reach of the control loop. This is due to time delays of the error

---

[1] Gsänger Optische Komponenten GMBH, Planegg, Germany.

signal as is passes through the circuitry; unavoidable phase changes of the error signal induced by the electronics; and also limited gain at high frequencies. These problems can be compensated for but are technically challenging.

(a) A laser frequency change of $\Delta \omega$.

(b) Voltage change to internal elements.
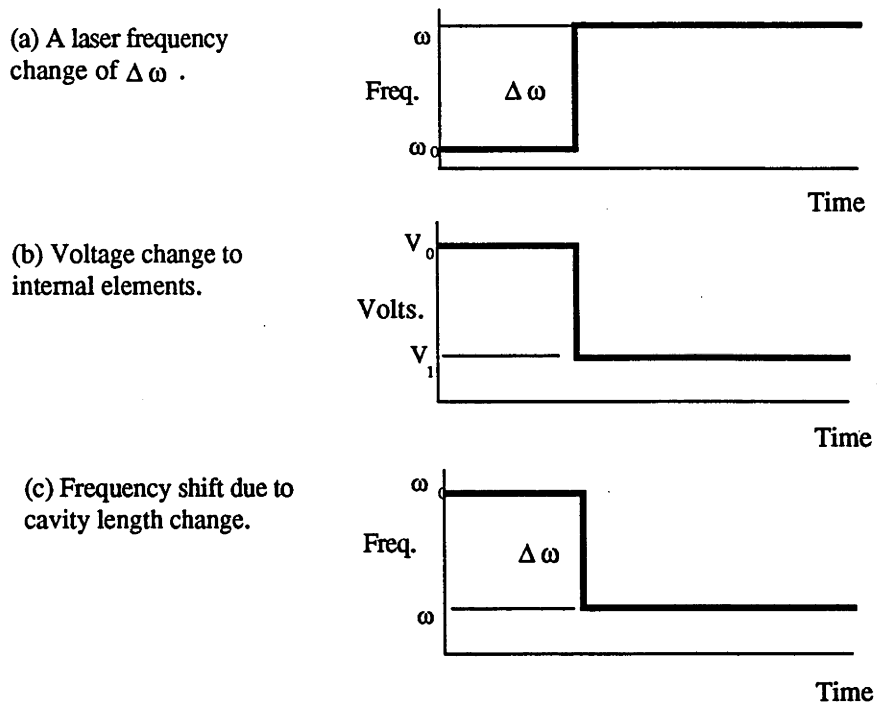
(c) Frequency shift due to cavity length change.

Fig. 4.1.1-2. The response of the internal stabilization system to a sudden change in frequency.

Internal stabilization systems have been capable of reducing the laser linewidth to the kHz regime, but have not yet been able to reduce the linewidth further. It is only a matter of time until they do reach the Hz regime as faster electronic circuitry is being developed continuously.

The primary advantage of internal stabilization is that the voltages required for the EOM are relatively small (tens of volts) and can be controlled by wide bandwidth amplifiers. The disadvantages are in the cost involved in developing the system and the difficulties involved in the optical alignment of the dye laser with this element inside the cavity. The expense lies not only in the purchase of the EOM, but in the acquiring other elements such as a Faraday isolator which prevents reflections back into the laser.

4.1.2   FEEDBACK EXTERNAL STABILIZATION

External stabilization systems attempt to regain the short term narrow linewidth by compensating for frequency jumps. Changes in the output frequency are measured and then reversed by the external transducer. In principle a lower frequency limit could be reached if the diagnostic and servo systems reacted without delay upon detection of a frequency change.

Hall [1984] reported the design for an external frequency stabilizer that combined an AOM and an EOM in the control loop. This technique links the two frequency correcting elements via a complex servo system. The system is complicated due to the unavoidable time delay of the AOM's frequency shift of the laser light. Intrinsic delays, due to the finite propagation time of the acoustic wave through the crystal are $0.2 - 0.8\mu s$. The EOM is thus used to give an instantaneous frequency shift of the light that lasts until the AOM is able to act as the frequency altering element. The system is shown in fig. 4.1.2-1.
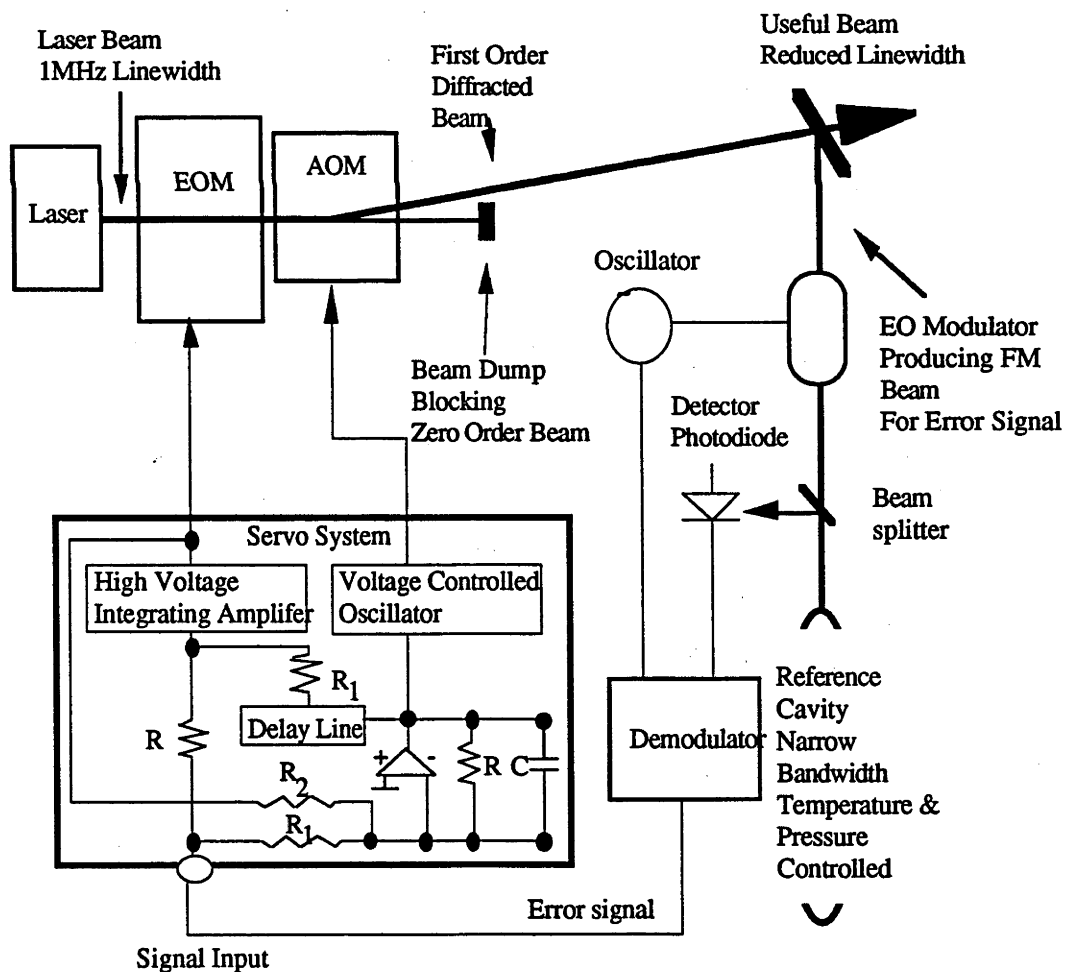

Fig. 4.1.2-1. The EOM/AOM external frequency stabilizer developed by Hall (1984) at JILA. This system uses Pound/Drever locking to a reference cavity.

An EOM is not able to be used on its own as a frequency shifter. A voltage U applied to an EOM changes the phase of the emerging light by an amount ϕ. A frequency shift is accomplished when the voltage is changed at some rate dU/dt, that is when the phase of the emerging light is being varied. In order to get a frequency shift Δv we electronically integrate the control voltage V(t) so that the EOM sees a voltage:

$$U = \frac{1}{\tau}\int_{t_1}^{t_2} V(t)dt \qquad (4.1)$$

and $\quad \Delta v = \frac{1}{2\pi}\cdot\frac{d\phi}{dt} = \frac{1}{2U_0}\cdot\frac{dU}{dt} = \frac{1}{2U_0\tau}V(t) \qquad (4.2)$

U_0 is the half-wave voltage of the EOM, and τ is the maximum integration time available. Typically, U_0 is $\approx$ 500V, τ is at best 1μs, and V(t) is 500V, so the maximum frequency change is Δv = 500kHz. We can, off course, produce V(t) that are up to 1kV but we sacrifice the available integration time. The EOM is, therefore, unable to sustain a frequency change and is also unable to change the frequency by a sufficient amount for some laser systems, such as dye lasers, where the frequency can change by several MHz.

Section 2.5.2 discussed the AOM and the output frequencies of the diffracted beams. In this stabilization system one the first order diffracted beams has its output frequency altered by a change of the frequency of the acoustic wave operating the AOM. The frequency of the acoustic wave is changed using a voltage controlled oscillator (VCO). The VCO needs to operate with a central frequency of about 150MHz with ±30MHz variation in frequency, and a response time less than 0.2μs. The VCO/AOM combination requires $\approx$1μs to alter the laser frequency. This is fast compared to resonator mirrors mounted on PZT stacks but is quite slow compared with the response time of an EOM.

Hall's system uses the fast response of the EOM to quickly adjust the laser frequency while the VCO/AOM are inoperable. The response curves for this system are shown in fig. 4.1.2-2.

Most workers do not use this technique because of the electronics required to control the frequency transducers. It is possible to simplify the arrangement by using only an AOM in feedback, as we have done in this work. The cost paid for this simplification is that the control loop cannot respond to fast frequency fluctuations. The laser linewidth can, however, be reduced to the tens of kHz regime, and
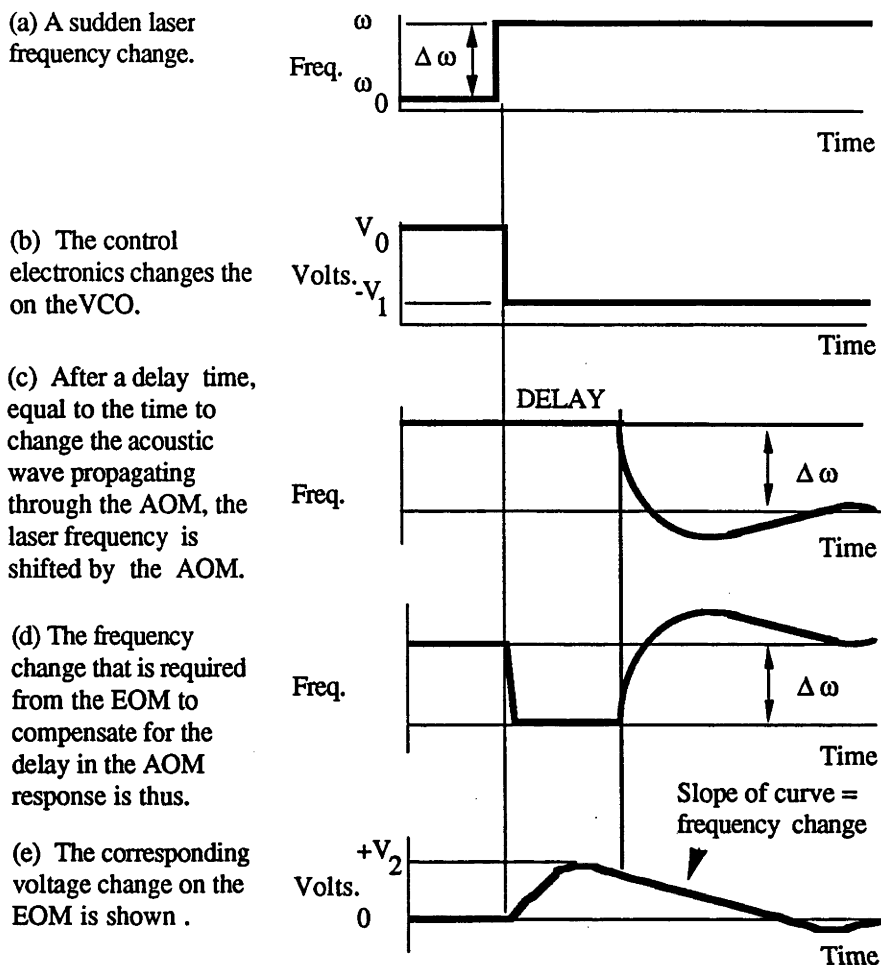
(a) A sudden laser frequency change.

(b) The control electronics changes the on the VCO.

(c) After a delay time, equal to the time to change the acoustic wave propagating through the AOM, the laser frequency is shifted by the AOM.

(d) The frequency change that is required from the EOM to compensate for the delay in the AOM response is thus.

(e) The corresponding voltage change on the EOM is shown.

Fig. 4.1.2-2. The response curves of the EOM/AOM external frequency stabilizer.

possibly less. This is suitable for most applications but not all. A larger concern is that the laser beam will be spatially tilted. There is a small shift (of milli-radians) but this did not pose a problem in the experiments carried out during the course of this work.

Using an AOM external stabilizer has several advantages over the other methods. The unit acts as an isolator because any light reflected back from an optical surface in the experiment experiences a frequency shift away from the operating frequency of the laser. We demonstrated the effectiveness of this isolation by reflecting all the light from one of the first order diffracted beams back into the laser and observed the effect on the laser's locking. We were unable to notice a change in the behaviour of the laser. Without the AOM in place the laser does not lock if a small fraction of laser light was reflected back.

The external system could be easily aligned when needed and removed when not required. It could be placed at any part of the experiment, and occupied little space.

The laser power dropped by about 20% on passing through the AOM, which gives it a similar efficiency to the internal system. This system, however, does not complicate the alignment of the laser.

4.1.3   FEEDFORWARD EXTERNAL STABILIZATION.

As an alternative to the feedback external system discussed above, we considered a feedforward external system that uses only an AOM as the frequency correcting element. This system is shown schematically in fig.4.1.3-1. This system was designed so that we could optically delay the laser light by the delay time of the in the AOM. The fibre optic replaces the EOM in fig. 4.1.2-1, and its corresponding electronics.
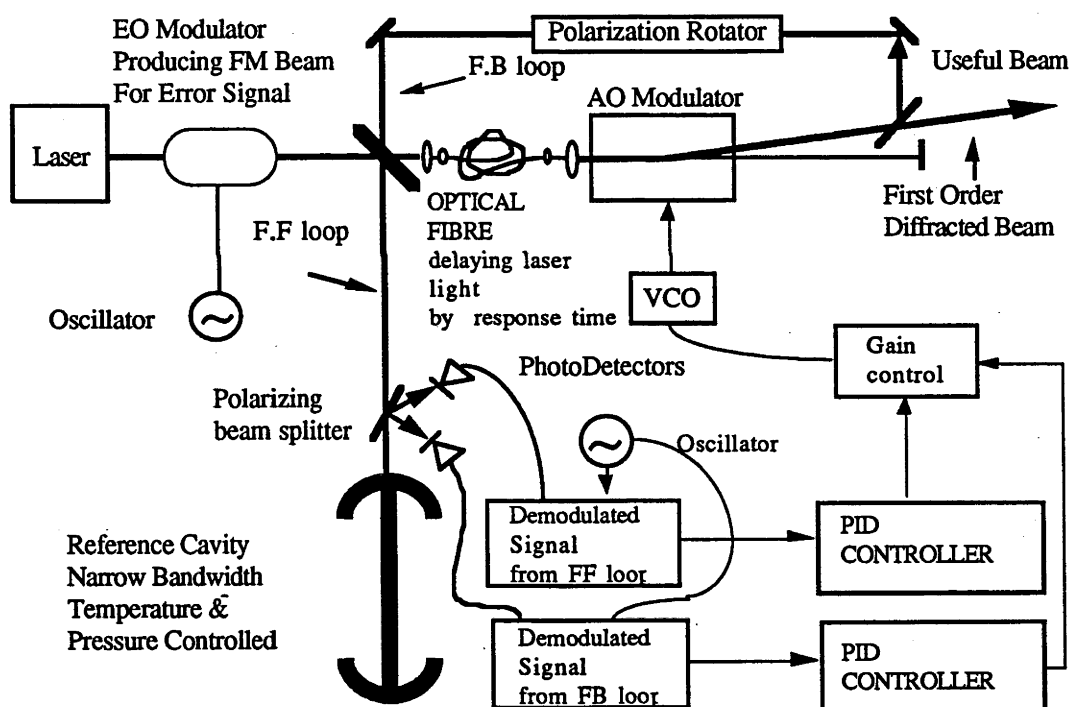

Fig. 4.1.3-1. The feedforward external frequency stabilizer.

The laser frequency is analysed as it leaves the laser cavity, and the error signal is then sent to the AOM. The AOM is placed after the test point, making this a feedforward system. Feedforward control loops have a disadvantage over feedback loops in that they cannot automatically adjust the controller's gain. Hence a second loop is required to test the output stage and correct for errors in the gain of the

feedforward loop. This second loop is the feedback loop indicated in fig. 4.1.2-1.

The optical fibre delay plays a major roll in this system. The length of fibre required for, say, $0.5\mu s$ delay of the laser light is $\approx 100m$. Single mode fibre of this length is expensive and at laser wavelengths of $\approx 560nm$ the power transmission efficient is around 50% due to losses in the input/output coupling.

(a) A laser frequency change of $\Delta \omega$.

(b) Optical delay of laser light using a fibre optic .

Laser input to AO as a result of fibre optic delay of laser output.

(c) Voltage change on VCO.

Gain adjusted using correction signal of feedback loop.

(d) AO response in feed forward system.

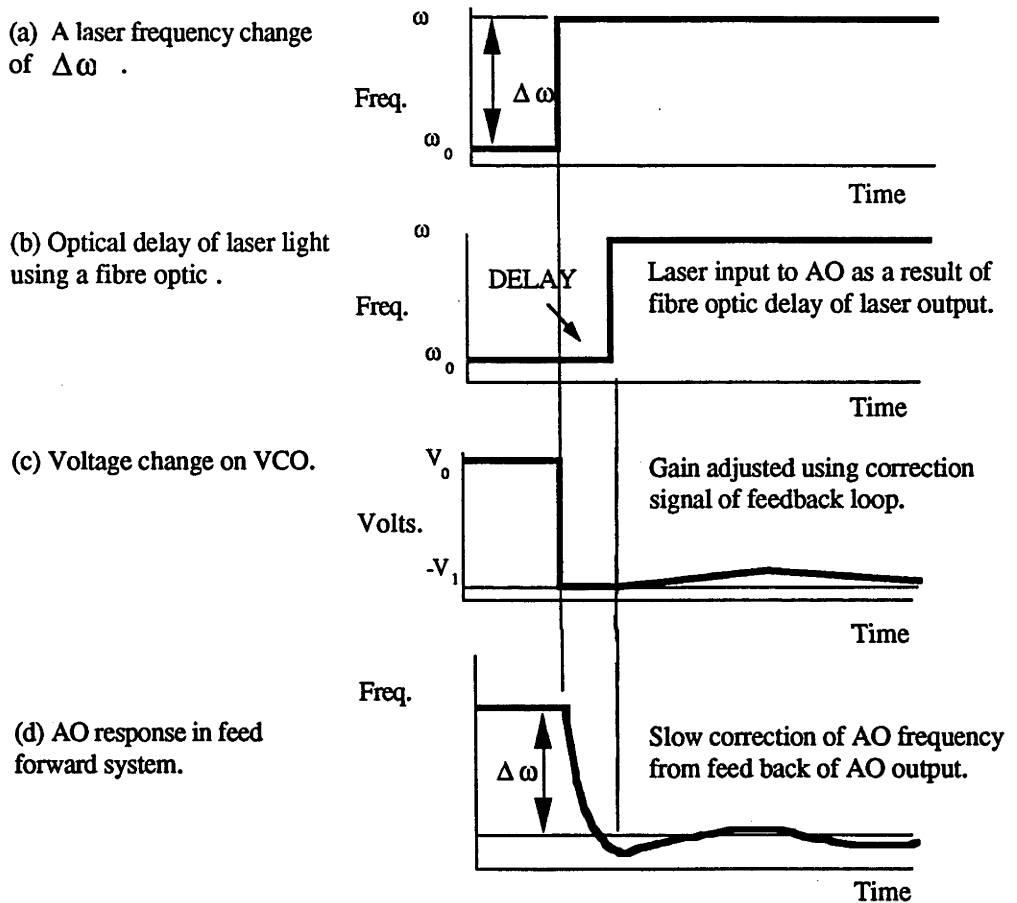Slow correction of AO frequency from feed back of AO output.

Fig. 4.1.3-2. The response curves for the feedforward external frequency stabilizer.

Once again the operation of this system can be understood more easily with the aid of its response curves. These are shown in figure 4.1.3-2. A detected frequency change (fig. 4.1.3-2a) is converted into a voltage change that is sent to the VCO. The VCO then changes the frequency of the acoustic wave operating the AOM, (fig. 4.1.3-2c). Meanwhile, the laser light is optically delayed in the optical fibre by the delay time of the AOM. These two stages result in a laser light reaching the AOM at the correct time. The resultant frequency change is shown in fig. 4.1.3-2d. As indicated in this diagram, the frequency change may be larger/smaller than required and must be controlled by some feedback loop. This feedback loop will

only need to operate at low frequencies as a gain control.

This system has the advantage that it simplifies the technical aspects associated with linking the EOM and AOM in one frequency transducer (fig. 4.1.2-1). Time restrictions did not allow us to investigate this technique and so I will not delve further into its advantages /disadvantages.

4.2   INTENSITY STABILIZATION

The laser is intensity stabilized external to the laser cavity. The basic principle involved is that the laser output intensity is monitored, by some low noise photodetector, and if it varies from some reference intensity then the stabilizer corrects for this change. We considered two techniques for stabilizing the laser's intensity. Both will be discussed here.

Before I discuss the two stabilizers I will quickly discuss the logic associated with intensity stabilization.

Figure 4.2-1 looks at the electronic concept behind the intensity stabilizer. The laser intensity is shown in fig. 4.2-1a as having some DC value with an AC component sitting on top of it. The laser's intensity is measured by a photodetector, and converted to a photocurrent. The intensity stabilizer compares the photocurrent measured by the detector with a reference current set by the controller. Any small change in the equality of the two currents will provide an error signal for the
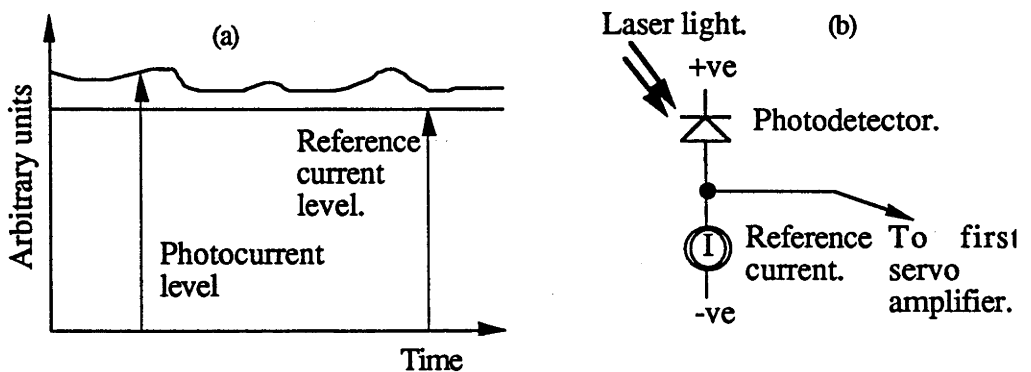
Fig. 4.2-1. Electronic concept behind the intensity stabilizer. The detected photocurrent is stabilized to a reference value by the stabilizer.

stabilizer. The reference current is set at a level that is below the minimum recorded photocurrent. This implies that a fraction of the laser intensity output is lost through the stabilizer. The fraction lost is generally dependent on the light fluctuations.

It should be noted that the theoretical limit for the intensity stabilization of a laser field is given the quantum-noise of the light. See [Yamamoto 90] for further details.

4.2.1   THE EOM INTENSITY STABILIZER

A schematic of the EOM intensity stabilizer is shown in fig. 4.2.1-1. It is based around the properties of an EOM. The laser light is passed through a polarizer and then the EOM. The optic axis of the EOM is set such that it differs from the polarization axis of the light. The optic axis is shown to be at 45^0 in the diagram because this gives the largest effect, it can in fact be at any angle other than 0^0. A second polarizer selects the light component at 0^0 with respect to the first polarizer.
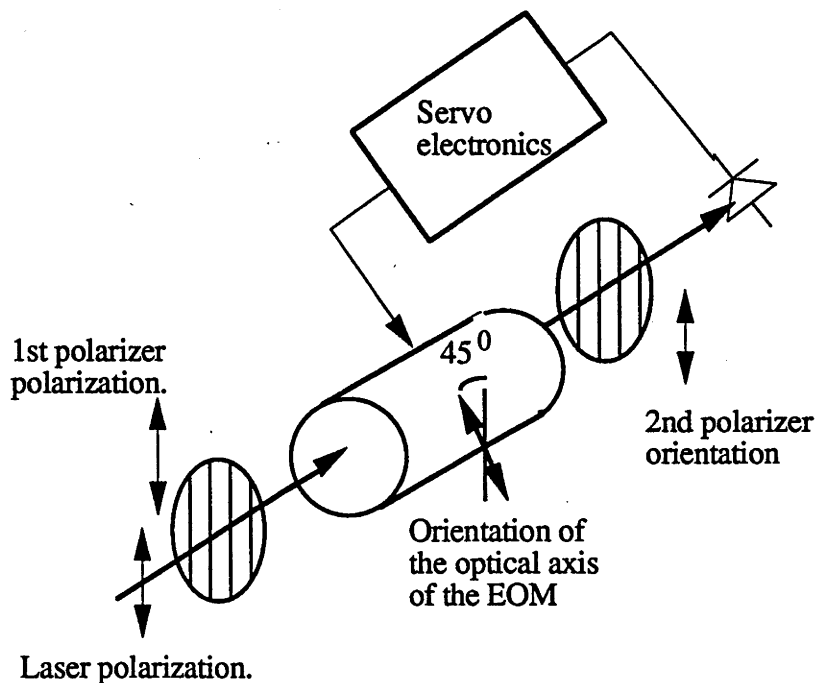

Fig. 4.2.1-1. Schematic of the EOM intensity stabilizer.

This stabilizer uses the property of the EOM to convert plane polarized light into elliptically polarized light by altering the electric field applied to it. The beauty of this system is that it's bandwidth, and it's noise suppression are dependent on the properties of the servo electronics. The EOM can respond very quickly to a change in the applied electric field.

4.2.2   THE AOM INTENSITY STABILIZER

The AOM intensity stabilizer [Layer 79] works on the principle that the diffraction efficiency of the AOM can be controlled by controlling the RF power operating it. Figure 4.2.2-1 illustrates the workings of this stabilizer.

A portion of the light from one of the first order diffracted beams is sent to a photodetector. A polarizer is placed in the beam to ensure that the intensity of one polarization is stabilized. This is to compensate for the unpredictable birefringence of the AOM. An AOM can give an output beam that has rotating polarization, and hence appears to be amplitude modulated if viewed through an analysing polarizer.
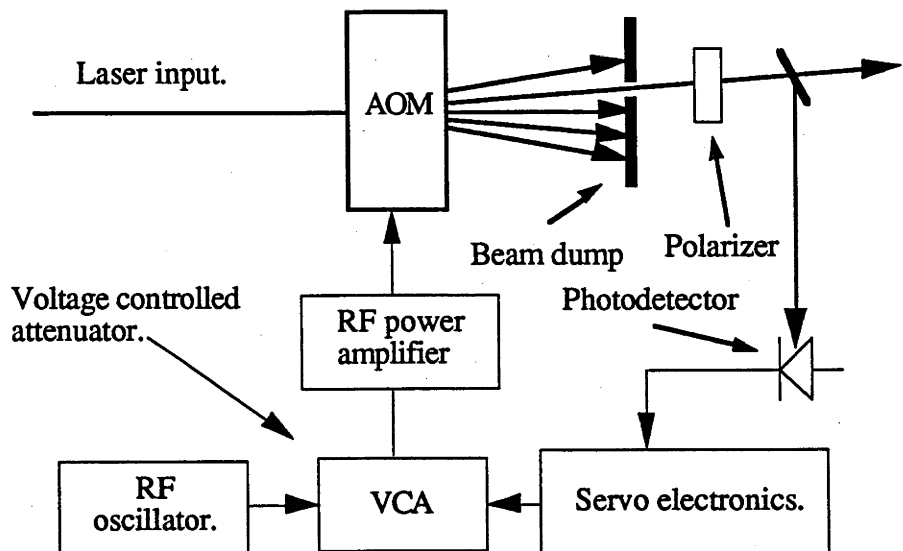
Fig. 4.2.2-1. The AOM intensity stabilizer.

The signal from the photodetector is sent to the servo electronics and then a voltage controlled attenuator (VCA). This attenuator has two inputs. The first input is for an RF sinewave which provides the acoustic wave frequency, and the second input is for a control voltage. The control voltage adjusts the transmitted amplitude of the RF signal through the attenuator. The output of the device is a signal at the same frequency as the input RF signal but is amplitude modulated by the servo signal. This signal is then amplified to the operating power of the AOM and sent to the AOM.

This system also has a very high bandwidth and is limited by the electronics. The diffraction efficiency can be altered as quickly as the maximum frequency of the VCA, which is over 10MHz

CHAPTER 5

ELECTRONICS

INTRODUCTION

We chose to develop the frequency stabilizer discussed in section 4.1-2 and the intensity stabilizer discussed in section 4.2-2 because they met the criteria mentioned in chapter 1. Developing these systems involved development of suitable electronics to control the stabilizers. This department had worked on cavity locking projects in the past [Fisk 87], where a 1m Fabry-Perot cavity was locked to a ring dye laser. The electronics used in this project were based on 741 chip technology. It was not possible to adapt this technology to the requirement of this project. The first task was, therefore, to update our technology and refine the techniques required to build high speed, low noise, low phase lag, high gain, low drift electronics.

The components developed included:

      (I)   Demodulators;

      (II)   High voltage amplifiers;

      (III)   Voltage controlled oscillators;

      (IV)   Photodetectors; and of course

      (V)   PIDs.

This chapter will discuss the development of these components and their performance. The circuit diagrams discussed in this chapter are shown in Appendix B.

5.1   THE DEMODULATOR

There are three sections required in order to produce a correction voltage that can be used in a servo system. This signal is called the system's *error signal*, ES. These are illustrated in fig. 5.1-1. The first component is a photodetector (PD) to convert the light from the frequency reference into a photocurrent, the second is a local oscillator (LO) that is tuned to the modulation frequency of the light field, and finally a demodulator that extracts the information out of the photocurrent producing an Intermediate Frequency (IF) which is the error signal. This demodulation process is called phase sensitive detection because the output of the demodulator is a DC signal which has an amplitude that is proportional to the phase difference between the local oscillator and the photodetector signals.

LASER LIGHT FROM
FREQUENCY
REFERENCE

PHOTO–DETECTOR (PD)

DOUBLE BALANCED MIXER (DBM)
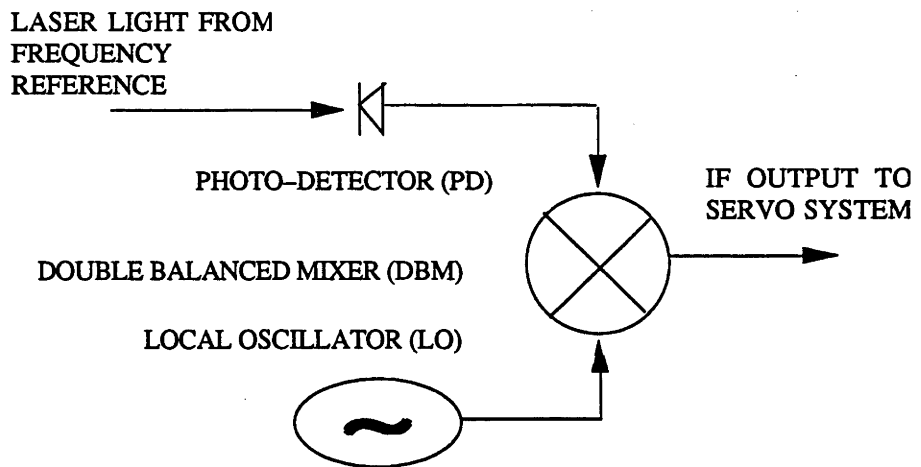
LOCAL OSCILLATOR (LO)

IF OUTPUT TO
SERVO SYSTEM

Fig. 5.1.1. Illustration of the ports of a demodulator

Our first project was to find a suitable high speed phase sensitive detector. The previous work was based around the balanced modulator-demodulator LM1596N (circuit diagram shown in fig. B1).

This is an active element with specifications that indicate suitable performance at the modulation frequencies we work at (2-20MHz). The circuit shown was designed for low frequency demodulation (10kHz say) and consequently had a lot of high frequency filtering on the output stage, the roll off frequency being at ≈32kHz. To obtain the largest possible control bandwidth we had to remove this filtering. Removing the filtering increased the bandwidth of the LM1596 chip but also introduced noise into the circuit. Further more, the chip was found to have excessive voltage

drifts (> 30mV over 1min) and the voltage noise exceeded 10mV. These were unsuitable characteristics which forced us to start working with passive phase sensitive detectors called double balanced mixers (DBM).

A mixer, of double balance type, is a passive electronic device that consists of four carefully matched schottky barrier diodes (fig. 5.1-2.) and two well balanced wideband hybrid transformers. This arrangement ensures that the LO, RF, IF mixer ports are isolated from each other.
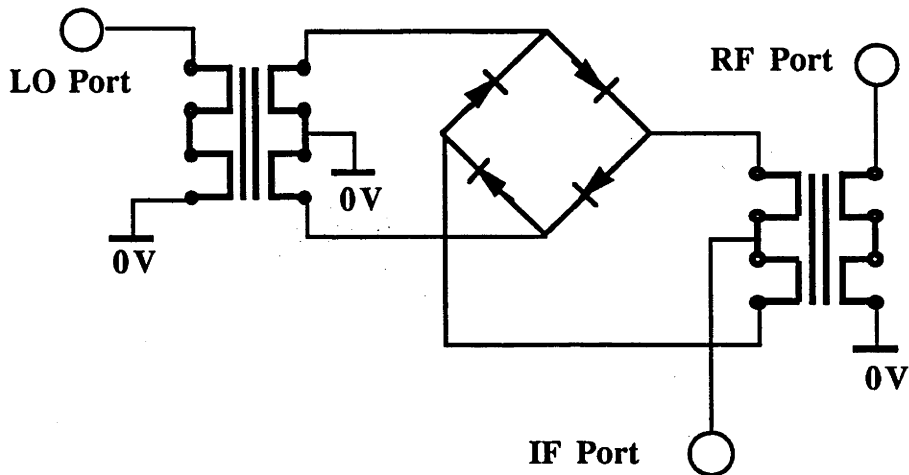
Fig. 5.1.2. The construction of a double balanced

The principle application of a DBM is as a frequency conversion (mixing) device. Two signals (LO, RF) are applied to the mixer which produce combinations of the sum and difference frequencies appearing at the IF port, that is, the frequencies (RF $\pm$ LO) are observed at the IF port.

However, in this type of locking experiment the DBM is used as a phase detector. The two signals input at LO & RF are at the same frequency so a DC voltage proportional to the phase difference between the two inputs appears at the IF port. A 90° phase relationship exists between the ports, so zero output at IF occurs at a relative phase quadrature condition. This is called a Cosine mixer and is the most common type. In addition to the DBM shown above, there exists a DBM that gives both the inphase and quadrature components and is called a Sine/Cosine mixer. This is useful in experiments where both components carry information.

The DBM used in this work was a Mini-Circuits ZP-10514. The LO/RF frequencies

can be between 0.2-500MHz and the IF output is between DC-500MHz. These devices require that the input signal to be at a certain level for correct operation. In this case the LO should have a signal strength of +7dBm and the RF signal can be up to +1dBm. The maximum voltage output at the IF port is 40mV P-P.

The ZP-10514, like all DBMs, requires to be isolated from any low impedance loads. We chose to send the IF output into a LH0033CG buffer amplifier as a form of isolation (the LH0033CG will be discussed at a later stage), and then to an amplifier stage. This DBM comes packaged with BNC connectors fitted. Interchanging the unit can therefore be done quickly, but for more compact electronics a PCB mounted DBM will be used in future.

5.2   THE HIGH VOLTAGE AMPLIFIER

We decided in our preliminary investigations that a high voltage amplifier would be required to control the EOM in the frequency stabilizer of section 4.1.2. The amplifier would need as large a frequency response bandwidth as possible, with low phase lag over that bandwidth and a voltage range up to 1kV.

The design developed (shown in fig. B2.) was inspired from a design for a 500V pulse amplifier circuit obtained from the Electronics Unit, Research School of Physical Sciences (RSPhysS). The original RSPhysS design could not be directly converted to suit our needs, but gave us the components for our design. These components were the three active elements: the LH0032CG operational amplifier; the LH0033CG buffer amplifier; and the MTM1N100 MOSFET.

The LH0032CG had many desirable features such as a slew rate of 500V/μs, 70MHz gain bandwidth product, and a high impedance FET input. This unit, however, was designed for comparator type applications where the relative phase between input and output is not important. This relative phase change (180^0 at 1MHz) ultimately limits the performance of the amplifier. The gain of this amplifier is also frequency dependent, dropping by 20dB at 100kHz. None the less, the amplifiers built using this chip worked to frequencies much higher than commercial high voltage amplifiers (>150kHz as shown in fig. B3).

The LH0033CG is an ultra fast device having a power bandwidth from DC to 100MHz. This unit has a $10^{10}\Omega$ input impedance and a high output drive (±10V at 50Ω). It is useful for many applications, namely; driving signals down coax cables; preventing signals from reflecting back through the circuit; and acting as a high input load for components that cannot drive low impedance loads.

The MTM1N100 MOSFET is a power field effect transistor. The voltage difference between the source and drain can be as large 1000V. A swing from 0 to 1000V can be achieved in a very short times (< 1µs). As shown in fig. B2 the drain is connected to the high voltage by some load resistor, while the source is held at ground (0V). The gate controls the current flow through the FET, and hence the potential at the drain. The operating threshold voltage range for the gate is between 2-4.5V. That is, no current flow when the gate voltage is set to 2V and maximum flow is when the gate voltage is set to 4.5V.

The amplifier design had some unforeseen problems. The major one being that the input-output isolation was not very good due to insufficient buffering between the input stage and the feedback loop. There was also some RF pick-up in the circuitry. These problems will be addressed in future designs.

The specifications for this high voltage amplifier are:

(1)   Fixed gain of 100 (0-10V input -> 0-1000V output);

(2)   Operates between 0 to 1000V;

(3)   Output gain flat to 100kHz with 3.4^0 phase lag;

(4)   maximum gain at 300kHz with 43.2^0 phase lag;

(5) 90^0 phase lag at 900kHz (gain drops by a factor of two);

(6) 180^0 phase lag at 10MHz (gain drops by a factor of thirty).

5.3   THE VOLTAGE CONTROLLED OSCILLATOR

The voltage controlled oscillators used in this project were supplied by Vari-L Company Inc. To our knowledge these are the only commercially available PCB mountable oscillators that operate at the RF frequencies suitable for AOMs. It is possible to purchase VCO drivers that are specifically designed for AOMs, but they are not suitable for this type of feedback control system because of excessive internal filtering.
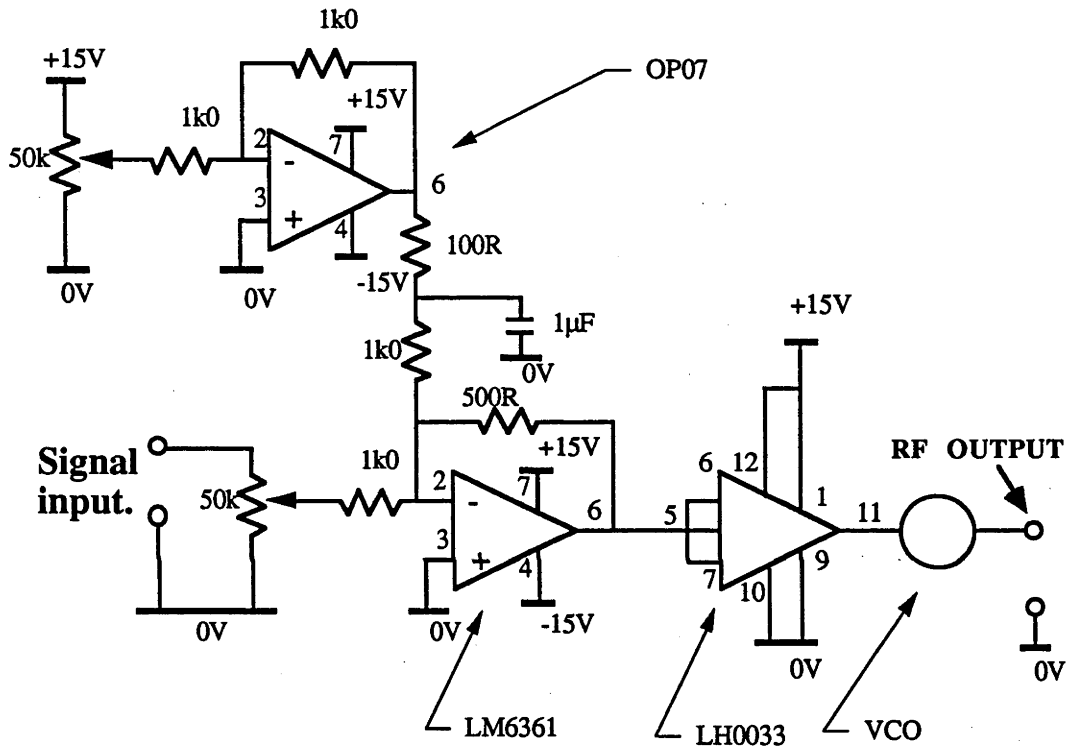
Fig. 5.3-1. Schematic diagram of the VCO electronic circuit.

The Vari-L VCOs come in three frequency ranges. The VCO-104 operates from 50-100MHz, the VCO-204 operates from 100-200MHz, and the VCO-304 operates from 200-400MHz. We purchased and constructed the VCO-104 and 204 models, using the 204 in the experiments. The circuit diagram for the VCO PCB is shown in fig. B4.

The specifications for the VCO are:

(1)   Output power +10dBm;

(2)   Modulation sensitivity 2.5 MHz/V;

(3)   Switching/slew 0% - 100% rise time 55ns;

(4)   Switching/slew 0% - 100% fall time 55ns.

The switching/slew is a measure of the response time of the VCO to a change in frequency, that is, how quickly the oscillator can follow the control voltage.

An AOM requires about +30dBm (1W into 50Ω) of RF power for maximum diffraction efficiency. The output of the VCO was amplified to +26dBm with a Mini-Circuits ZHL-1A +16dB RF amplifier.

5.4   THE PHOTODETECTORS

The photodetector plays a major role in any optical experiment. The properties of the light field can easily be masked by noise if the photodetector is not properly constructed. We have devoted much time and work to the construction of quiet photodetectors in the past three years. Producing a shot-noise limited photodetector requires good isolation of the photodetector from RF noise sources, filtering of power noise, and quiet amplification. RF isolation is achieved by enclosing the detector in a Faraday cage (cast Iron or Nickel plated box for example). The power supply is filtered with capacitors, inductors, and if necessary extra voltage regulation. Finally, the photocurrent signal is amplified by sending it through a current to voltage converting operational amplifier. This is called a transimpedance amplifier.

A transimpedance amplifier can be a low noise operational amplifier (such as an OP27) arranged in the configuration of fig. 5.4-1. The transimpedance amplifier can be understood simply if we examine the current flow in the amplifier. In an operational amplifier the currents i_d and i_f are equal. We thus have the situation:

$$i_d = i_f = \frac{v_{out}}{R_f} \qquad (5.1)$$

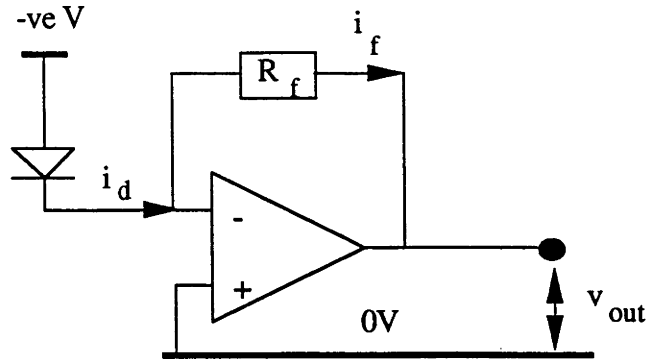or $$v_{out} = i_d R_f \qquad (5.2)$$

Fig. 5.4-1. Schematic of the transimpedance amplification of photocurrent. The photodiode is initially reverse biased and any photocurrent is fed directly into the negative input port of an operational amplifier.

Hence the output voltage is simply the photocurrent times the feedback resistance.

The noise in transimpedance amplification is dominated by the Johnson noise [Horowitz Ch 7] of the feedback resistor. This is because the leakage current of good PIN diodes is typically less then 1nA, which induces a shot noise that is much less than Johnson noise for resistances less than 100MΩ.

We designed two photodetector circuits for this project. One for the intensity stabilizer and one for the frequency stabilizer error signal. The schematic of the two circuits are shown in appendix B.

The intensity stabilizer photodetector circuit consists of a reverse biased Radio Spares BPX-65 photodiode being feed into a PMI OP-27 operational amplifier, operating in transimpedance mode. We selected this op-amp for the intensity stabilizer because of its noise properties, and bandwidth. The OP-27 has a voltage noise density [Horowitz Ch 7] of $3nV/\sqrt{Hz}$; a drift of $0.2\mu V/^{\circ}C$; and a gain bandwidth product of 8MHz. The feedback resistance chosen was 100kΩ.

The photodetector circuit was designed as a differential amplifier. An adjustable DC voltage was applied to the non-inverting input of the op-amp. This voltage cancelled any DC component coming from the photodetector. The OP-27 cannot drive any low impedance loads and hence requires buffering. This was accomplished by placing a LH0033CG buffer amplifier at its output. The photodetector circuit has an operating range from DC to beyond 1MHz.

The frequency stabilizer photodetector[1] circuit consists of a reverse biased EG&G FND-100 being amplified by a Philips NE-5212 transimpedance amplifier. This amplifier is specifically designed to operate as a transimpedance amplifier. It has a current noise density [Horowitz Ch-7] of 2.5pA/√Hz, and a 140MHz operating bandwidth.

The NE5212 has one input and two complimentary outputs. We are looking for signals that are at RF frequencies (above 2MHz) and hence only require the AC component of the photocurrent. The outputs are passed through an RF transformer to extract the AC signals. Once again, the signal at the output of the RF transformer is passed through a LH0033CG for buffering. The photodetector has a an operating frequency range from ≈2MHz to beyond 100MHz.

5.5   THE PID

The development of a correctly functioning PID was by far the most challenging task of this project. Difficulties arose when we tried to make high speed operational amplifiers into integrators and differentiators. Our first attempts were with LH0032CG op-amps, but we found that they could not be used as anything other than proportional amplifiers. Oscillations would set in if they were configured as integrators or differentiator.

Initially, we tried to design the PID circuit so that it was compact and universal. The circuit design is shown in fig. 5.5-1. It was not possible to build this circuit so that the three sections functioned independently. In hindsight, the poor isolation is probably due to, firstly, insufficient buffering and also the use of the LH0032CG amplifiers in the circuit. The LH0032CG amplifiers are constructed in metallic cases and require very good shielding and grounding to ensure minimal pick-up.

The phase characteristics of the LH0032CG was another factor that needed to be addressed if it was to be used in a PID circuit. As mentioned earlier this amplifier has appreciable phase lag from 100kHz on. More modern amplifiers such as the OP-61 and LM6361 have much better phase characteristics. Their phase lag only becomes evident at frequencies well above 1MHz. These chips are inexpensive

---

[1] This circuit was designed by C. Penn during his stay in 1990/91.

compared to the LH0032CG amplifier, and circuit designs are much easier because the new chips come in 8 pin DIL configuration rather than the 12 pins in a square shape.

The final PID designs are shown in appendix B. We decided to isolate each stage of the PID by placing each stage on a different PCB. One circuit was designed which could be constructed into a P, I, D, summing amplifier, or pre-amplifier. This arrangement made the PID versatile, and easily interchangeable. We also found this was more convenient experimentally.

CHAPTER 6

RESULTS

INTRODUCTION

There are many methods measuring the performance of a stabilization system. As an example, the frequency stability can be measured by recording the Allan variance [see appendix A and Wallard 73] of two identical lasers; or by examining the residual noise on the systems' error signal; or by a direct experimental measurement. It was not possible to measure the Allan variance because there was insufficient equipment and time. We were, however, able to investigate the performance of the stabilization unit using the remaining two methods.

This chapter will present the stability performances of both the frequency and the intensity stabilizers. The performance of the stabilizers is demonstrated through error signal analysis. I also presented the results of two experiments that were designed to test the performance of the stabilization unit. These experiments did not give conclusive evidence of the stability of the laser due to experimental difficulties that will be discussed later.

6.1   THE FREQUENCY STABILIZER

The frequency stabilizer used in all the experiments was a simplified version of the system discussed in section 4.1.2. The experimental arrangement of the external stabilizer is shown in fig. 6.1-1. The laser field was phase modulated by an EOM, an AOM was used as the frequency control element, and the reference cavity was either the Tropel confocal cavity (hole burning experiment) or the Newport SuperCavity (high resolution spectroscopy experiment and error signal analysis). We had the option of placing the EOM after the AOM, in the reference cavity arm,

but this increases the number of optical components needed to derive the locking error signal so we chose to have the EOM as shown in fig. 6.1-1.
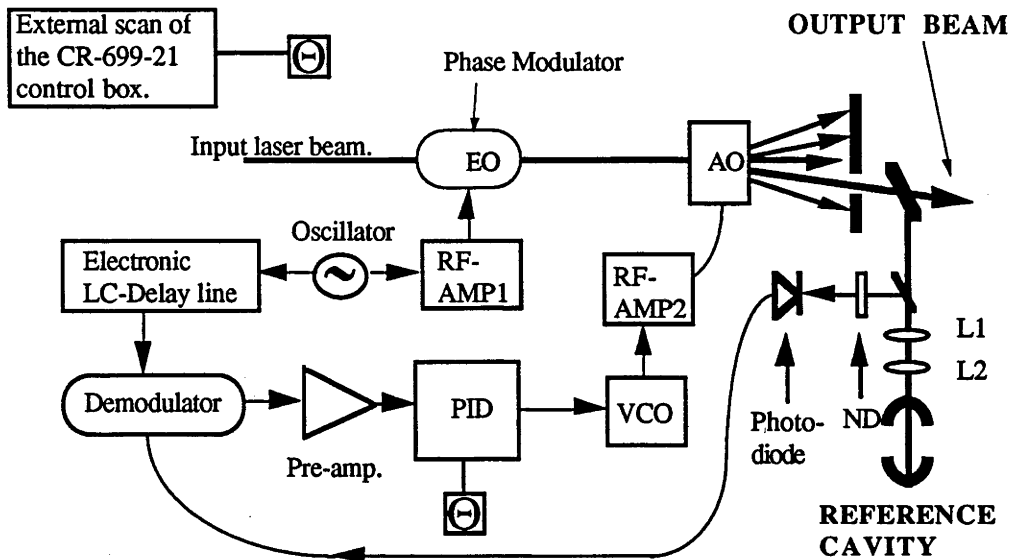

Fig. 6.1-1. The external stabilization system changes the frequency in two stages. The error signal is derived by detecting the response of the reference cavity to frequency modulated light (typically 10MHz FM signal). The low frequency error components are sent to the external scan input of the 699 (corrections < 200Hz), and the high frequency error components are sent to the AOM. The points marked as ϕ are linked together.

In this set up the AOM (Inrad/Matsushita EFL-120) operating at 120MHz is used as the frequency correcting element. The AOM crystal was made from TeO_2 which has a speed of sound equal to 4260m/s. The wavelength of the grating is thus 35.5μm. Hence, the greatest efficiency is achieved when the laser spot size is smaller than 35.5μm. The dye laser light is first sent through an EOM (Lasermetrics Model 1039D), which frequency modulates the light, and is then passed through the AOM. Typically, an RF power of 20-25W (RF-AMP1 was an EIN Model 325LA RF Power Amplifier) was sent to the EOM to produce ≈ 5% modulation of the laser beam.

The first order Doppler shifted beam from the AOM is selected to be stabilized. A beam splitter takes a portion of this beam and sends it to the reference cavity. The beam is mode matched into the cavity [Anderson 84, Sampas 90, Penn 91] using the appropriate focussing lenses (L1 & L2), and the reflected light off the cavity is sent to a photodiode (PD - custom designed circuitry around an FND 100 working in transimpedance mode, see section 5.4).

The locking error signal [Section 2.3.1.4] (ES) was derived from the reflected light off the reference cavity by demodulating the PD signal with respect to the FM local oscillator (LO), and applying an appropriate phase delay between the LO and the PD. The modulation frequency used was 10MHz, which was ≈100 times as large as the bandwidth of the SuperCavity and ≈ 3 times as large as the bandwidth of the Tropel. The phase delay was controlled by passing the output of the RF oscillator signal (National AM/FM Signal Generator Model VP-8177A) into an electronic LC delay line (EG&G/ORTEC Model DB-463 Delay Box). Delays of typically 32ns could change the phase from one quadrature to the other.

The demodulator used was a Mini Circuits double balanced mixer (DBM - ZP 10514). The error signal produced by the demodulation process was first sent to a buffer amplifier and then pre-amplifier, before being passed through the PID. The Buffer and pre-amp stages were constructed using the amplifiers discussed in section 5.5. The amplification stage increases the signal from the demodulator from 40mV to over 10V (i.e., about 50dB gain).
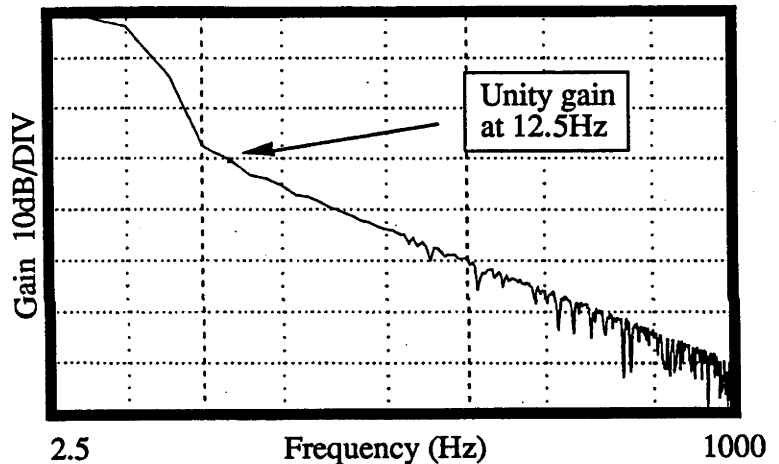

Fig. 6.1-2a. Magnitude Bode plot for the low frequency integrator stage sent to the external scan of the CR-699-21 control box.

The PID has two output channels. The first has high gain at low frequencies and was sent to the external scan input of the CR-699-21 control box. The circuit diagram for this section is shown in appendix
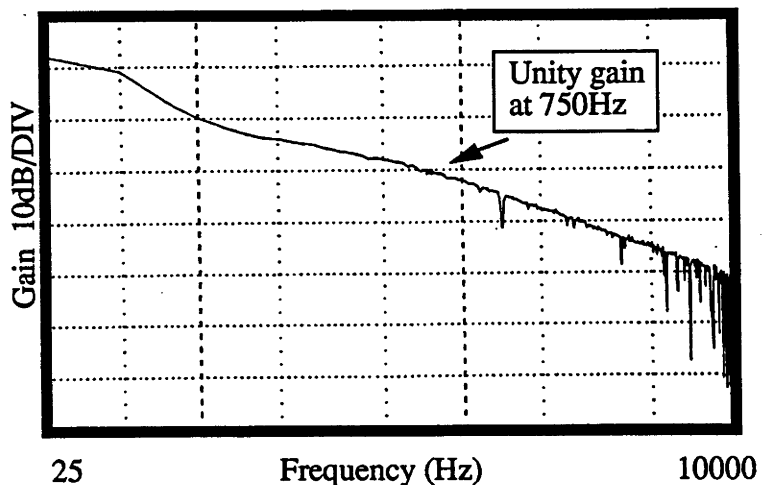

Fig. 6.1-2b. Magnitude Bode plot for the integrator stage sent to the VCO.

B. Channel two was sent to the VCO and had its low frequency gain limited, so as not to compete with the first channel. This limitation was imposed by holding the gain to a fixed value using a gain limiting feedback resistor. The magnitude Bode plots for both sections are shown in figure 6.1-2.

Finally, the VCO output was amplified to the power required to drive the AOM using an RF amplifier (Mini-Circuits ZHL-1A). The time required for the VCO/RF amp./AOM chain to alter the laser frequency is measured by monitoring the spacial sweep of the laser beam induced by a sinusoidal modulation of the AOM's drive frequency. It was observed that the chain could respond to sinusoidal modulations approaching 1MHz. However, the laser beam had to be passed very close to the AOM's RF sound wave transducer in order for this response to be obtained. If the laser was displaced by as little as 1mm away from the transducer then the frequency response drops to 200-300kHz This indicates that the time delay in setting up the diffraction grating is $\approx 1\mu s$ near the transducer and increases to $\approx 4\mu s$ as the spot is moved 1mm away from the transducer.

6.2   ERROR SIGNAL ANALYSIS

Both the system's error signal and the laser field transmission through the reference cavity can be used to judge the stability of the control loop. In this section an analysis of these signals will be presented.

Let us start with an analysis of the Pound/Drever error signal. A typical, experimentally obtained error signal is shown below (fig. 6.2-1a). This signal is recorded after the pre-amp stage of fig. 6.1-1 on a Tektronix 2211 digital storage oscilloscope. A modulation frequency of 10MHz was used, hence a capture range of 20MHz is possible.

The slope of the curve at the centre of the error signal (lock point) gives us the transfer function (D(f$\Rightarrow$v) section 2.1) of the frequency discriminator (also see Appendix A). This has been measured to be 2.5kHz/V using fig. 6.2-1b, which shows the central slope on an expanded scale. The residual error signal obtained in the lock loop is shown in fig. 6.2-1c. This figure shows that the average deviation

around the lock point is ≈ 8V, which is equivalent to a 20kHz frequency variation.

A second feature to note from fig. 6.2-1c is that the fluctuations in frequency are occurring at ≈ 200kHz. Either we were exciting some resonant frequency at 200kHz, or we were observing the effect of the build-up time of the reference cavity. The Bode plots for the two stages of the PID, shown in fig. 6.1-2, indicate that excitation of a resonance at 200kHz is unlikely because the PID has very low gain at high frequencies. It seems more likely that the build-up time was the cause of the oscillatory motion of the error signal. In fact it is possible to reduce the oscillations at 200kHz frequencies by adding the P and D channels to the VCO loop [Sellars 91]. However, we did not add the P and D to the servo loop because it was not necessary for the experimental work. This method gives an accurate indication of the servo loop stability. This is the standard method used by most manufacturers when they quote the stability of their lasers.
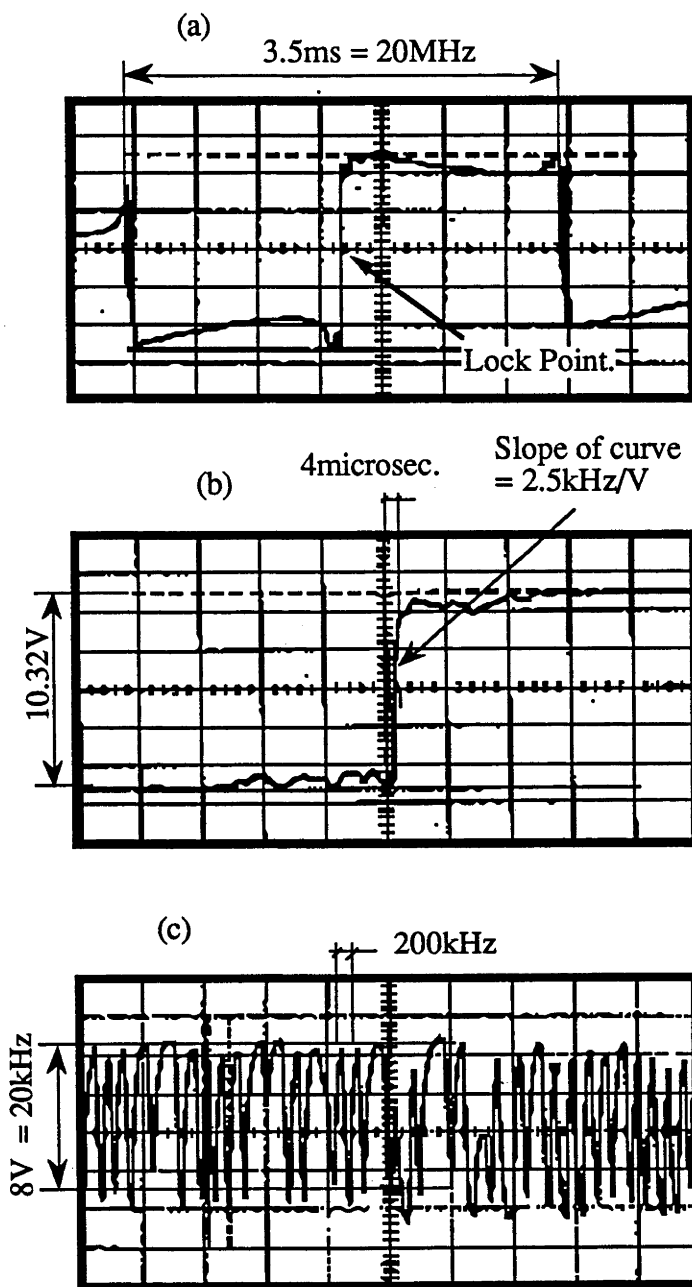
Fig. 6.2-1. Experimentally obtained Pound/Drever signal.
(a) the Pound/Drever signal;
(b) expansion of (a) to show the slope of the central feature;
(c) the residual error signal obtained while the laser was locked to the SuperCavity.

A second test of the performance of the stabilizer was obtained by measuring the

signal transmitted through the reference cavity (SuperCavity in this case; see appendix A for an explanation of the measurement process) . Figure 6.2-2 is an experimentally obtained diagram of the transmitted field through the reference cavity (top) and the transmitted field when the laser is locked to the reference cavity (bottom). The laser frequency was locked to within 15% of the peak transmission. Assuming that the laser frequency was oscillating symmetrically around the peak of

Fig. 6.2-2a. Transmitted field through the reference cavity (Newport SuperCaviy). This figure shows the FM sidebands at 10MHz.

Fig. 6.2-2b. Laser field locked to 15% of the peak of the reference cavity transmission.

the transmission function and that the transmission can be approximated by a triangular function, the results corresponds to a frequency variation of $\approx$ 50kHz. This is twice as large as the value obtained from the residual error signal. However, the laser could have been locked to one side of the peak (a common occurrence) implying that the frequency variation would be less than 25kHz, which is in agreement with the error signal analysis. This technique is not reliable since the Airy function is not linear around peak transmission. It does, however, indicate that we were in fact locking to within a few tens of kHz to the resonant frequency of the reference cavity.
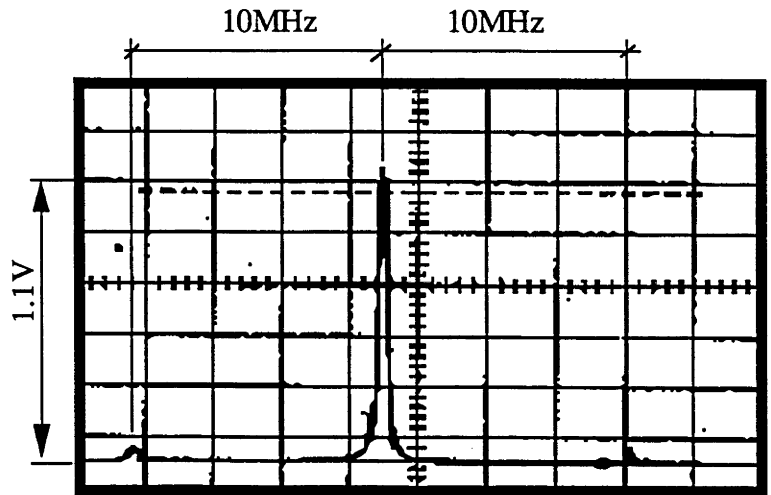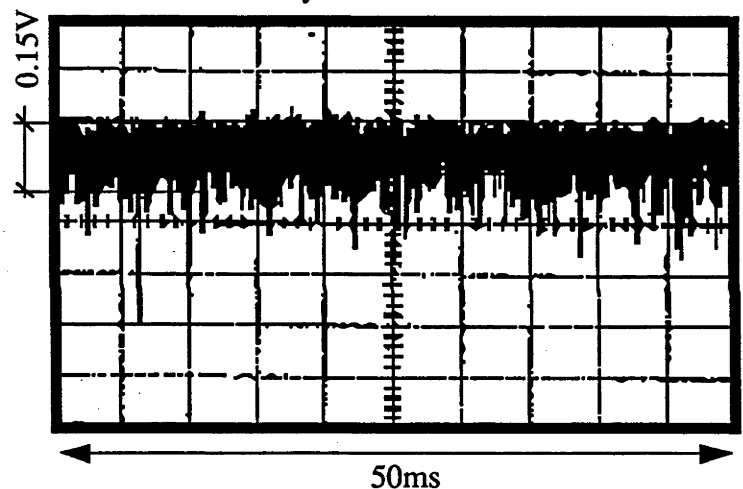
6.3 EXPERIMENTS PERFORMED USING THE STABILIZATION UNIT

Two experiments were carried out to demonstrate the capability of the external stabilizer and in attempt to determine directly the laser linewidth. The first was a spectral hole burning experiment performed in collaboration with Dr. P.T.H. Fisk & Mr. M. Sellars at their laboratories in the Laser Physics Centre, Research School of Physical Science, ANU. The second was an experiment on saturated absorption in an atomic vapour carried out at the ANU with the assistance of Dr. R.J. McLean and Dr. P. Hannaford from CSIRO Division of Materials Science and Technology. The experiments were designed and the results were interpreted by my co-workers. My input was to supply a stabilized laser for the experiments. The techniques used are summarized in the following sections.

6.3.1 SPECTRAL HOLE BURNING IN A SOLID

Spectral hole burning [Siegman 85, Ch. 30] is a phenomenon that can occur in certain crystals. This is a process where we saturate one of the crystals electronic transitions with an optical field (the pump) and probe the population by sweeping a second beam through this transition. The pump 'burns a hole' in the ground state population of the crystal making this spectral region transparent to the probe field. The width of the hole is dependent on the decay rate of the transition, collisional damping, and the stability of the laser source. There are many crystals that have transitions with decay rates on the order of 1ms [Fisk 91]. We therefore require a laser source that has frequency noise in the kHz regime to probe these transitions.

The experiment was designed to probe the material $K Eu (WO_4)_2$. This material was placed inside a cryogenic chamber where it was examined by two light fields. The first field was passed through an EOM and then an AOM operating at 85MHz, and the second field was passed through an AOM operating at 50MHz. The beam at +50MHz (relative to the unshifted beam), and the beam at +85MHz were selected to produce the pump and probe beams, respectively. These two beams were passed (almost collinearly) through the sample so that they were examining the same atoms. The experimental arrangement is shown in figure 6.3.1-1.
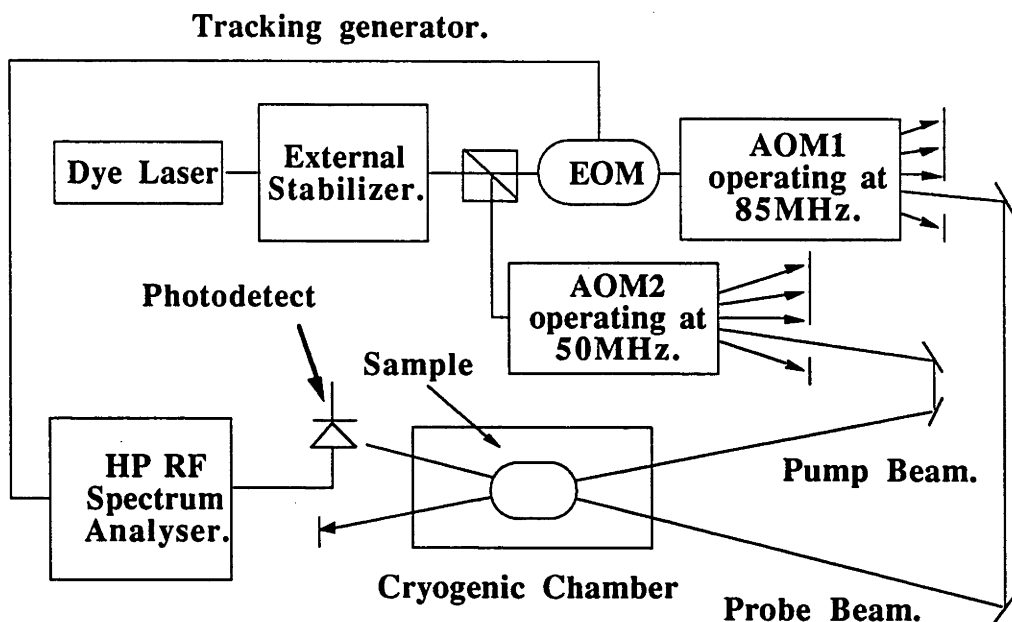
Tracking generator.

Fig. 6.3.1-1. Experimental arrangement of the hole burning experiment.

An RF phase modulation was superimposed onto the 85MHz beam by passing the beam through the EOM oscillating at an RF frequency, which was taken from the tracking generator output of the Hewlett-Packard RF Spectrum Analyser. The resulting field had frequency components at (85MHz and 85MHz± tracking generator frequency). In the experiment the probe field was one of the sidebands generated by the phase modulation. We monitored the transmission of the probe field through the sample using a photodetector. The tracking generator was swept from 25MHz to 45MHz so that the probe could be scanned through the pump without altering the initial laser frequency.

Figure 6.3.1-2 shows results obtained using externally stabilized laser light (locked to a Tropel cavity in this case) to produce a hole in the material K Eu (WO$_4$)$_2$. The top traces show the hole profile & background of the dye laser in actively stabilized mode, and the second set of traces show the hole profile & background with the external stabilization on. The hole width was reduced from ≈ 2MHz FWHM to ≈ 1MHz FWHM, and the background noise was also reduced by the external stabilization. This experiment illustrated that the hole width was narrowed when we used the stabilizer. It was not, however, able to give a definite value for the frequency stability of the external system. The hole produced by our external stabilization was later shown [Sellars 92] to be limited by the crystal not the laser source. Sellars showed that hyperfine pumping with an RF field allows significant reduction (≈ 1-10kHz FWHM) of the hole width. Without the RF pumping the
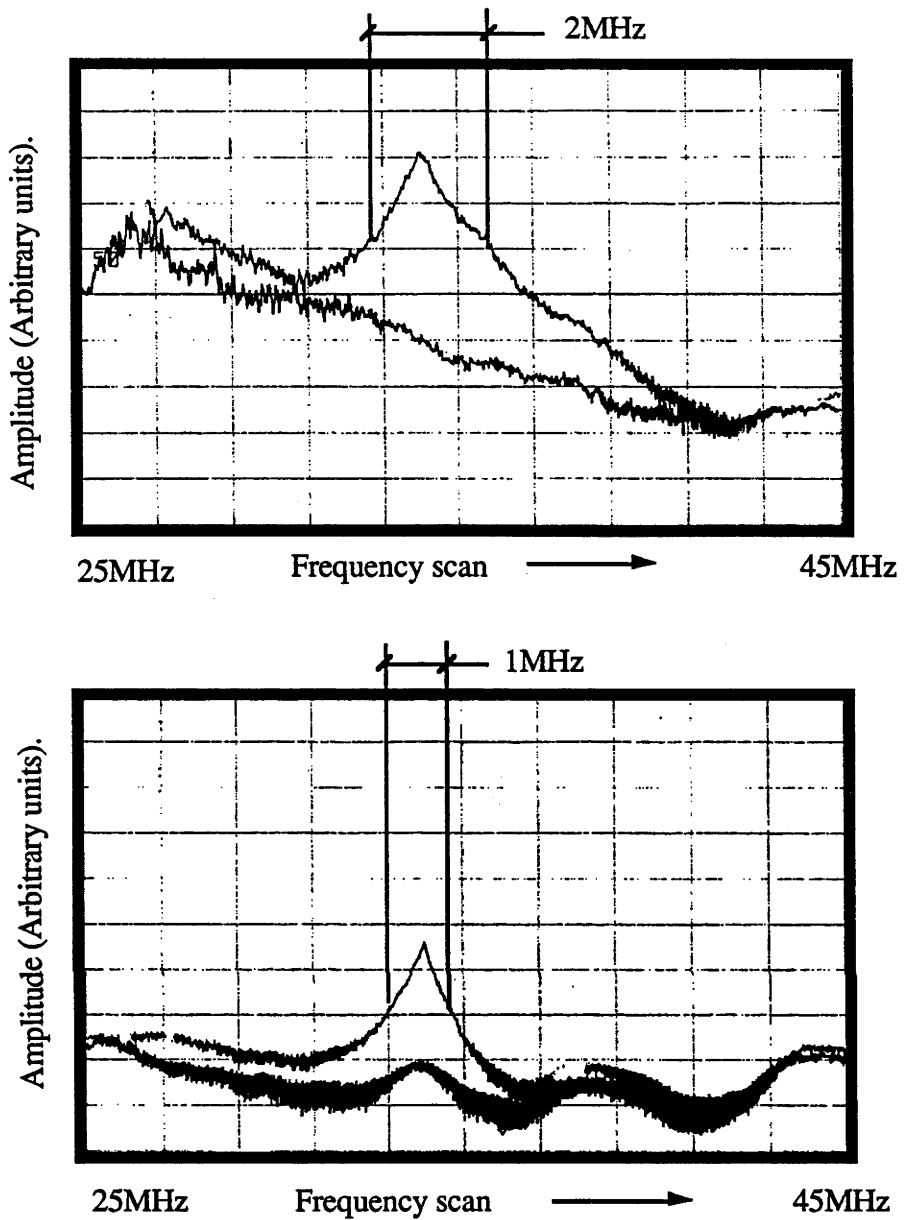
Fig. 6.3.1-2. Results of hole burning experiment. The top traces were recorded with the laser locked to its internal cavity only. The two scans are the signal and the background scans. The bottom traces are with the laser externally locked using only an AO in feedback. The linewidth of the hole was reduced from ≈ 2MHz to ≈ 1MHz.

hole width could not be reduce further than is shown in fig. 6.3.1-2 because collisional damping of the excited electrons was too great.

6.3.2 HIGH RESOLUTION LASER SPECTROSCOPY IN AN ATOMIC VAPOUR

The second experiment was designed to probe a narrow linewidth transition in Samarium [Hannaford 86], (λ = 5874.21Å : $4f^6 6s^2$ $^7F_2$ -> $4f^6 6s6p$ $^7F_3^0$, lifetime $\tau \approx$ 100ns and linewidth $\approx$ 100kHz) using the standard saturated absorption [Siegman 85 Ch. 30] setup, which consists of excitation of an atomic vapour using collinear and counter propagating beams. The linewidth has thus far been estimated to be less than 5MHz by CSIRO in both sputtering [McLean 86] and thermal discharge cells. Smaller linewidths could not be obtained due to the limitations of the laser used for those measurements. Our externally stabilized laser should allow us to eliminate laser noise from the experiment, and hence measure sub-megahertz transition linewidths.

The cells are manufactured at CSIRO in Melbourne out of Pyrex formed into a cross shape, and are fitted with windows, as shown in figure 6.3.2-1. They have demountable conical bases housing two tungsten pins to which the electrodes and heating filaments are spot-welded. The cell and base are vacuum sealed together using a thin coating of black wax. A home built glass vacuum system is used to pump the cell down to $\approx$ 1E-5 Torr.

The sputtering cell creates an atomic vapour by electron bombardment of the sample. A buffer gas is required in the cell (to limit the current flow between the electrodes),
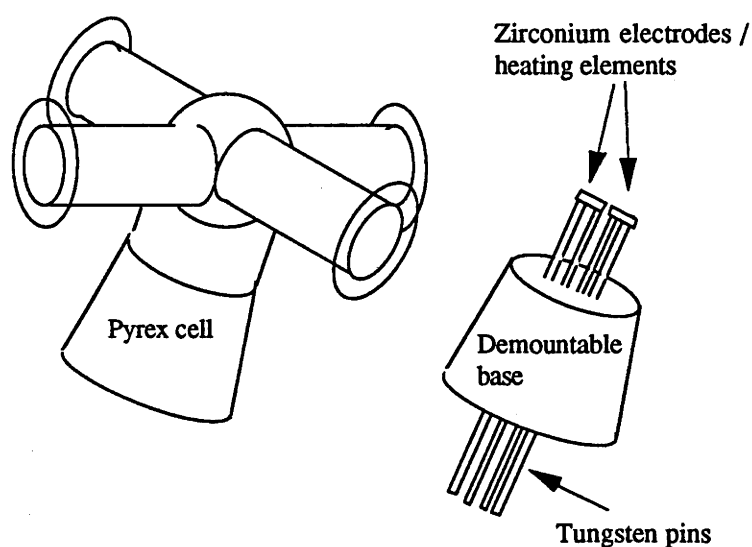

Fig. 6.3.2-1. Diagram of the cell used in the experiment (supplied by CSIRO Division of Material Science and Technology).

typically 0.01 to 0.1 torr of an inert gas such as Xenon or Argon. Typical voltages and currents are 1500V at 1mA to 3000V at 10mA respectively.

The thermal cell creates an atomic vapour by heating the sample. No buffer gas is used in the cell, hence collisional broadening is kept at a minimum. High currents are required to bring the filament to a temperature that will vaporise the sample, typically 10 - 12A at 5V. The current subjects the sample to a large magnetic field which acts to broaden the transition via the Zeeman effect. We minimise the effect of the magnetic field on the sample by sending an equivalent current in the reverse direction placed in close proximity (2mm) to the heating filament.

The experimental arrangement is shown in figure 6.3.2-2. The dye laser output was passed through the frequency stabilization stage (EOM and AOM1) via a 3.0 dioptre focussing lens so that the spatial waist was at the AOM1. The beam was defocused with a second 3.0 dioptre lens to return the laser beam to its original condition. One of the first order diffracted beams from AOM1 was allowed to proceed to the experiment. A second unused beam was sent to the wavemeter for gross wavelength selection. All other beams were blocked at this point using an aperture. Beam splitter 1 (BS1) divided the experimental beam into two, sending 70% to the saturated absorption experiment and 30% to the analysis section.

The saturated absorption experiment was arranged in a triangular shape. A pellicle selected $\approx$10% of the beam and sent it via a folding mirror through the Sm cell. This beam was used as the probe beam. The remaining 90% was used as the pump beam. This beam was first sent through a AOM2 (80MHz), which was being used as a high frequency chopper ($\approx$100kHz). We were using a high chopping frequency to overcome the formation of pedestals on the saturated absorption signal arising from velocity changing collisions [Willis 89]. Once again the laser beam was focused-defocused through the AOM using a pair of 3.0 dioptre lenses. An aperture was used to select one of the first order diffracted beams and a folding mirror sent it through the Sm cell. The pump and probe were aligned such that they counter propagated precisely through the cell, using the folding mirrors. An aperture and a ND filter were placed in each beam to limit the beam's diameter and power. The probe signal was selected using a microscope objective and sent to a DC PD (UDT PIN 6), amplifier and then passed to a lock-in amplifier (Princeton Applied Research Model 5204 : reference frequency being the chopping frequency of AOM2). Both in-phase and quadrature signals were sent to the data acquisition system (DAS).
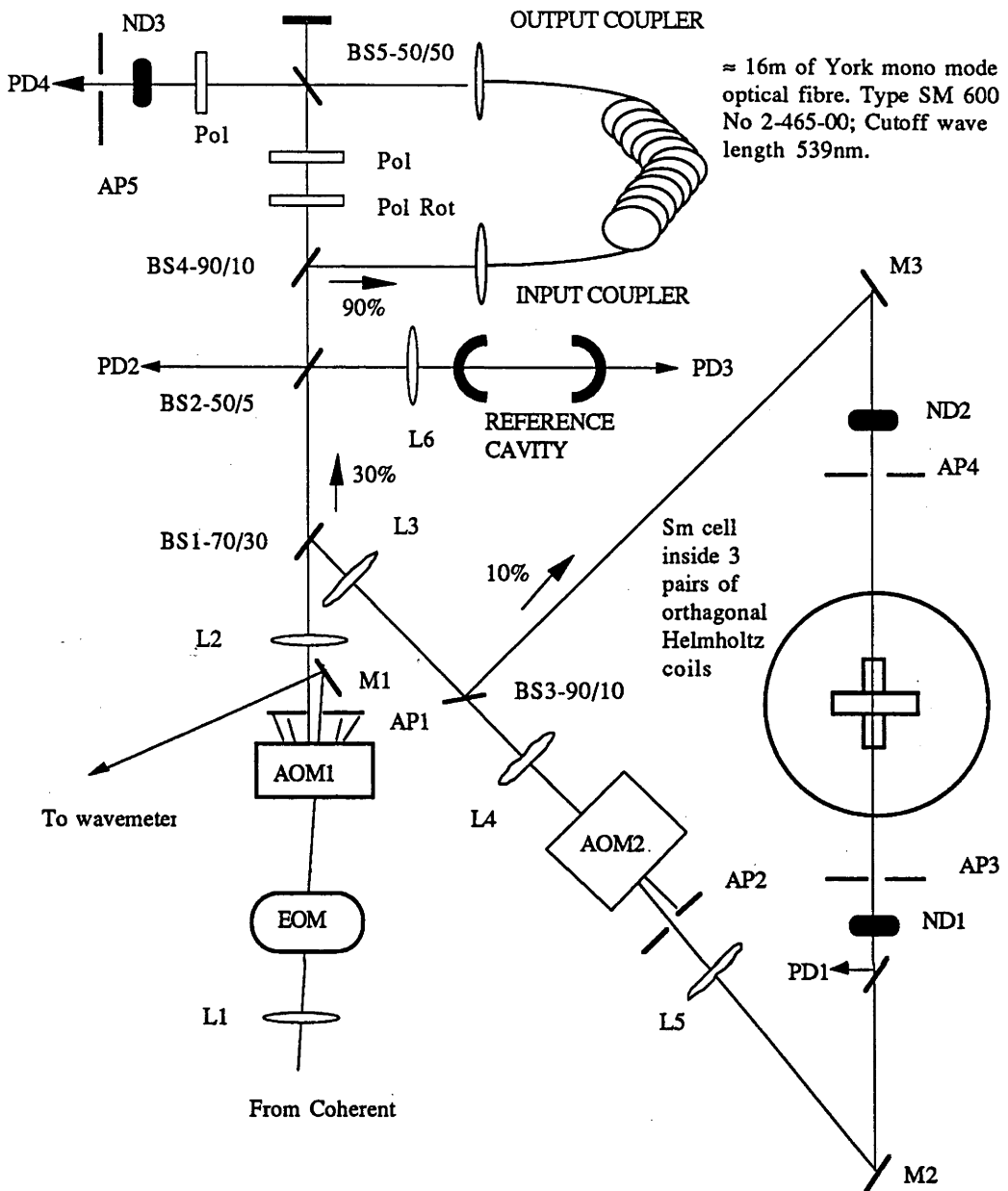
Fig. 6.3.2-2. Schematic representation of the three stages in the experiment. L = Lens; M = Mirror; PD = Photo Diode; AP = Aperture; BS = Beam Splitter; ND = Neutral Density filter; Pol = Polarizer; Pol Rot = Polarization Rotator. The output of PD1 is sent to a lockin amplifier and then to the data acquisition system (DAS). The output of PD2 is sent to stabilization electronics and a digital storage oscilloscope. The output of PD3 is sent to the reference cavity control box and a digital storage oscilloscope. The output of PD4 is sent to a lowpass filter and then to the

The analysis section consisted of the reference cavity (for frequency stabilization as discussed earlier), and a home built (17.2 ± 0.5)MHz Mach-Zehnder interferometer for scan length calibration. In one arm of the interferometer there was ≈16m of single mode optical fibre (York mono mode optical fibre: type SM600; No 2-465-00; cutoff wavelength 539nm) with appropriate input and output couplers. The second

arm had a polarization rotator and a polarizer which were used to balance the intensity and polarization in each arm. BS3 sent 90% of the light to the fibre and 10% through the other arm. The two beams were recombined on BS4 (50-50 BS). The recombined beams are sent to a DC PD via a polarizer and pinhole aperture, the signal from this is then sent to the DAS via a low pass filter. The fibre interferometer has been calibrated against a commercial Tropel (300 ± 0.5)MHz FP confocal optical spectrum analyser and is shown in figure. 6.3.2-3.
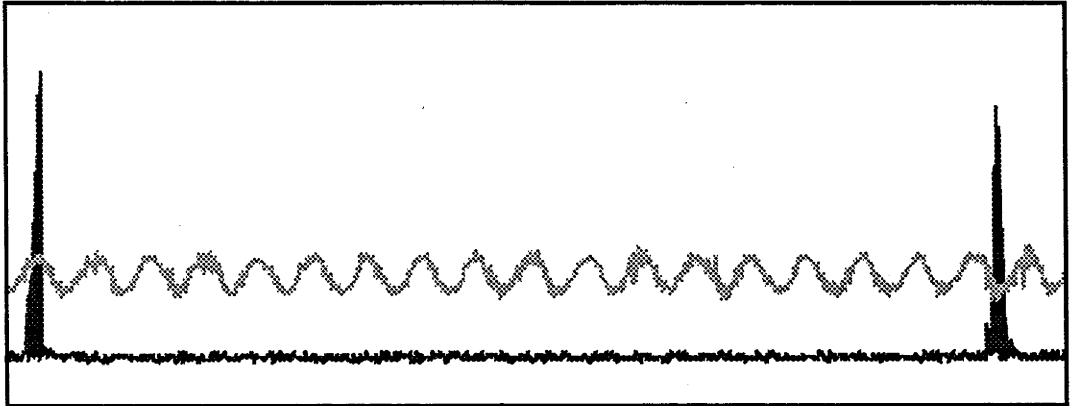

Fig. 6.3.2-3 Calibration of the home built Mach-Zehnder optical fibre interferometer using a commercial Tropel confocal Fabry-Perot interferometer. The Tropel has a FSR of 300MHz, as is indicated, and the Mach-Zender has ≈ 17.5 fringes over that frequency span. Its FSR is thus ≈ 17.2MHz.

Below are the results obtained on the 30th of May 1991 using the experimental arrangement shown above. The curves show the profile of the electronic transition mentioned earlier.

Figure 6.3.2-4 is the profile obtained by examining the line with a dye laser that is locked only to its own reference cavity. The measured FWHM of the line was 5.4MHz, and the profile appears to be asymmetric and noisy.

Figure 6.3.2-5 shows the profile of the line as obtained in a sputtering cell when the laser was locked to an external reference cavity using an AOM as the frequency correcting transducer. The FWHM of this profile is 3.3MHz. The profile in this case is symmetric, and there is, as expected, some broadening in the wings. This broadening could be due to many mechanisms but the most likely is velocity changing collisions, as the pressure of the buffer gas was high and could not be reduced because of restrictions imposed by our voltage supply.
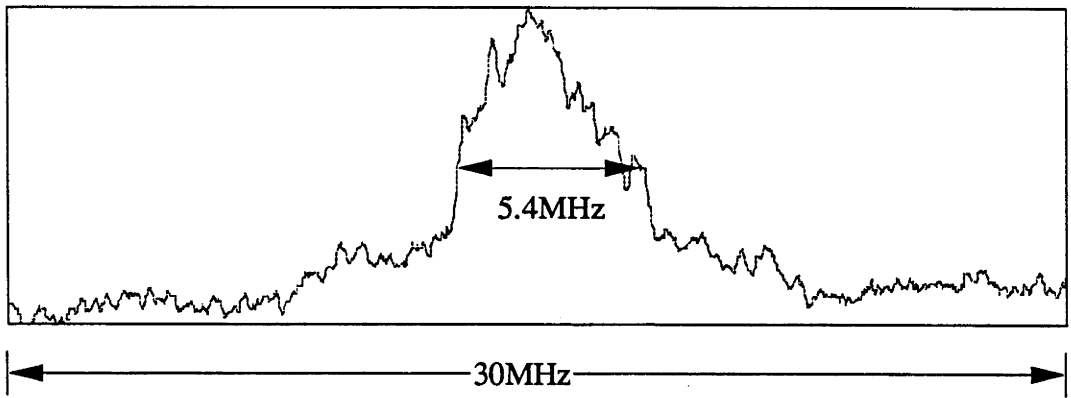
5.4MHz

30MHz

Fig. 6.3.2-4. Line profile obtained using internally stabilized dye laser. Pump power = 0.15mW; Probe power = 0.015mW; < 20% absorption of pump; Beam Diameter ≈ 2mm.

Pedestals from VCC or possibly unresolved hyperfine structure.
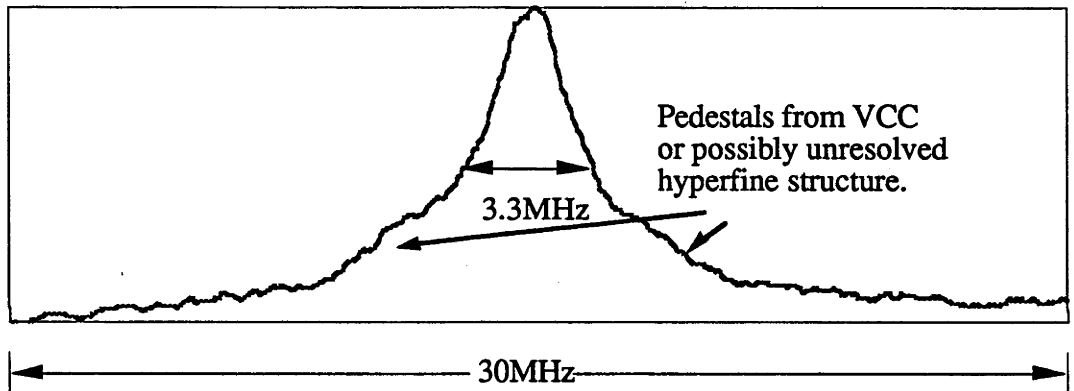
3.3MHz

30MHz

Fig. 6.3.2-5. Line profile obtained using external stabilizer whilst examining a sputtering cell. Pump power = 1.6mW; Probe power = 1.6mW; < 20% absorption of pump; Beam Diameter ≈ 2mm; 0.3cm Xe buffer; Sputtering cell current = 6mA, and voltage = 1700V.

2.2MHz

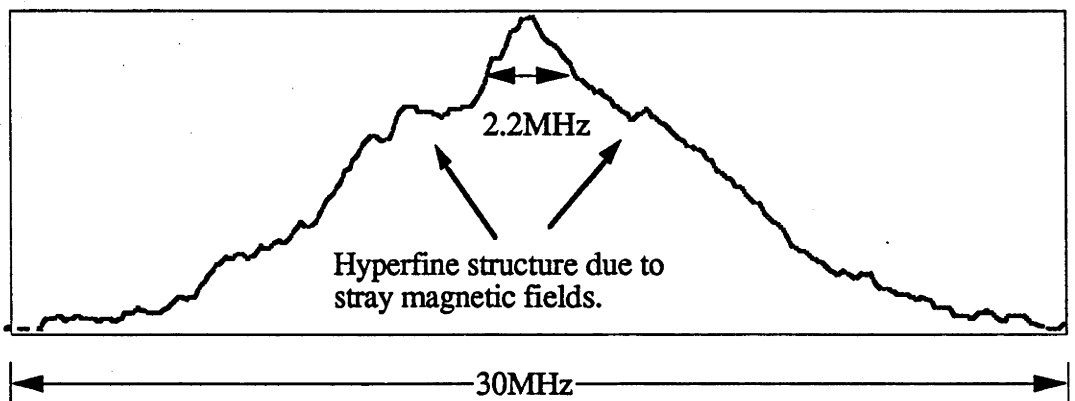Hyperfine structure due to stray magnetic fields.

30MHz

Fig. 6.3.2-6. Line profile obtained using external stabilizer, and examining a thermal cell. Pump power = 0.15mW; Probe power = 0.015mW; < 20% absorption of pump; Beam Diameter ≈ 2mm; Thermal cell current = 11A, and voltage = 12V.

Figure 6.3.2-6 is a profile obtained in a thermal cell. The width stated is the minimum resolvable linewidth and not the FWHM. The broadening seen in this profile is splitting of the hyperfine structure due to large local magnetic fields generated by the current in the heating element. The secondary peaks observed in the profile support this deduction. We were unable to measure the magnetic field experienced by the atoms because of technical difficulties with the cell.

The results obtained in this experiment were able to show that conventional dye lasers are unable to probe the profile of electronic transitions that have linewidths of the order of 1MHz or less. Figures 6.4-4 illustrates that the profiles obtained by commercial lasers are poorly resolved because of the excess intensity noise on the signal due to frequency noise from the laser.

Figure 6.3.2-5 illustrates that the line profile can be dramatically improved by external frequency stabilization of the laser light. Both intensity noise on the line and the width of the line are reduced by the external stabilization. The profile obtained is symmetric and $\approx$3.3MHz FWHM. The raised section in the wings of the line could be due either to velocity changing collisions or Zeeman splitting of the hyperfine structure. We could not investigate this further due to experimental time restrictions and unavailability of appropriate voltage supply for the sputtering cell, as mentioned earlier.

The profile obtained in figure 6.3.2-6, taken in the thermal cell, shows that the locking system enables us to resolve structure that is ≤ 2.2 MHz. The broadening of the profile and the two secondary peaks on the profile are attributed to large localised magnetic fields present in the cell that are generated by the current through the heating element. These results couldn't be repeated because of time restrictions and technical problems with the cells.

Unfortunately, we were unable to produce the appropriate conditions in the test cells that would give the narrowest line profiles (low pressure <1 Torr, high potential > 1000V). Hence, the main result obtained from these experiments is that the frequency jitter on the laser, which is manifested as intensity noise on the line profile, can be reduced by the external stabilization system built at this university. As a consequence of our stabilization, the width of the smallest resolvable feature is considerably less than can be obtained by commercial devices.

6.4 THE INTENSITY STABILIZER

The intensity stabilizer developed was discussed from a theoretical point of view in section 4.2.2, (see fig.4.2.2-1). The intensity stabilizer's performance was tested experimentally by Ms. D.M. Hope in the experiment shown schematically in figure 6.4-1. She was investigating quadrature squeezing in a high transmission near-bistable cavity atom system [Hope 91]. The laser source was a Spectra-Physics 380D ring dye laser, which had about 2.5% intensity noise on its output (see fig. 1-2). Fluctuations of this magnitude buried the desired signal under noise. The intensity stabilizer was used to reduce the laser's intensity noise.
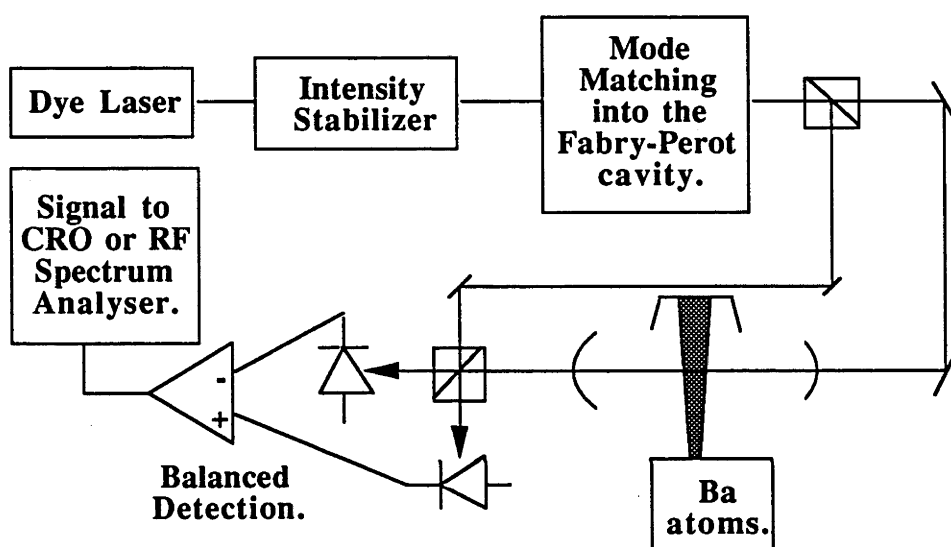
Fig. 6.4-1. Schematic of the squeezing experiment using this intensity stabilizer. I refer the reader to Hope et. al. 1991 for further details on the experiment.

The AOM (Isomet Model 1205C-2) was operated at a fixed frequency of 80MHz. A fraction of one of the first order diffracted beams was sent to a DC photodetector via a polarizer and neutral density filter. The photodetector signal was then sent to an integrator stage (see appendix B) of a PID (the proportional and differentiator stages were not required) and from there to a voltage controlled attenuator (VCA), Mini-Circuits Model ZAS-3. The VCA requires a 0 to 1.5V signal to give an output from 0 to maximum input (the VCA operates from DC to 10MHz). The RF oscillator signal was generated by a National Signal Generator. The output of the VCA was amplified by an INR RF power amplifier, to a power of 1W, which was the operating power of the AOM.

The integrator stage was designed to have maximum gain at low frequencies (up to

200Hz). The gain was set to approximately 40dB. It had a roll-off of -6dB/Octave (or -20dB/Decade), reaching unity gain at 9kHz. The DC component from the photodetector signal could be cancelled using an in-built DC offset adjustment. The phase of the output was also adjustable, it could be switched by 180^0. This was accomplished by sending the signal from the integrator stage through an inverting amplifier. The op-amps that amplified the output signal were powered by ±5V regulators mounted on the PCB. This regulation greatly reduced the stray noise as well as 50Hz mains pick-up, and power supply noise.

Figure 6.4-2 shows the performance of the intensity stabilizer. This graph shows that the residual noise on the laser has been suppressed to less than 0.4% from an initial noise level of 2.5% (see fig. 1-2). The period of oscillation of the residual error signal was ≈ 10ms, that is, ≈ 100Hz. The frequency is due to Argon ion laser fluctuation. The noise output could be improved further by increasing the gain and bandwidth of the control loop. This was not done as the achieved degree of stability was more than sufficient for the experimental work shown in fig. 6.4-1.
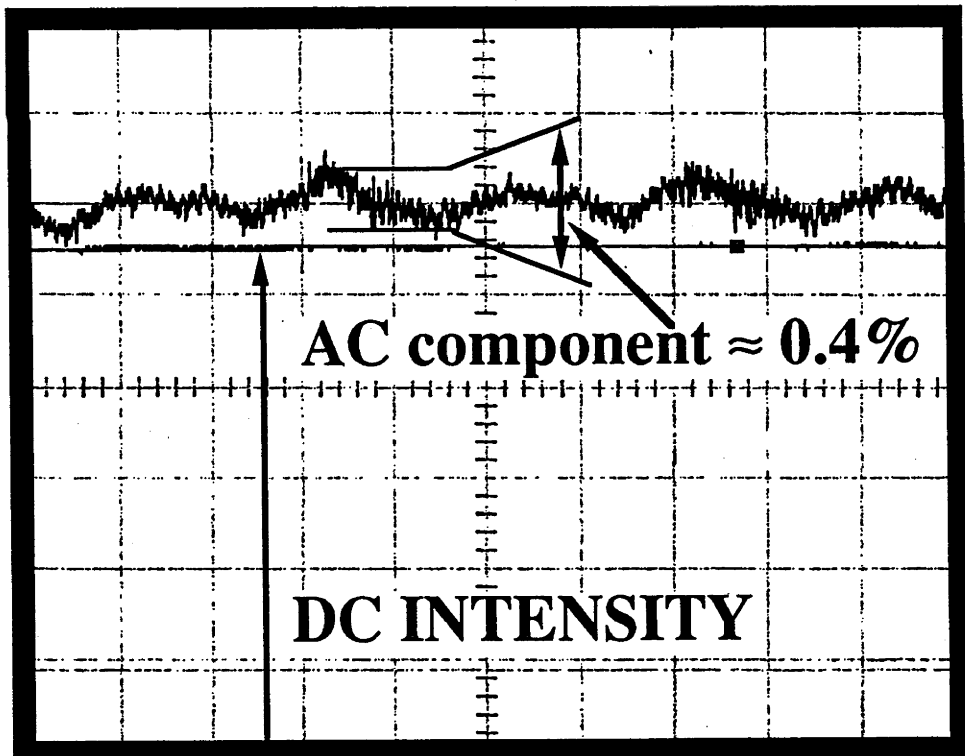
DC signal at 0.5V/DIV. AC signal at 20mV/DIV. Time base is 5ms/DIV.

Fig. 6.4-2. Performance of the intensity stabilizer. The residual noise on the laser beam is approximately 0.4%.

In conclusion, the results from the stability tests outlined in this section show that the linewidth of the laser was determined to have a long term stability of approximately 20kHz. This value was obtained from the calibration of the residual fluctuations of the error signal. This method proved, under these circumstances, to be the most reliable method for determining the stability of the lasers. Neither the transmission or the spectroscopic experiments could give a lower limit to the laser stability. The other techniques showed that the laser was locked to within 15% of the peak transmission, and that neither the hole burning nor the saturated absorption were any longer limited in resolution by the laser because the lasers linewidth was much less than the narrowest measured profile, 1MHz.

CHAPTER 7

CONCLUSION

To summarize, I have built an external stabilization unit for a ring dye laser that can be used to control the frequency and intensity of the laser. An AOM was the only control element in the feedback loop. The frequency stability of the dye laser was reduced from ≈8MHz to ≈20kHz (both measured over a 30 second time interval), and the intensity stabilization was reduced from ≈2.5% to below 0.5%. The stabilization unit satisfied the criteria set at the onset of this project. We were able to produce a single unit that could be used as a frequency and intensity stabilizer, as well as being an isolator.

I have measured the transfer functions of the elements in the feedback loop and designed and built the control electronics noting their properties. I have also given examples of spectroscopic experimental results that were improved by this stabilization unit.

A system with an EOM internal to the laser has been reported [Fisk 91, Sellars 92, Grezesik 85] to have frequency stabilities approaching 1kHz. However, the system is more complex to operate than our system. An additional element inside the laser cavity increased the difficulty in aligning and maintaining the power output for extended periods. Furthermore, the laser can not be used in its original form once the internal system has been setup because the laser control electronic needs permanent modification.

An AOM-EOM external system has been reported [Hall 90] to have reached frequency stabilities in the kHz regime. The advantage of this system is that the laser requires no modifications, however, it does require very specific design and fine tuning of the electronics to ensure success of the system.

In comparison with these stabilization methods our unit fares well. We can reach frequency stabilities three orders of magnitude better than commercial systems, which is more than sufficient for most spectroscopic applications. Our unit has the

additional advantage that it can be used simultaneously as an intensity stabilizer and isolator.

This work has shown that the delay time of the AOM is not a limiting factor in the performance of the stabilization system. The ability to alter the laser frequency (and intensity) at a MHz rate is sufficient to iron out most of the frequency fluctuations. A more important consideration is the build-up time (τ_B) of the reference cavity which can be greater than several microseconds. As we reduce the linewidth of the reference cavity, in an attempt to lock the laser frequency more tightly, we face the inevitable problem that the laser frequency information has an unavoidable delayed and phase shift imposed on it from the cavity. Consequently the servo can break into oscillation about the frequency ($1/\tau_B$).

APPENDIX A

NOISE

A.1   BASIC DEFINITION

This appendix is included in the thesis as a short tutorial of how we deal with noise. Ideally the optical field described by (A-1) is only measured by the detection system.

$$v_S(t) = a_S \cos(\omega t) \qquad \text{where } a_S \text{ is some amplitude.} \qquad \text{(A-1)}$$

However, the field (A-1) is influenced by many kinds of stray noise. Before discussing these noise sources I shall introduce the basic definition of noise.

A noise field, $v_N(t)$, has a component in-phase with the signal (A-1) and a component in-quadrature with the signal.

$$v_N(t) = a_{NC}(t) \cos(\omega t) + a_{NS}(t) \sin(wt) \qquad \text{(A-2)}$$

The amplitudes of the quadrature components, $a_{NC}(t)$ & $a_{NS}(t)$, are time varying quantities that have ramdom magnitudes. They are also uncoralated. The total field at a detector due to both signal and noise is given by :

$$
\begin{aligned}
v(t) &= a_S \cos(\omega t) + a_{NC}(t) \cos(\omega t) + a_{NS}(t) \sin(wt) \\
&= \text{Re}\left\{ [a_S + a_{NC}(t) - ja_{NS}(t))] e^{j\omega t} \right\} \\
&= \text{Re}\left[a(t) e^{j\omega t} \right]
\end{aligned}
\qquad \text{(A-3)}
$$

In order to obtain the noise components in the field v (t) we need a knowledge of the various frequencies contained within the field. The Fourier transform $V(\omega)$ of

v (t) gives us that information. That is,

$$V(\omega) = \frac{1}{2\pi} \int_{-\infty}^{\infty} v(t) e^{-j\omega t} \, dt \qquad \qquad \text{(A-4)}$$

&

$$v(t) = \int_{-\infty}^{\infty} V(\omega) e^{j\omega t} \, d\omega \qquad \qquad \text{(A-5)}$$

In principle an infinite time is required to evaluate $V(\omega)$ precisely, however, this is not practical. Instead we measure over a time period T and consider the function v(t) to be zero for $t \le -T/2$ & $t \ge T/2$ making (A-4) & (A-5)

$$V(\omega) = \frac{1}{2\pi} \int_{-T/2}^{T/2} v(t) e^{-j\omega t} \, dt \qquad \qquad \text{(A-6)}$$

&

$$v(t) = \int_{-T/2}^{T/2} V(\omega) e^{j\omega t} \, d\omega \qquad \qquad \text{(A-7)}$$

T is known as the integration time of the system.

The instantaneous power in the field v(t) is given by $P = v(t) v*(t)$. The average power is thus:

$$P = \frac{1}{T} \int_{-T/2}^{T/2} v(t) v*(t) \, dt \qquad \qquad \text{(A-8)}$$

or

$$P = \frac{2\pi}{T} \int_{-\infty}^{\infty} V(\omega) V*(\omega) \, d\omega$$

$$= \frac{4\pi}{T} \int_{0}^{\infty} V(\omega) V*(\omega) \, d\omega \qquad \qquad \text{(A-9)}$$

If we define the *spectral density function* , $S_v(\omega)$, of v(t) to be :

$$S_v(\omega) = \lim_{T \to \infty} \frac{4\pi \, |V_T(\omega)|^2}{T} \qquad \qquad \text{(A-10)}$$

then $S_v(\omega).d\omega$ is the portion of the average power of v(t) that is due to the frequency components between ω and $\omega + d\omega$. Physically, $S_v(\omega)$ is measured by selectively filtering the spectrum of v(t) into its various frequency classes and measuring the power output in each of the classes.

A.2   DETECTION OF NOISE

The noise on the lasers output is in two forms. There is intensity and frequency noise. Detecting each of these is the problem at hand. Before we can measure the laser noise we must understand the noise components at the detection point. That is, the electronic noise emanating at and beyond the photodiode.
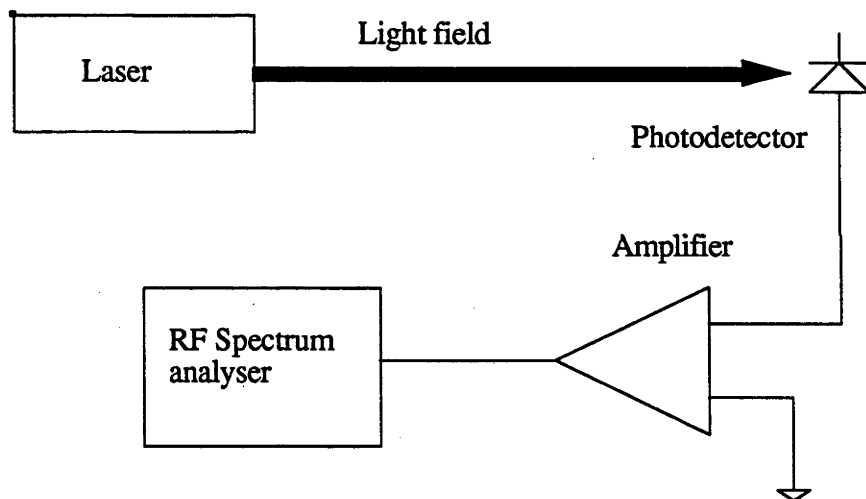

Fig. A.2-1. Schematic of a typical detection system.

A generalised detection system has been summarized in fig. A.2-1. The system consists of a photodiode that converts the laser radiation to an electronic current, and some amplifier that boosts the signal to a level that can be measured. An electronic spectrum analyser is used to obtain the spectral density function of the detected system.

Each of these stages contain noise.   There is shot noise (which is a property of the light field), Johnson noise, amplifier noise, spectrum analyser noise, and stray

noise due to pick-up from external sources. These noise sources have been described in many texts [Yariv 91 Ch10; Ott 88]. The reader is referred to these texts for further details.

A.3   LASER INTENSITY NOISE

The experimental arrangement for measuring the noise on the lasers output intensity (or power) is shown below.
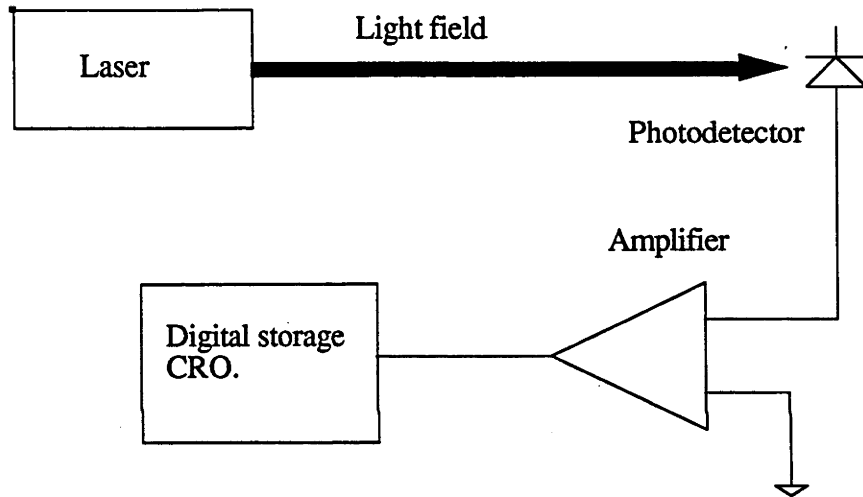

Fig. A.3-1. Schematic of a typical detection system.

The optical signal emitted by the laser is given by (A-3). The instantaneous power in v(t) is given by :

$$P(t) = v(t)v*(t) = a_s^2 + 2\, a_s\, a_{NC} + a_{NC}^2 + a_{NS}^2 \qquad \text{(A-11)}$$

The long term average power is then :

$$\bar{P} = \overline{P(t)} = \overline{a_s^2} + 2.\overline{a_s.a_{NC}} + \overline{a_{NC}^2} + \overline{a_{NS}^2} \qquad \text{(A-12)}$$

and if we note that the ensemble average $\overline{a_{NC}} = 0$ then (A-12) simplifies to:

$$\overline{P} = \overline{a_s^2} + \overline{a_{NC}^2} + \overline{a_{NS}^2} \qquad (A\text{-}13)$$

The uncertainty in the power measurement is given by the root mean square (RMS) power deviation,

$$\Delta P = \left[\overline{\left(P(t) - \overline{P}\right)^2}\right]^{0.5} \qquad (A\text{-}14)$$

We can express ΔP as a percentage error of the average power using the relation:

$$\% \text{ Error} = (\Delta P / \overline{P}) * 100\% \qquad (A\text{-}15)$$
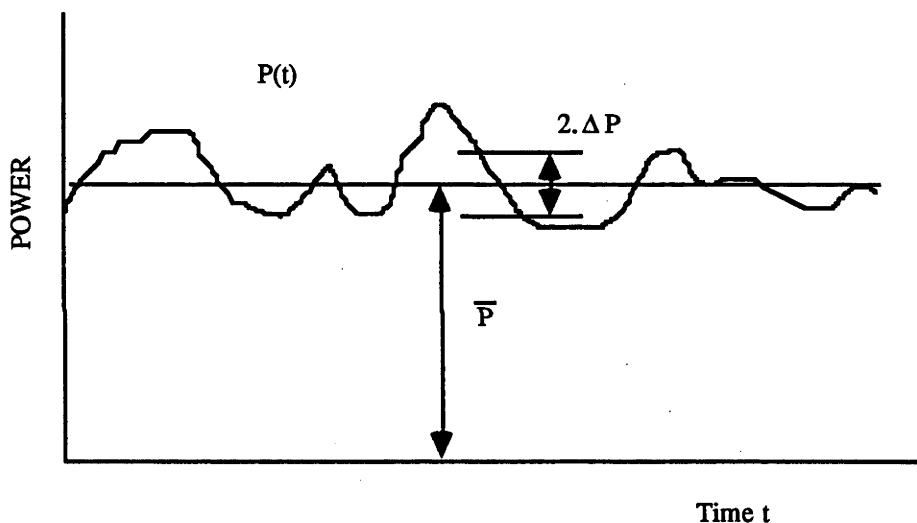
Fig. A.3-2. The rms power measurement performed by the setup of fig. A.3-1.

A.4   LASER FREQUENCY NOISE

There are several methods used to measure the frequency noise on the lasers' output. These include measuring the Allan variance [Allan 66, Wallard 73] of the stabilized laser; observing the lasers' frequency jitter through an optical spectrum analyser; a direct spectroscopic measurement; or measuring residual noise on the stabilized lasers' error signal. I will briefly discuss these methods in this section.

Frequency stability is a function of both the bandwidth of the frequency measuring system used to observe the fluctuations and the total observation time, τ. A measure of the frequency stability can be written as :

$$S_{Freq} = \frac{[\Delta v_{RMS}]_t^{t+\tau}}{\frac{1}{\tau}\int_t^{t+\tau} v(t)dt} = \frac{\Delta v_{RMS}(\tau)}{\overline{v}}$$

(A-16)

where $v(t)$ is the frequency at any time t within the observation period t to t+τ, $\overline{v}$ is the mean laser frequency during this period, and $\Delta v_{RMS}(\tau)$ is the root mean square value of the frequency deviations observed within the measurement bandwidth during the observation period. During the time period τ some extremely large fluctuations can occur that may bias the estimated frequency stability. These fluctuations should have less weight, when measuring the frequency stability, than a typical variation. For this reason the RMS deviation is specified.

The observation time limits the slowest observable fluctuation. An electronic detection system is able to measure laser frequency fluctuations from DC to hundreds of MHz, but it can only measure for periods of the order of tens of seconds hence no sensible information can be obtained involving fluctuations with periods longer than the measurement period. On the other hand, it is possible to measure the average frequency fluctuation over many seconds but this measurement prohibits the measurement of fast frequency changes. We thus have two situations to consider. The short-term and the long-term frequency stability. The short-term stability usually refers to measurement periods approaching 1s, and the long-term refers to integration periods exceeding 1s.

The Allan variance is generally used to measure the stability of a laser. The classical variance σ of the laser frequency v_i is :

$$\sigma^2(M,\tau) = \frac{1}{M-1}\left\{\sum_{i=1}^{M} v_i^2 - \frac{1}{M}\left(\sum_{i=1}^{M} v_i\right)^2\right\}$$

(A-17)

where M is the number of samples of the laser frequency and τ is the sample

integration time.

Ideally the variance should decrease to some finite value as the noise fluctuations are averaged out using longer sample integration times. However, for noise sources which contain a most of their noise power in the Fourier frequency ranges corresponding to long times, the value of $\sigma^2(M,\tau)$ diverges as the number of samples is increased. This type of noise (for example 1/f noise) is commonly found in laser oscillators. To remedy this problem two adjacent samples of the laser frequency are taken, both averaged over the same time period τ. Hence, we find :

$$\sigma^2(2,\tau) = \frac{1}{2}(v_1 - v_2)^2$$

(A-18)

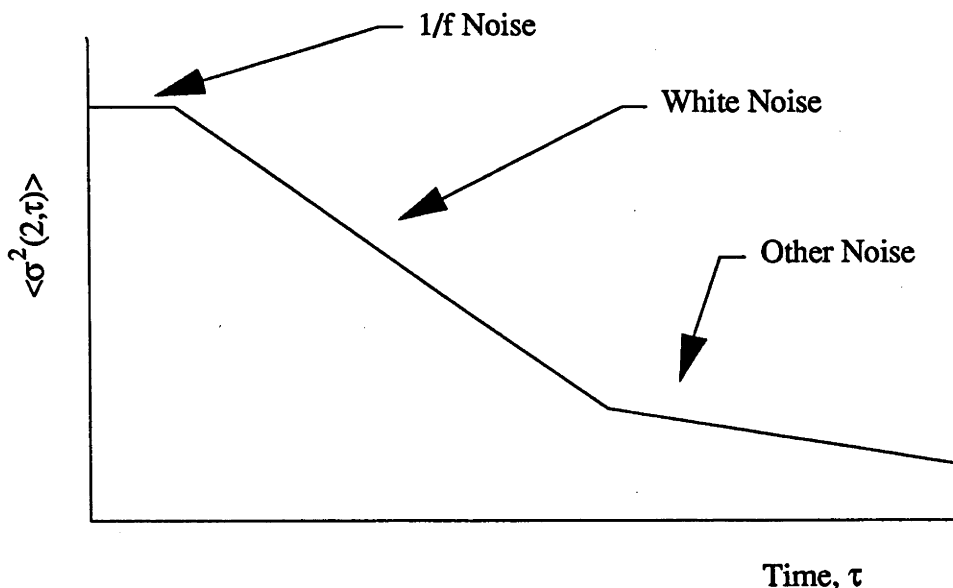The Allan variance is the average of N pairs of adjacent readings of laser frequency:

Fig. A.4-1. Typical Allan variance plot.

$$\langle \sigma^2(2,\tau) \rangle = \frac{1}{2N}\sum_{i=1}^{N}\left(v_{2i} - v_{(2i-1)}\right)^2$$

(A-19)

This value does decrease with increasing N for the noise sources that make (A-17) diverge.

The Allan variance gives information about the average difference between two adjacent samples of the frequency as a function of the sampling time. $<\sigma^2(2,\tau)>$ is plotted logarithmically as a function of τ, and the slope of the plots gives information as to the noise processes acting on the laser oscillator.

1/f noise, for example, has an Allan variance

$$<\sigma^2(2,\tau)> \; = \; 2\alpha \ln 2 \qquad\qquad (A-20)$$

where α is a constant that determines the magnitude of the noise. Form this relation we can see that the slope of the 1/f noise is zero on a Allan variance plot.

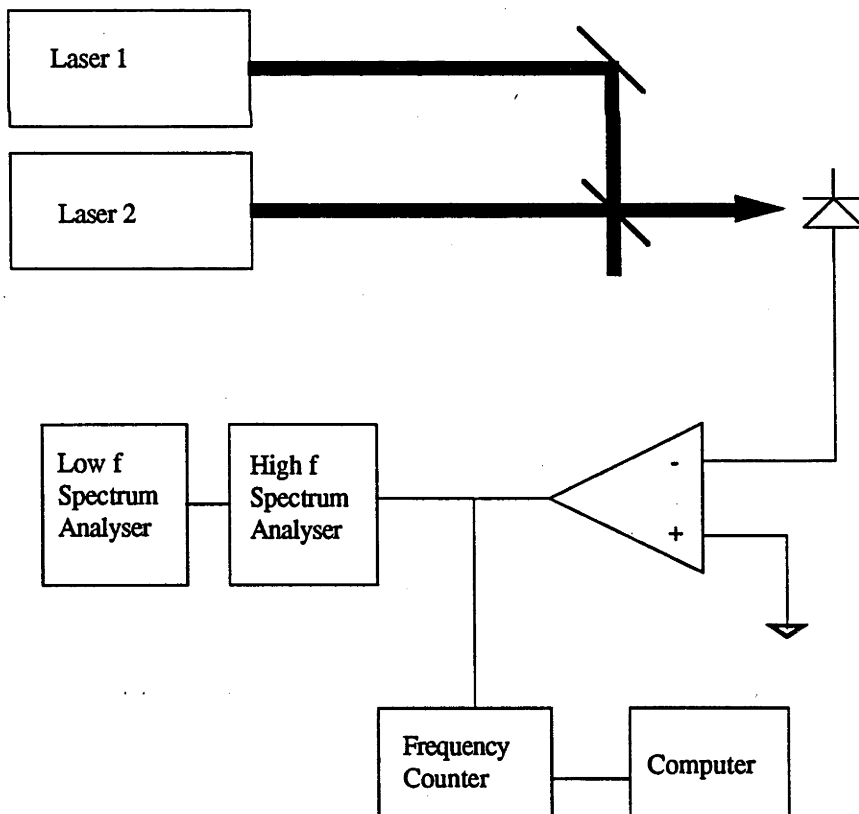White noise has the same magnitude β independent of bandwidth. In this case we

Fig. A.4-2. Schematic of the experimental arrangement for measureing the Allan variance. The light from two independent lasers is combined on a beam splitter and detected on a photodiode. The beat frequency is measured by a frequency counter and computer or by two spectrum analysers.

find

$$<\sigma^2(2,\tau)> = (\beta/2\tau) \qquad\qquad\qquad (A-21)$$

and so the plot has a slope of -1.

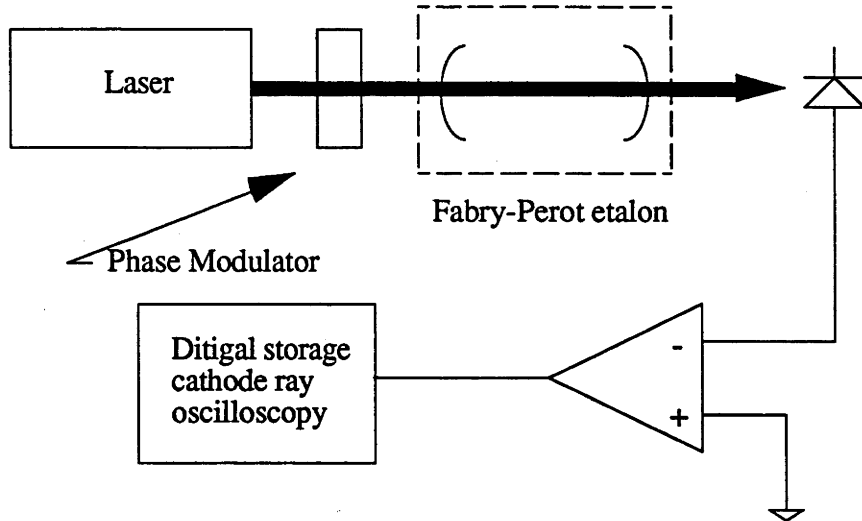The setup shown in figure A.4-2 [Hough *et. al.* 84] is the standard method of

Fig. A.4-3. The experimental arrangement for measuring the lasers' frequency jitter using a Fabry-Perot cavity as a frequency discriminator.

experimentally determine the Allan variance. The frequency stability is measured by an experiment that looks at the beat signal between two identical lasers, operating at slightly different frequencies (300MHz say). The two laser beams are combined on a beam splitter, and the combined beam is sent to a photodiode. The photo current is amplified then sent to the data collecting system. This could be a frequency counter connected to a computer, or possibly two spectrum analysers. In the latter case the first spectrum analyser is used to observe the beat signal and to act as a frequency discriminator. The output of the first spectrum analyser is sent to
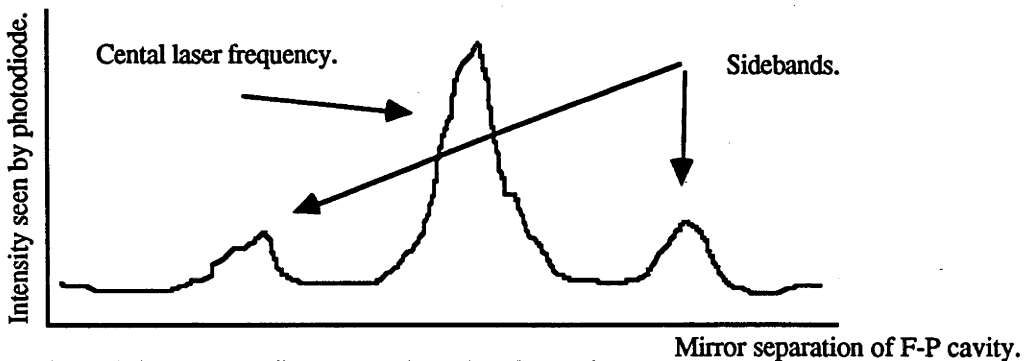

Fig. A.4-4. Laser profile as seen through a F-P cavity.

the low frequency spectrum analyser where the Fourier spectrum of the beat signal is displayed. The Allan variance can then be obtained from this information.

The second method that I will discuss uses an optical spectrum analyser to determine the laser frequency jitter. The experimental arrangement is shown in figure A.4-3.

The laser light is firstly passed through a phase modulator, then a non-confocal Fabry-Perot cavity and is finally detected by a photodiode. The signal is amplified and sent to a digital storage CRO. The phase modulator is used to place sidebands on the laser field at a known RF frequency (2MHz say). These sidebands are used as a calibration. A scanning Fabry-Perot cavity then examines the laser field, resulting in a curve similar to that shown in figure A.4-4.

A single scan gives information as to the frequency stability of the laser over the period of the scan, provided that the Fabry-Perot cavity has a linewidth that is smaller than the lasers. To gain information as to the long-term stability of the laser we can take multiple scans and display them together. The Hewlett-Packard [Model 54200A/D] digitizing oscilloscope has the capability to measure and store many such traces (as is shown in fig.1-1). Hence, with this machine we can record the long-term stability of the laser. The disadvantage of using such a system is that the cavities stability is in question. So when we use this system we need to state the stability of the reference cavity and state which cavity was used.

A third approach is to measure the frequency jitter experimentally in a spectroscopic experiment. Two such experiments were discussed in chapter 6. The difficulty with this approach is in finding a suitable spectroscopic reference. They do exist, as has been shown by [Fisk 91], but their production is technically challenging because they need to have a linewidth that is comparable to that of the laser, or preferable laser linewidth limited. In general it is not easy to be sure that the test sample has these properties. We found that in both our experiments the samples were not suitable. However, with more time we could have improved our experimental technique and produced suitable samples.

By far the most convenient way to measure the stability of the laser is to measure the residual error signal. This technique is used by most manufacture of laser systems. In this method the slope of the error signal is measured (MHz/V) and also the voltage swing of the error signal is measured (V) while the laser is locked. The frequency stability is deduced by multiplying these two values. This method gives

the closed loop stability of the laser as seen by the stabilizing circuitry. It does not, however, give any absolute measurement of the lasers' performance.

Finally, we also have the option of looking at the laser field transmitted through the reference cavity. This technique should (if the stabilizer electronic is working correctly) confirm the result obtained from measuring the residual error signal. In this method we measure the Airy function for the reference cavity and then the field intensity passing through the reference cavity (while the laser is locked). We deduce the laser frequency stability by examining how closely the laser field remains near peak transmission.

APPENDIX B
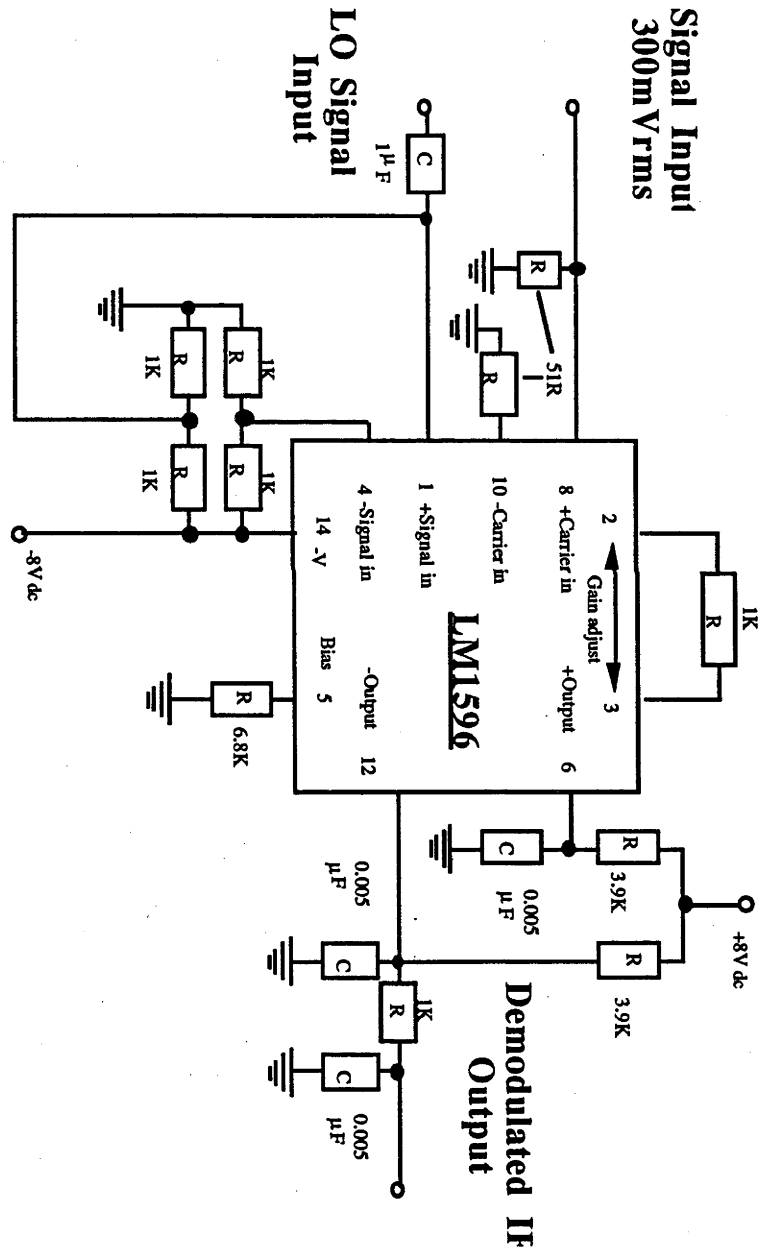
ELECTRONIC CIRCUITRY
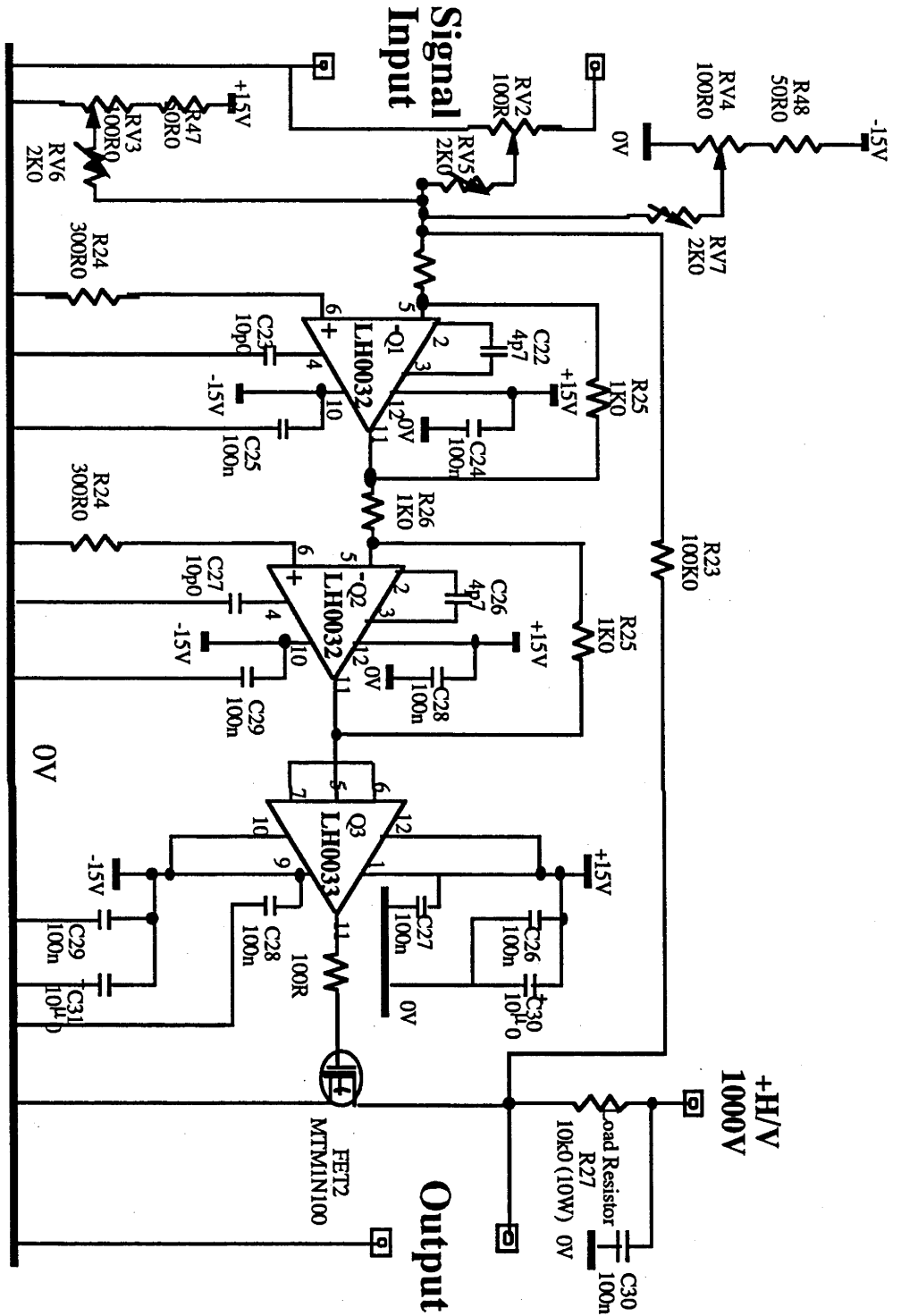

Fig. B1. LM1596 modulator/demodulator circuit.
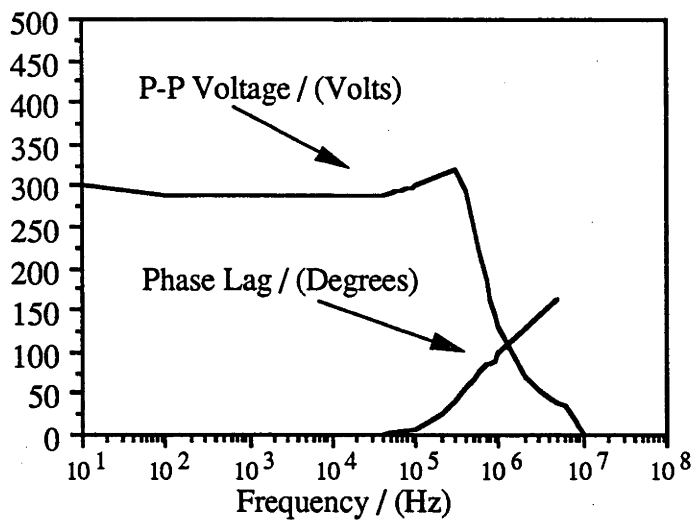
Fig. B2. The high voltage amplifier.

Fig. B3. Phase and frequency response of the high voltage amplifier.

BP65 PHOTODIODE

-15V

100kΩ

BUFFER AMP LM0033CG

−

+

OUTPUT

TRANSIMPEDANCE
AMP OP27

0V

0V
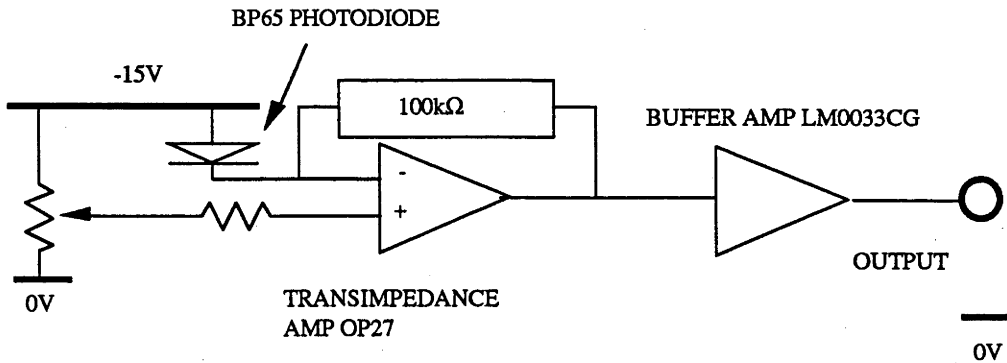
Fig. B4. Low frequency photodiode for dye laser intensity stabilization. (±15V supply).

-15V   1µH   100Ω   FND 100

47µF   0.01µF   1µF   0.01µF   NE5212

0V

+15V   7805   1µH   33Ω

+5V   0.1µF

1µF   1µF   47µF   0.01µF   TM0-1
TRANSFORMER

0V

OUTPUT

Fig. B5. High speed photodiode circuit using an FND-100 photodiode and a NE-5212 transimpedance amplifier.

For the low frequence integrator to the 699
external scan input:
RIV = 20k0 ; RII = 470R ; RIF = 0R;
RIS = 0R ; CI = 1μF; C23 = 1μF; R3 = 330R.
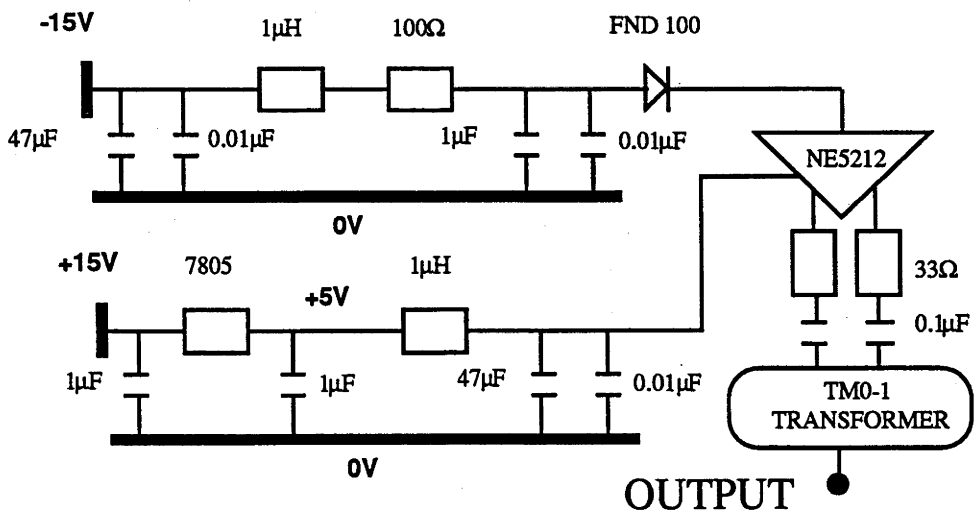The roll over point is set to start at 0Hz.
The maximum gain is > 50dB.
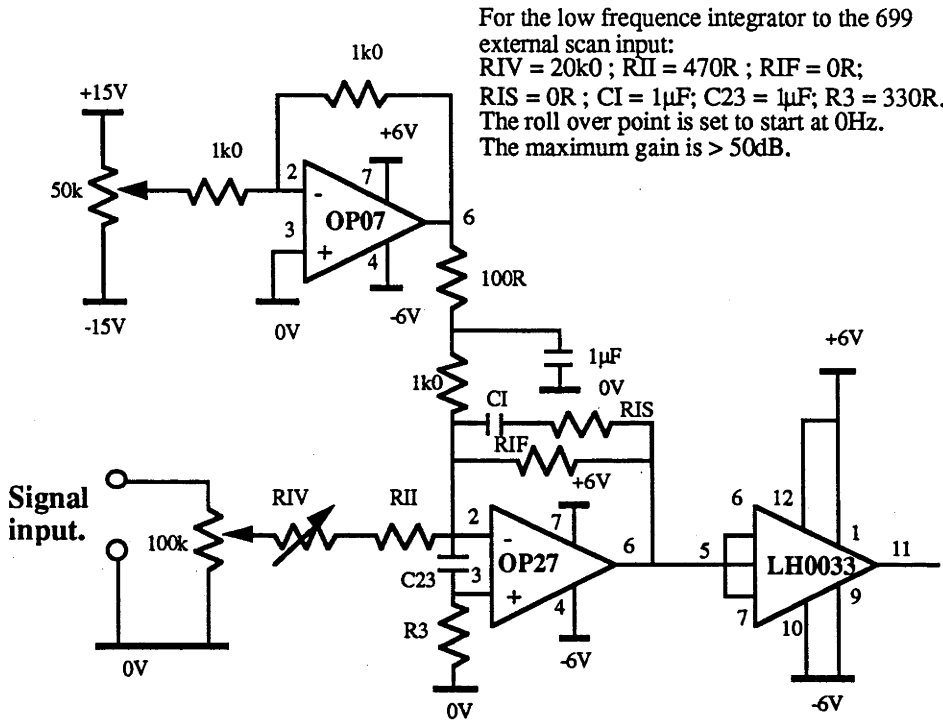
Fig. B6. Low frequency integrator to the external scan of the CR-699-21 control unit.

Output amplitude is flat to > 1MHz
(operating at max gain) with 40 deg
phase lag. Maximum gain is 25dB.
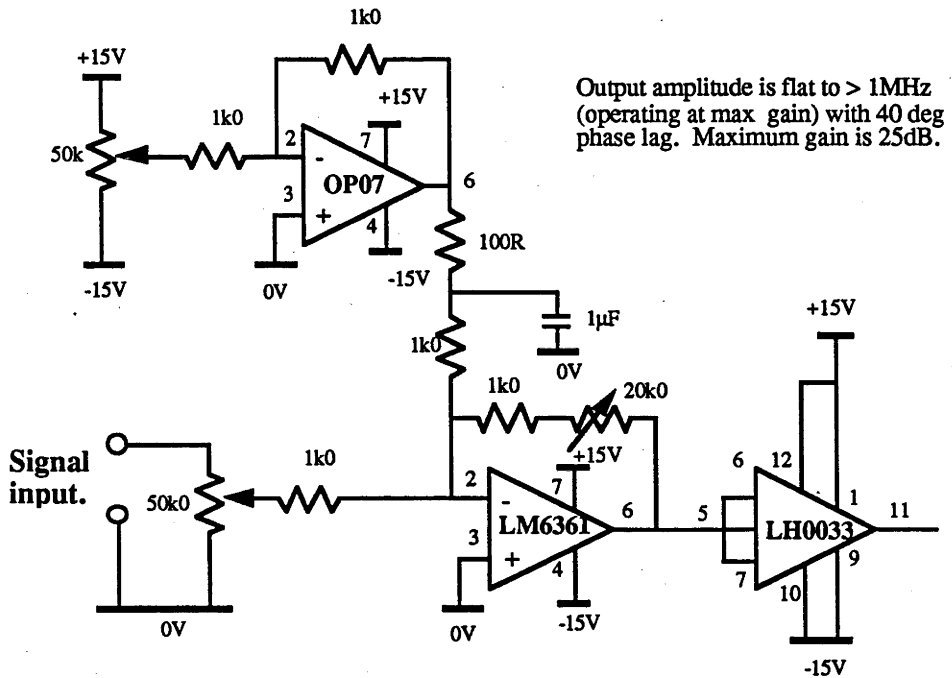
Fig. B7. Proportional stage of the PID going to the VCO.

For the low frequence integrator:
RIV = 0R ; RII = 47R ; RIF = 500k pot;
RIS = 0R ; CI = 160nF.
The roll over point can be changed from
11Hz to 11kHz.
The maximum gain is 47dB.

For the high frequence integrator:
RIV = 10k ; RII = 47R ; RIF = 0R;
RIS = 1k0 ; CI = 3n3.
The roll over point can be changed from
4kHz to 480kHz.
The maximum gain is 50dB.
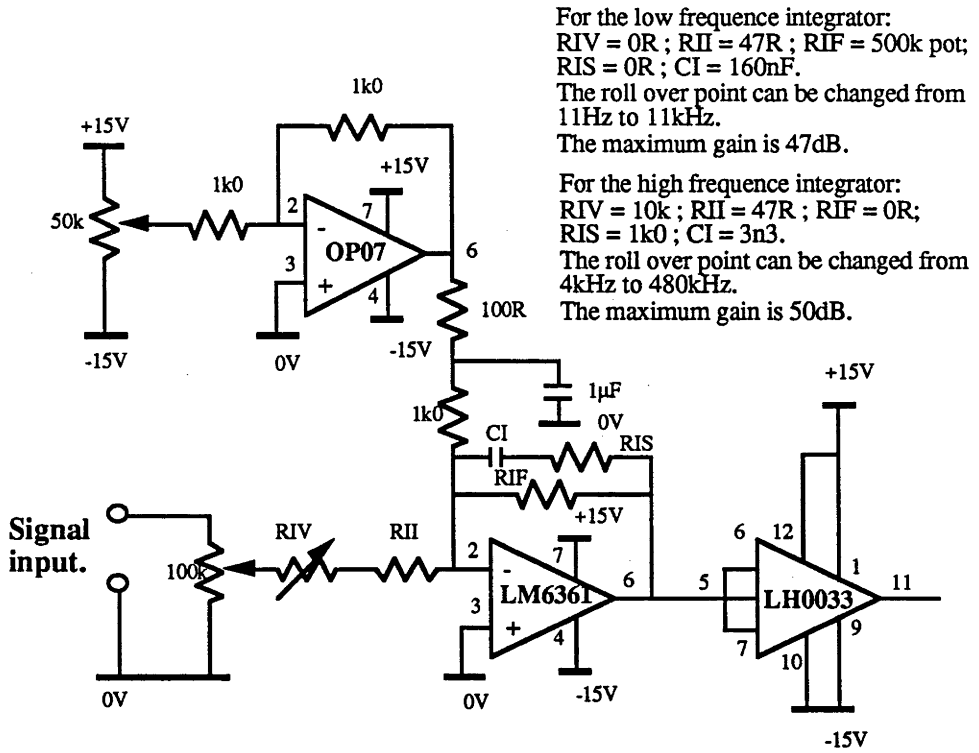
Fig. B8. Integrator stages of the PID going to the VCO.

Differentiator was not used
in the experiments.
The basic configuration is
shown here, with out
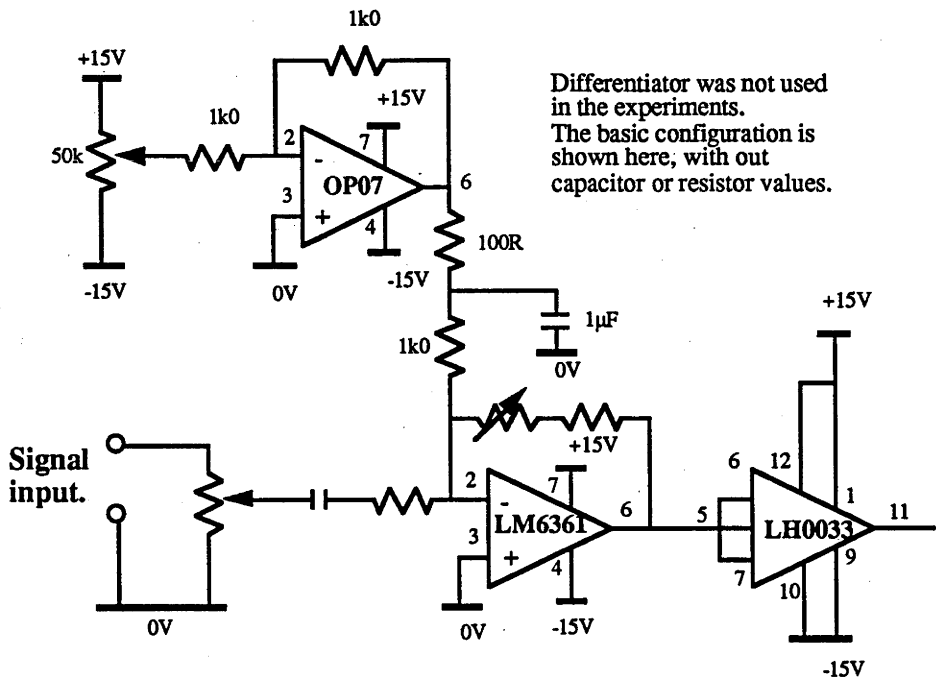capacitor or resistor values.

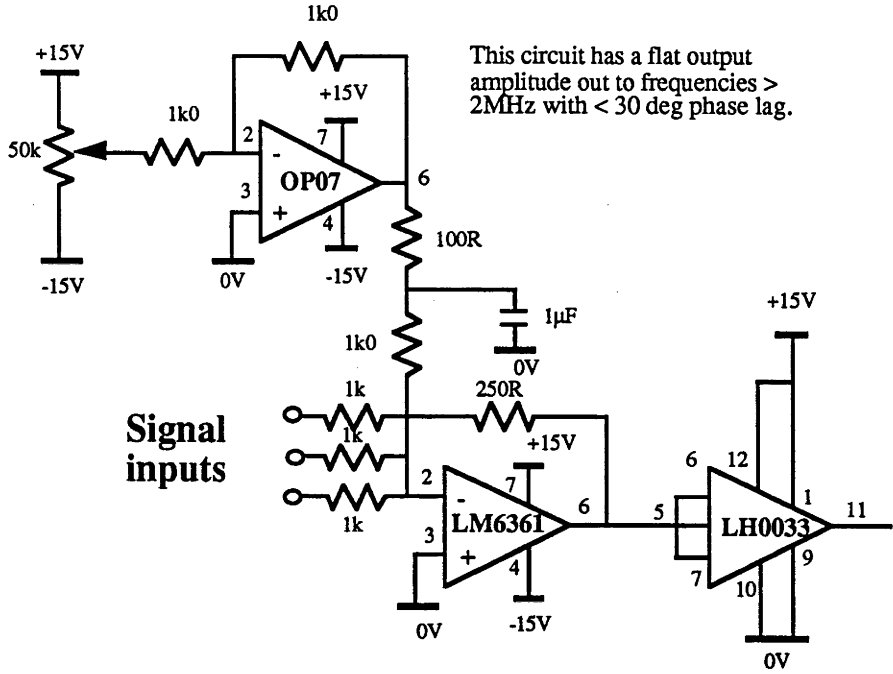Fig. B9. Differentiator stage of PID going to VCO.

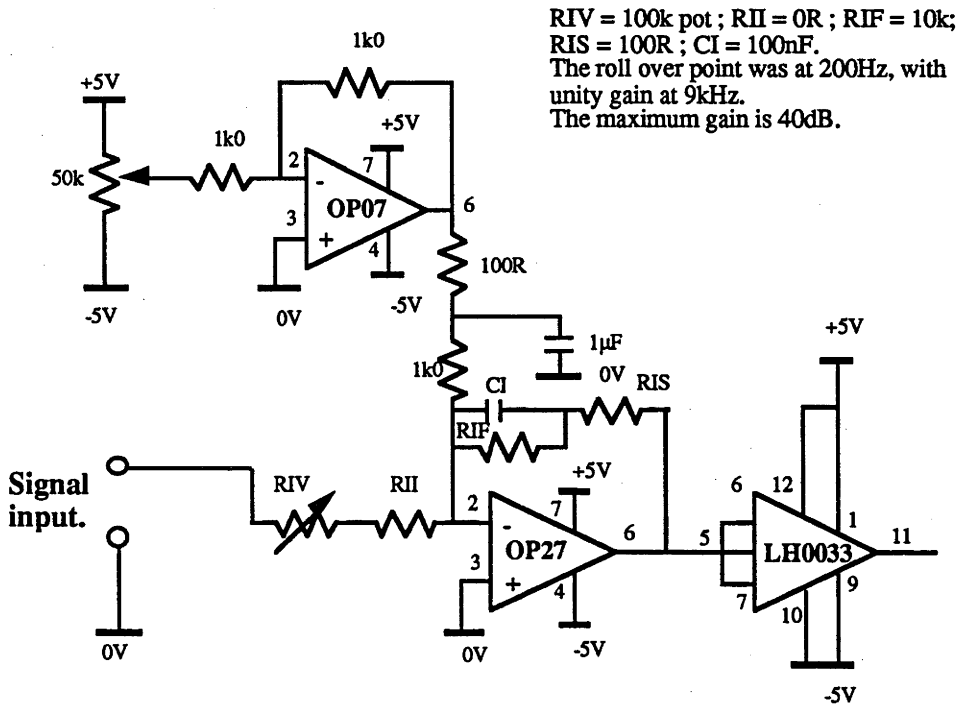Fig. B10. Summing circuit of the PID.

Fig. B11. PID for intensity stabilizer.

REFERENCES AND FURTHER READING

S.R. Amin, C.D. Caldwell, & W. Lichten, 'Crossed-beam spectroscopy of Hydrogen: A new value for the Rydberg constant.', Phys. Rev. Lett., Vol. 47, No. 18, pp. 1234-1238, 1981.

D.Z. Anderson, 'Alignment of resonant optical cavities.', Appl. Opt., Vol. 23, No. 17, pp. 2944-2949, 1984.

T. Baer, F.V. Kowalski, & J.L. Hall, 'Frequncy stabilization of a 0.633micrometer He-Ne longitudinal Zeeman laser.', Appl. Opt., Vol. 19, No. 18, pp. 3173-3177, 1980.

R. Balhorn, H. Kunzmann, & F. Lebowsky, 'Frequency stabilization of internal-mirror Helium-Nenon lasers.', Appl. Opt., Vol. 11, No. 4, pp. 742-744, 1972.

R.L. Barger & J.L. Hall, 'Pressure shift and broadening of Methane line at 3.39micrometers studied by laser-saturated molecular absorption.', Phys. Rev. Lett., Vol. 22, No. 1, pp. 4-8, 1969.

R.L. Barger, M.S. Sorem & J.L. Hall, 'Frequency stabilization of a cw dye laser.', Appl. Phys. Lett., Vol. 22, No. 11, pp. 573-575, 1973.

A.D. Berg, 'Etalon laser mode selector.', United States Patent 4 081 760, 1978.

J.C. Bergquist, S.A. Lee, & J.L. Hall., 'Saturated absorption with spatially separated laser fields: Observation of "Ramsey" fringes.', Phys. Rev. Lett., Vol. 38, No. 4, pp. 159-162, 1977.

G.C. Bjorklund, 'Frequency-modulation spectroscopy: a new method for measuring weak absorptions and dispersions.', Opt. Lett., Vol. 5, No. 1, pp. 15-17, 1980.

G.C. Bjorklund & M.D. Levenson, 'Sub-Doppler frequency-modulation spectroscopy of I2.', Phys. Rev. A, Vol. 24, No. 1, pp. 166-169, 1981.

D.S. Bomse, 'Dual-Modulation laser line-locking scheme.', Appl. Opt., Vol. 30, No. 21, pp. 2922-24, 1991.

N. Brown, 'Frequency stabilized lasers: Optical feedback effects.', Appl. Opt., Vol. 20, No. 21, pp. 3711-3714, 1981.

G. Camy, D. Pinaud, N. Courtier & Hu Chi Chuan, 'Recent developments in high resolution saturation spectroscopy obtained by means of acousto-optic modulators.', Revue de physique Appliquee, Vol. 17, pp. 357-363, 1982.

C.B. Carlisle & D.E. Cooper & H. Preier, 'Quantum Noise-limited FM Spectroscopy with a lead-salt diode laser.', Appl. Opt., Vol. 28, No. 13, pp. 2567-2576, 1989.

P.E. Ciddor and R.M. Duffy, 'Two-mode frequency-stabilized He-Ne (633nm) lasers: studies of short- and long-term stability.', J. Phys. E: Sci. Instrum., Vol. 16, pp. 1223-1227, 1983.

B. Dahmani, L. Hollberg, & R. Drullinger, 'Frequency stabilization of semiconductor lasers by resonant optical feedback.', Opt. Lett., Vol. 12, No. 11, pp. 876-878, 1987.

T. Day, E.K. Gustafson and R.L. Byer, 'Sub-hertz relative frequency stabilization of two diode laser pumped Nd:YAG lasers locked to a Fabry-Perot interferometer.', 'To be published',

T. Day, E.K. Gustafson, & R.L. Byer, 'Active frequency stabilization of a 1.062micrometer, Nd:GGG, diode-laser-pumped nonplanar ring oscillator to less than 3 Hz of relative linewidth.', Opt. Lett., Vol. 15, No. 4, pp. 221-223, 1990.

R.G. DeVoe & R.G. Brewer, 'Laser-frequency division and stabilization.', Phys. Rev. A, Vol. 30, No. 5, pp. 2827-2829, 1984.

R.C. Dorf, 'Modern control systems.', Addison Weisley, 1989.

R.W.P. Drever, J.L. Hall, F.V. Kowalski, J. Hough, G.M. Ford, A.J. Munley, & H. Ward., 'Laser phase and frequency stabilization using an optical resonator.', Appl. Phys. B, Vol. 31, pp. 97-105, 1983.

D.S. Elliott, R. Roy, & S.J. Smith, 'Extracavity laser band-shape and bandwidth modification.', Phys. Rev. A, Vol. 26, No. 1, pp. 12-18, 1982.

P. Fisk, 'Report on progress made during the first attempt at running the squeezed state experiment in May/June/July 1987.', Technical Report, 1987.

P.T.H. Fisk, Private Communication, 1991.

Charles Freed, 'Stability measurements of CO2-N2-He lasers at 10.6 micrometers wavelength.', IEEE Journal of Quan. Elect., pp. 203-205, 1967.

Charles Freed, 'Design & short-term stability of single frequency CO2 lasers.', IEEE Journal of Quan. Elect., Vol. QE-4, No. 6, pp. 404-408, 1968.

P. Fritschel, A. Jeffries, & T.J. Kane, 'Frequency fluctuations of a diode-pumped Nd:YAG ring laser.', Opt. Lett., Vol. 14, No. 18, pp. 993-995, 1989.

D.A. Glenar, D.E. Jennings, & S. Nadler, 'Electrooptic modulation methods for sensitivity tunable diode laser spectroscopy', Appl. Opt., Vol. 29, No. 15, pp. 2282-2287, 1990.

D.S. Gough and P. Hannaford, 'High quality saturated absorption spectroscopy in a sputtered vapour: Application to hyperfine structure in Zr I.', Opt. Comm., Vol. 67, No. 3, pp. 209-213, 1988.

H. Greenstein, 'Theory of single mode gas lasers.', Physical Review , Vol. 175, No. 2, pp. 438-452, 1968.

U. Grzesik, 'Frequenzstabilisierung eines farbstoffringlasers.', PhD Thesis for Physics, Ludwig-Maximilian-Universitat Munich, 1985.

J.L. Hall & T.W. Hänsch, 'External dye-laser frequency stabilizer.', Opt. Lett.,

Vol. 9, No. 11, pp. 502-504, 1984.

J.L. Hall, 'Stabilizing lasers for applications in quantum opics.', 'Quantum Optics IV', Ed: J.D. Harvey and D.F. Walls, Springer-Verlag, pp. 273-284, 1986.

J.L. Hall, M. Long-Sheng, and G. Kramer., 'Principles of optical phase-locking: Application to internal mirror He-Ne lasers phase-locked via fast control of the discharge current.', IEEE Journal of Quan. Elect., Vol. QE-23, No. 4, pp. 427436, 1987.

J.L.Hall, Private Communication, 1990.

J.M. Halley & J.E. Midwinter, 'Competitive Instability in non-linear Fabry-Perot etalons.', IEEE Journal of Quan. Elect., Vol. 26, No. 2, pp. 348, 1990.

G.R. Hanes & C.E. Dahlstrom, 'Iodine hyperfine structure observed in saturated absorption at 633nm.', Appl. Phys. Lett., Vol. 14, No. 11, pp. 362-364, 1969.

G.R. Hanes, K.M. Baird, & J. DeRemigis, 'Stability, reproduceibility, and absolute wavelength of a 633nm He-Ne laser stabilized to an iodine hyperfine component.', Appl. Opt., Vol. 12, No. 7, pp. 1600-1605, 1973.

P. Hannaford and R.M. Lowe, 'Some recent developments in atomic lifetime determinations', Aust. J. Phys., Vol. 39, pp. 829-244, 1986.

P. Hannaford and D.S. Gough, 'High quality staurated absorption spectroscopy in a sputtered vapour: Application to isotope shift in Zr I.', Laser Specrtoscopy IX, Academic press, 1989.

T.W. Hänsch, M.D. Levenson, & A.L. Schawlow., 'Complete hyperfine structure of a molecular Iodine line.', Phys. Rev. Lett., Vol. 26, No. 16, pp. 946-949, 1971.

T.W. Hänsch and B. Couillaud, 'Laser frequency stabilization by polarization spectroscopy of a reflecting reference cavity.', Opt. Comm., Vol. 35, No. 3, pp. 441-444, 1980.

J. Helmcke, S.A. Lee, & J.L. Hall, 'Dye laser spectrometer for ultrahigh spectral resolution: design and performance.', Appl. Opt., Vol. 21, No. 9, pp. 1686-1694, 1982.

D. Hils & J.L. Hall, 'Response of a Fabry-Perot cavity to phase modulated light.', Rev. of Sci. Instrum., Vol. 58, No. 8, pp. 1406-1412, 1987.

D.M. Hope, H.-A. Bachor, P.J. Manson, D.E. McClelland and P.T.H. Fisk, 'Observation of quaderature squeezing in a cavity-atom system.', 'To be published',

Horowitz and Hill, 'The art of electronics.', Cambridge University Press, 1988.

J. Hough, D. Hils, M.D. Rayman, Ma L.-S., L. Hollberg, & J.L.Hall., 'Dye-laser frequency stabilization using optical resonators.', Appl. Phys. B, Vol. 33, pp. 179-185, 1984.

M. Houssin, M. Jardino, B.Gely, & M. Desaintfuscien, 'Design and performance of a few-kilohertz-linewidth dye laser stabilized by reflectionin an optical resonator.', Opt. Lett., Vol. 13, No. 10, pp. 823-825, 1988.

D.A. Jennings, C.R. Pollock, F.R. Petersen, R.E. Drullinger, K.M. Evenson, J.S. Wells, J.L. Hall, & H.P. Layer, 'Direct frequency measurement of the I2-stabilized He-Ne 473-THz (633nm) laser.', Opt. Lett., Vol. 8, No. 3, pp. 136-138, 1983.

T.F. Johnston, Jr., J.L. Hobart, R.C. Rempel, & G.H. Williams., 'Method and apparatus for automatically reacquiring a predetermined output radiation frequency in a tuneable laser system despite momentary perturbations of laser oscillation.', United States Patent 4 150 342, 1979.

T.F. Johnston, Jr., R.H. Brady, & W. Proffitt, 'Powerful single-frequency ring dye laser spanning the visible spectrum.', Appl. Opt., Vol. 21, No. 13, pp. 2307-2316, 1982.

M. H. Jones, 'A practical introduction to electronic circuits.', Cambridge University Press, 1985.

P. Jung, 'Absolute frequenzstabilisierrung von farbstofflasern mittels eines bichromatischen referenzresonators.', Diplomarbeit, Universitat Kaiserslautern, 1989.

R. Kallenbach, C. Zimmermann, D.H. McIntyre, T.W. Hänsch, 'A blue laser with sub-kilohertz stability.', Opt. Comm., Vol. 70, No. 1, pp. 56-60, 1989.

G.A. Kerr, N.A. Robertson, J. Hough, & C.N. Man, 'The fast frequency stabilization of an Argon laser to an optical resonator using an extra-cavity electro-optic modulator.', Appl. Phys. B, Vol. 37, pp. 11-16, 1985.

F.V Kowalski, R.E. Teets, W. Demtröder, & A.L. Schawlow, 'An improved wavemeter for cw lasers.', J. Opt. Soc. Am., Vol. 68, No. 11, pp. 1611-1613, 1978.

H. P. Layer, 'Acoustooptic modulator intensity servo.', Appl. Opt., Vol. 18, No. 17, pp. 2947-49, 1979.

M.D. Levenson, W.E. Moerner, & D.E. Horne, 'FM Spectroscopy detection of stimulated Raman gain.', Opt. Lett., Vol. 8, No. 2, pp. 108-110, 1983.

M.D. Levenson, Private Communication, 1991.

Shen-ping Li & Qi-Ming Yang, 'Optical stabilizer using a Michelson interferometric bistable device with a ceramic electrostictor', J. Mod. Opt., Vol. 28, No. 15, pp. 3358-3361, 1989.

R.J. McLean, P. Hannaford, H.-A. Bachor, P.T.H. Fisk, and R.J. Sandeman, 'Absorption line narrowing measurements of hyperfine structure in highly excited levels of Yttrium.', Z. Phys. D - Atoms, Mol., and Clust., Springer-Verlag, Vol. 1, pp. 253-259, 1986.

P. Nachman, J. Munch, & R. Yee, 'Diode-pumped, frequency stabilized, tunable, continuous-wave Nd:Glass laser.', IEEE Journal of Quan. Elect., Vol. 26, No. 2, pp. 317, 1990.

T.M. Niebauer, J.E. Faller, H.M. Godwin, John L. Hall, & R.L. Barger, 'Frequency stability measurements on polarization-stabilized He-Ne lasers.', Appl. Opt., Vol. 27, No. 7, pp. 1285-1289, 1988.

M. Ohtsu, M. Murata, and M. Kourogi., 'FM noise reduction and subkilohertz linewidth of AlGaAs laser by negative electrical feedback.', IEEE Journal of Quan. Elect., Vol. 26, No. 2, pp. 231-41, 1990.

H.W. Ott, 'Noise reduction techniques in electronic systems.', Wiley Interscience, 1988.

C. Penn, H-A. Bachor & D.E. McClelland, 'Automatic alignment and mode-matching of a laser beam to an optical resonator.', Technical Report, No. 2, 1991.

W.D. Phillips & H. Metcalf, 'Laser deceleration of an atomic beam.', Phys. Rev. Lett., Vol. 48, No. 9, pp. 596-599, 1982.

M.D. Rayman, C.G. Aminoff, & J.L. Hall, 'Precise laser frequency scanning using frequency-synthesised optical frequency sidebands: application to isotope shifts and hyperfine structure of mercury', J. Opt. Soc. Am. B, Vol. 6, No. 4, pp. 539-549, 1989.

N.A. Robertson, S. Hoggan, J.B. Mangan & J. Hough, 'Intensity stabilization of an Argon laser using Electro-optic modulator - Performance and limitation', Appl. Phys. B, Vol. 39, pp. 149-153, 1986.

M. Romagnoli, M.D. Levenson, & G.C. Bjorklund, 'Frequency-modulation-polarization spectroscopy.', Opt. Lett., Vol. 8, No. 12, pp. 635-637, 1983.

Ch. Salomon, D. Hils & J.L. Hall, 'Laser stabilization at the MilliHertz level.', J. Opt. Soc. Am. B, Vol. 5, No. 8, 1988.

N.M. Sampas & D.A. Anderson, 'Stabilization of laser beam alignment to an optical resonator by heterodyne detection of off-axis modes.', Appl. Opt., Vol. 29, No. 3, pp. 394-403, 1990.

G.S. Sasagawa & M.A. Zumberge, 'Five-year frequency stability of A Zeeman stabilized laser.', Appl. Opt., Vol. 28, No. 5, pp. 824-825, 1989.

A. Sasaki, K. Wakabayashi, & S. Masuda, 'Stabilization of sinble frequency internal mirror He-Ne lasers.', Appl. Opt., Vol. 28, No. 9, pp. 1608-1609, 1989.

A.L. Schawlow & C.H. Townes, 'Infrared and optical masers', Physical Review , Vol. 112, No. 6, pp. 1940-1949, 1958.

Alex Schenzle, R.G. DeVoe, & R.G. Brewer, 'Phase-modulation laser spectroscopy.', Phys. Rev. A, Vol. 25, No. 5, pp. 2606-2621, 1982.

W.G. Schweitzer, Jr., E.G. Kessler, Jr., R.D. Deslattes, H.P. Layer, & J.R. Whetstone, 'Description, performance, and wavelengths of Iodine stabilized lasers.', Appl. Opt., Vol. 12, No. 12, pp. 2927-2938, 1973.

A.E. Seigman, 'Lasers', Oxford University Press, 1986.

M. Sellars, Private Communication, 1992.

C.-H. Shin and M. Ohtsu, 'Stable semiconductor laser with a 7-Hz linewidth by an optical-electrical double-feedback technique.', Opt. Lett., Vol. 15, No. 24, pp. 1455-57, 1990.

D. Shoemaker, A. Brillet, C.N. Man, O. Crégut, & G. Kerr, 'Frequency-stabilized laser-diode-pumped Nd:YAG laser.', Opt. Lett., Vol. 14, No. 12, pp. 609-611, 1989.

C.M. Shum & E.A. Whittaker, 'Resonantly enhanced radio frequency electrooptic phase modulator.', Appl. Opt., Vol. 29, No. 3, pp. 422-428, 1990.

D.A. Smith & D.I. Shernoff, 'Simple measurement of gain andloss in ultralow loss optical resonators.', Appl. Opt., Vol. 24, No. 12, pp. 1722-1723, 1985.

D.N. Stacey and K. Burnett, 'High-resolution laser spectroscopy of atoms.', Sci. Prog., Oxf., Vol. 73, pp. 351-388, 1989.

I. Steiner, V. Enders, F. Elsner, W. Neuhauser, P.E. Toschek, R. Blatt, and J. Helmcke., 'A dye ring-laser spectrometer for precision spectroscopy.', Appl. Phys. B, Vol. 49, pp. 251-256, 1989.

L.V. Tarsov, 'Laser Physics', MIR Publishers Moscow, 1983.

H.R. Telle, 'Narrow linewidth laser diodes with broad continuous tuning range.', Appl. Phys. B, Vol. 49, pp. 217-266, 1989.

U. Tietze and Ch. Schenk, 'Electronic Circuits: Design and applications', Springer-Verlag, 1991.

M.A. Title & S.H. Lee, 'Modeling and characterization of embedded electrode performance in transverse electrooptic modulators.', Appl. Opt., Vol. 29, No. 1, pp. 85-98, 1990.

H. Tsuchida & Y. Mitsuhashi, 'Novel ring interferometer for frequency stabilization of semiconductor lasers.', Appl. Opt., Vol. 27, No. 2, pp. 302-305, 1988.

N. Umeda, M. Tsukiji, and Hi Takasaki, 'Stabilized 3He-20Ne transverse Zeeman laser.', Appl. Opt., Vol. 19, No. 3, pp. 442-450, 1980.

F. Vachss & I. McMichael, 'Efficient optical enhancement of acousto-optic diffraction using optimized overlap of coupled waves.', Opt. Lett., Vol. 15, No. 16, pp. 921-923, 1990.

A.J. Wallard, 'The frequency stabilization of gas lasers', J. Phys. E, Vol. 5, pp. 926, 1972.

A.D. White, 'Frequency satbilization of gas lasers.', IEEE Journal of Quan. Elect., Vol. 1, No. 8, pp. 349-357, 1965.

E.A. Whittaker, M. Gehrtz, and G.C. Bjorklund, 'Residual amplitude modulation in laser electro-optic phase modulation.', J. Opt. Soc. Am. B, Vol. 2, No. 8, pp. 1320-26, 1985.

W. Wiesemann, 'Longitudinal mode selection in lasers with three-mirror reflectors.', Appl. Opt., Vol. 12, No. 12, pp. 2909-2912, 1973.

D.J. Wineland, R.E. Drullinger, & F.L. Walls, 'Radiation-pressure cooling of bound resonant absorbers.', Phys. Rev. Lett., Vol. 40, No. 25, pp. 1639-1642, 1978.

W.L. Wise, 'Feedback loop control system employing method and apparatus for stabilizing total loop gain and bandwidth.', United States Patent 4 092 530, 1978.

N.C. Wong and J.L. Hall, 'Servo control of amplitude modulation in frequency-modulation spectroscopy: demonstration of shot-noise-limited detection.', J. Opt. Soc. Am. B, Vol. 2, No. 9, pp. 1527-33, 1985.

C. Xie, L. Wang, L. Chen, L. Xie, & Y. Wang, 'Frequency stabilization of an AlGaAs laser diode by a Fabry-Perot interferometer locked to a laser beam frequency-locked to the D2 line of a Cs atomic beam.', Appl. Opt., Vol. 28, No. 21, pp. 4552-4555, 1989.

Y. Yamamoto, S. Machida, S. Saito, N. Imoto, T. Yanagawa, M. Kitagagawa, and G. Bjork., 'Quantum mechanical limit in optical precision measurement and communication.', E. Wolf, Progress in optics XXVIII, Elsevier Science Publishers B.V, pp. 87-179, 1990.

D.-H. Yang and Y.-Q. Wang, 'A simple method to stably lock a diode laser frequency to an atomic transition line for a long period.', Opt. Comm., Vol. 80, No. 1, pp. 23-25, 1990.

A. Yariv, 'Optical electronics', Holt, 1991.

P. Zorabedian & W.R. Trutna, Jr., 'Alignment-stabilized grating-tuned external-cavity semiconductor laser.', Opt. Lett., Vol. 15, No. 9, pp. 483, 1990.

M.A. Zumberge, 'Frequency stability of a Zeeman-stabilized laser.', Appl. Opt., Vol. 24, No. 13, pp. 1902-1904, 1985.